

Fault systems of the eastern Indonesian triple junction: evaluation of Quaternary activity and implications for seismic hazards

IAN M. WATKINSON* & ROBERT HALL

*SE Asia Research Group, Department of Earth Sciences, Royal Holloway
University of London, Egham, Surrey TW20 0EX, UK*

**Correspondence: ian.watkinson@rhul.ac.uk*

Abstract: Eastern Indonesia is the site of intense deformation related to convergence between Australia, Eurasia, the Pacific and the Philippine Sea Plate. Our analysis of the tectonic geomorphology, drainage patterns, exhumed faults and historical seismicity in this region has highlighted faults that have been active during the Quaternary (Pleistocene to present day), even if instrumental records suggest that some are presently inactive. Of the 27 largely onshore fault systems studied, 11 showed evidence of a maximal tectonic rate and a further five showed evidence of rapid tectonic activity. Three faults indicating a slow to minimal tectonic rate nonetheless showed indications of Quaternary activity and may simply have long interseismic periods. Although most studied fault systems are highly segmented, many are linked by narrow (<3 km) step overs to form one or more long, quasi continuous segment capable of producing $M > 7.5$ earthquakes. Sinistral shear across the soft linked Yapen and Tarera Aiduna faults and their continuation into the transpressive Seram fold thrust belt represents perhaps the most active belt of deformation and hence the greatest seismic hazard in the region. However, the Palu Koro Fault, which is long, straight and capable of generating super shear ruptures, is considered to represent the greatest seismic risk of all the faults evaluated in this region in view of important strike slip strands that appear to traverse the thick Quaternary basin fill below Palu city.

Several of the devastating earthquakes that occurred on faults around the world during the last decade were either poorly understood or not recognized at all. The M_w 6.6 Bam earthquake (Iran) of 26 December 2003 ruptured a section of the Bam Fault that had a poor surface expression and had not caused a destructive earthquake for 2000 years (Eshghi & Zare 2003; Fu *et al.* 2004). The M_w 8.0 Wenchuan earthquake (China) of 12 May 2008 resulted from complex rupture of part of the Lonmen Shan tectonic belt (Burchfiel *et al.* 2008), an area that was previously considered not to be at risk from large earthquakes (Chen & Hsu 2013). The M_w 7.1 Haiti earthquake of 12 January 2010 occurred on the well known Enriquillo Fault, part of the fault system marking the northern boundary of the Caribbean plate, but which had previously been mapped as having low seismic hazard based on recent seismicity (Stein *et al.* 2012). The Canterbury earthquake sequence (New Zealand) ruptured the Greendale Fault, which was previously unrecognized because it was buried beneath alluvial sediments (Quigley *et al.* 2012). The Canterbury sequence culminated in the M_w 6.3 Christchurch earthquake of 22 February 2011. These events emphasize the need for the accurate identification of faults that have been active during the Quaternary and have the potential for modern tectonic activity.

Eastern Indonesia is a region of complex and rapid neotectonics. Convergence between Australia, Eurasia, the Pacific and the Philippine Sea plates (e.g. Hamilton 1979; DeMets *et al.* 1994; Hall 1996, 2012; Bock *et al.* 2003; Charlton 2010) results in both contraction and extension from subduction hinge rollback, lithospheric delamination and slab break off (e.g. Harris 1992; Spakman & Hall 2010; Hall 2012).

Great uncertainty surrounds the position, tectonic role and modern activity of eastern Indonesia's many Quaternary faults (e.g. Hamilton 1979; Okal 1999; Bailly *et al.* 2009; Charlton 2010). New fault systems continue to be identified using both modern geophysical/remote sensing and conventional field techniques (e.g. Stevens *et al.* 2002; Spencer 2010, 2011; Watkinson *et al.* 2011; Pownall *et al.* 2013) and it is likely that many others remain unknown, with important implications for seismic hazard analysis.

Despite intense seismicity in eastern Indonesia, there have been few catastrophic earthquake disasters in the last 100 years compared with other rapidly deforming areas such as China, Iran, Japan and Pakistan (e.g. Holzer & Savage 2013; National Geophysical Data Center/World Data Service). Significant events include: the 25 June 1976 M_w 7.1 Papua earthquake, which killed 3000 6000

59 people; the 12 December 1992 M_w 7.8 Flores earth
 60 quake, which killed 2500 people and destroyed
 61 31 800 houses; the 17 February 1996 M_w 8.2 Biak
 62 earthquake, which caused a 7 m tsunami and killed
 63 at least 100 people (Okal 1999); the 16 November
 64 2008 M_w 7.4 Minahasa earthquake, which killed six
 65 people and displaced 10 000; and the 16 June 2010
 66 M_w 7.0 Yapen earthquake, which killed 17 people
 67 and destroyed 2556 houses (National Geophysical
 68 Data Center/World Data Service; USGS Earth
 69 quake Hazards Program). With increasing urban
 70 development and the replacement of traditional
 71 wooden dwellings with concrete constructions, it
 72 is likely that damaging earthquakes will become
 73 more frequent in the future (e.g. Wyss 2005).

74 This paper catalogues Quaternary fault systems
 75 onshore eastern Indonesia from Sulawesi to Papua,
 76 providing evidence for Quaternary tectonic activity
 77 and a reconnaissance evaluation of the seismic haz
 78 ard of the faults (Fig. 1).

79 Methods

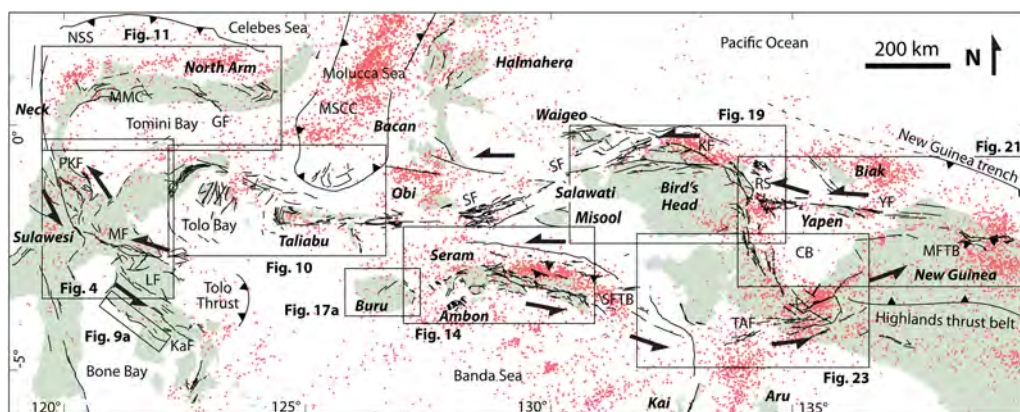
80 Definitions and extent of study

81 This study was concerned with evaluating Quater
 82 nary (Pleistocene and Holocene, 2.59 0 Ma) fault
 83 activity. Quaternary activity lies within the realm
 84 of neotectonics, the study of broadly post Miocene,
 85 ‘young’ and still active tectonic events, the effects
 86 of which are compatible with modern seismotec
 87 tonics (Pavlidis 1989). Neotectonics is distinct
 88 from palaeoseismology – the study of deformation
 89 related to specific past earthquakes (e.g. Michetti

90 *et al.* 2005). Thus faults that show evidence of Qua
 91 ternary activity may or may not also show evidence
 92 of palaeoseismicity, depending on whether they
 93 have recently ruptured the surface, the rates of sed
 94 imentation and erosion, and whether they are truly
 95 ‘active’ in the sense that they have failed during
 96 the Holocene. Equally, Quaternary faults may or
 97 may not be present in records of instrumental or his
 98 torical seismicity, depending on whether they have
 99 recently become inactive, have a long interseismic
 100 period, or have yielded historical earthquakes in
 101 locations where there was no written documenta
 102 tion. Quaternary fault activity is therefore distinct
 103 from, but influential in, the field of active tectonics,
 104 which includes future fault activity that may affect
 105 human society (Wallace 1986).

106 Quaternary fault activity was evaluated in
 107 this study by the following criteria: (1) instrum
 108 ental/historical seismicity and geodetic observations;
 109 (2) deformation of Quaternary sediments, often
 110 indicated by topographic lineaments that could be
 111 linked to an underlying fault; (3) the systematic
 112 offset of modern streams across a topographic line
 113 ament; (4) evidence of structurally controlled drain
 114 age network modification where signs of an earlier
 115 arrangement were preserved; (5) geomorphic indi
 116 ces recording the relative youthfulness of fault
 117 controlled mountain fronts; and (6) evidence of
 118 landslips localized to faults.

119 The study extent was a 2200 × 800 km swath
 120 of the Indonesian archipelago centred on the triple
 121 junction between Australia, Eurasia, the Pacific
 122 and the Philippine Sea plates. It includes much of
 123 eastern Indonesia from Sulawesi eastwards, except



111 **Fig. 1.** Map of eastern Indonesia showing upper crustal structures with geomorphic evidence of Quaternary tectonic activity and seismicity (1973–2014, focal depths < 35 km). CB, Cenderawasih Bay; GF, Gorontalo Fault; KaF, Kolaka Fault; KF, Koor Fault; LF, Lawanopo Fault; MF, Matano Fault; MFTB, Mamberamo fold thrust belt; MMC, Molino Metamorphic Complex; MSCC, Molucca Sea Collision Complex; NSS, North Sulawesi Subduction; PKF, Palu–Koro Fault; RS, Ransiki Fault; SF, Sorong Fault; SFTB, Seram fold thrust belt; TAF, Tarera–Aiduna Fault; YF, Yapen Fault. Locations of other figures as indicated.

117 the islands of the southern Banda Arc. Because of
 118 the focus on geomorphic expression, the study
 119 mainly dealt with onshore faults, except where mul-
 120 tibeam bathymetry was available.

122 *Datasets*

124 Our interpretations of Quaternary fault activity are
 125 based on a variety of remote sensing data, field
 126 observations by both authors and their students
 127 over several years (e.g. Roques 1999; Watkinson
 128 2011; Pownall *et al.* 2013; Hennig *et al.* 2014) and
 129 published geodetic/geophysical data. Digital ele-
 130 vation models (DEMs) based on Shuttle Radar
 131 Topography Mission (SRTM) 3 arc second/90 m
 132 resolution and ASTER 30 m resolution data were
 133 processed using ERMapper software. These data
 134 were also used to extract topographic contours and
 135 drainage networks using ArcGIS. Landsat TM and
 136 ETM+ scenes composed of the 30 m resolution
 137 bands 432, 451, 531 and 742 (red green blue com-
 138 binations) were used and, where appropriate, sharp-
 139 ened with ETM+ band 8 panchromatic 15 m
 140 resolution data. Where available, high resolution
 141 visible spectrum imagery from Google Earth and
 142 Bing Maps (compiled from a variety of sources)
 143 and the ESRI World Imagery compilation, which
 144 includes 2.5 m SPOT and <1 m DigitalGlobe
 145 imagery, was also interpreted. ESRI World Imagery
 146 is compiled from Esri, DigitalGlobe, GeoEye,
 147 Earthstar Geographics, CNES/Airbus DS, USDA,
 148 USGS, AEX, Getmapping, Aerogrid, IGN, IGP,
 149 swisstopo, and the GIS User Community.

150 Multibeam bathymetric data (kindly provided by
 151 TGS) from parts of the offshore Sorong Fault Zone
 152 and Cenderawasih Bay were interpreted in the
 153 same way as the DEMs. The multibeam data were
 154 acquired using a Kongsberg Simrad EM120 Multi-
 155 beam Echo Sounder using 191 beams at equidistant
 156 spacing. Positioning control used a C Nav Starfire
 157 DGPS. During processing, positioning, tidal and
 158 calibration corrections were applied, random noise
 159 and artefacts were removed, and a terrain model
 160 using a 25 m bin size was gridded and exported to
 161 ESRI format. The multibeam data were further pro-
 162 cessed in ERMapper to remove voids.

163 All data were integrated in ArcGIS together
 164 with previously published georeferenced maps. The
 165 CMT focal mechanisms were from the International
 166 Seismological Centre catalogue, plotted using Mir-
 167 one software. We considered only earthquakes with
 168 a focal depth ≤ 35 km to avoid contamination from
 169 deeper structures that have little surface expression.

171 *Geomorphic indices*

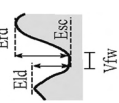
172 Geomorphic indices are a valuable tool to rapidly
 173 evaluate the relative tectonic rate of surface faults
 174

on a reconnaissance scale (Keller 1986). We utilized
 mountain front sinuosity (S_{mf}) and the valley floor
 width to valley height index (V_f) following the
 method of Bull & McFadden (1977) and Bull
 (1978). The key parameters are summarized in
 Table 1. An excellent description of the method and
 its uncertainties is given in Bull (2007). Although
 conventionally applied to normal faults, geomorphic
 indices can be used in any setting where there is
 vertical motion, including regions of transpression
 and transtension. However, they are of little value
 in regions of pure strike slip and were not applied
 to pure strike slip segments in this study.

Mountain front sinuosity is the ratio $S_{mf} = L_{mf}/L_s$,
 where L_{mf} is the straight line length of the moun-
 tain front and L_s is the true, or sinuous, length along
 the mountain front following topographic contours
 at the contact between alluvial fans and the solid
 geology of the range front (Table 1). This method
 assumes that a fault bounded range front will
 become more sinuous over time in the absence of
 tectonic activity (e.g. Bull & McFadden 1977;
 Rockwell *et al.* 1984). The method is well estab-
 lished for Quaternary fault evaluation in regions of
 extension (e.g. Ramírez Herrera 1998), contraction
 and strike slip (e.g. Dehbozorgi *et al.* 2010), trans-
 tension (e.g. Silva *et al.* 2003; Yıldırım 2014), com-
 bined extension and contraction (Wells *et al.* 1988)
 and differential uplift (e.g. Sohoni *et al.* 1999). Crit-
 ical uncertainties include the interpreter's definition
 of the sinuous mountain front, which is partly
 dependent on the quality of the input satellite data,
 and the recognition of discrete mountain front seg-
 ments. Climate also has an impact on S_{mf} indepen-
 dent of the tectonic rate. In a humid environment
 like eastern Indonesia it is expected that erosion
 and hence S_{mf} will be higher than in an arid region
 for a given tectonic rate.

The valley floor width to valley height index, V_f ,
 measures the ratio between the valley floor width
 and the valley depth: $V_f = 2V_{fw}/(E_{ld} - E_{sc})$
 ($E_{rd} - E_{sc}$), where V_{fw} is the valley floor width,
 E_{ld} and E_{rd} are the topographic elevations of the
 left and right valley watersheds and E_{sc} is the eleva-
 tion of the valley floor (Table 1). The method
 assumes that recently excavated river channels
 (i.e. those into which a river has incised as a result
 of recent uplift) are V shaped and become more U
 shaped over time (e.g. Bull & McFadden 1977;
 Rockwell *et al.* 1984). Like S_{mf} , V_f has been applied
 in a wide range of tectonic settings (e.g. Wells *et al.*
 1988; Ramírez Herrera 1998; Yıldırım 2014). V_f is
 sensitive to a number of variables apart from tec-
 tonic rate, so we standardized as much as possible
 by: measuring V_f in all cases 1 km upstream from
 the mountain front; measuring the valley width as
 the width of the river channel visible on the highest
 resolution satellite imagery available or the width

Table 1. Summary of geomorphic indices used in mountain front analysis, modified after Wells et al. (1988)

Parameter	Definition	Derivation*	Measurement†	Purpose	Potential difficulties
S_{mf}	Sinuosity of topographic mountain fronts	L_{mf}/L_s		Defines the degree of topographic modification of mountain front from the position of possible controlling structures	Defining actual topographic junction Defining discrete mountain front segments
V_f	Valley floor width to valley height index	$2V_{fw}/[(E_{fd} - E_{sc}) - (E_{rd} - E_{sc})]$		Defines the ratio of the valley floor width to the mean height of two adjacent divides, measured at given locations along a stream channel within the range block	Resolution of satellite imagery in defining V_{fw} and divide elevations Effects of changes in lithology Need to minimize variations in stream size (length and area)

* L_{mf} , straight line length of mountain front; L_s , sinuous length along mountain front; V_{fw} , valley floor width; E_{fd} and E_{rd} , topographic elevations of left and right valley watersheds; E_{sc} , elevation of valley floor.
 †Schematic map view for S_{mf} , schematic cross-section view for V_f .
 Both indices after Bull & McFadden (1977) and Bull (1978).

175
176
177
178
179
180
181
182
183
184
185
186
187
188
189
190
191
192
193
194
195
196
197
198
199
200
201
202
203
204
205
206
207
208
209
210
211
212
213
214
215
216
217
218
219
220
221
222
223
224
225
226
227
228
229
230
231
232

of the valley to the point where the floor rose 10 m above the minimum elevation in individual transects; measuring only streams that reached the mountain front without joining a higher order stream; and measuring only streams oriented $\geq 70^\circ$ from the mountain front. Noise in the V_f signal was reduced by averaging between three and ten separate V_f measurements along each fault segment.

High quality topographic maps are not available for eastern Indonesia, so both S_{mf} and V_f were measured in ArcGIS software using a combination of 30 m ASTER GDEM satellite data and the ESRI World Imagery compilation. This allowed the finest possible resolution of L_s and V_{fw} , which are crucial, but potentially subjective, parameters. High quality satellite imagery may be better for such measurements than conventional maps (Bull 2007).

Schemes for the classification of relative tectonic activity based on a combination of geomorphic indices have been proposed (e.g. Bull & McFadden 1977; Bull 1978, 2007). Here we applied a modified scheme from McCalpin (2009). This uses S_{mf} and V_f to classify relative tectonic activity as follows: $S_{mf} < 1.1$, mean $V_f < 0.15$, maximal activity; $S_{mf} 1.1 - 1.3$, mean $V_f 0.15$, rapid activity; $S_{mf} 1.6 - 2.3$, mean $V_f 1.5$, slow activity; $S_{mf} \geq 2.5$, $V_f 1.7 - 2.5$, minimal activity; and $S_{mf} 2.6 - 4.0$, mean $V_f 7.4$, inactive. This classification allows a comparison between faults with different relative tectonic rates and corresponding geomorphic expression. Because the indices record undated Quaternary fault activity expressed by geomorphology, the classes also correspond to a Quaternary tectonic rate and not necessarily to a modern tectonic rate comparable with geodetic measurements. It should also be remembered that the schemes were developed using faults in arid areas of the western USA where tectonic landforms are preserved for longer than in humid areas (e.g. Bull 1978), meaning faults in the tropics will generally be classified as tectonically 'slower' than equivalent faults at higher latitudes.

We analysed both S_{mf} and V_f for a total of 111 segments from 24 fault systems across the study area (Fig. 2a-r, Table 2) and found a good correlation between S_{mf} and V_f (Fig. 3), supporting the reliability of each method. A previous study of geomorphic indices along a segment of the Palu-Koro Fault (Vecchiotti 2008) obtained similar results to those presented here. However, we used these indices only as a simple quantitative means to support other evidence for Quaternary fault activity and did not classify faults on the basis of these data alone.

Sulawesi

Sulawesi lies at the triple junction between the Australian, Eurasian and Philippine Sea plates (e.g.

Hamilton 1979; Silver *et al.* 1983a, b; Hall 1996). North of Sulawesi, the Celebes Sea is being subducted beneath Sulawesi (e.g. Hamilton 1979; Silver *et al.* 1983a). Convergence across the subduction margin increases from $20 \pm 4 \text{ mm a}^{-1}$ in the east to $54 \pm 10 \text{ mm a}^{-1}$ in the west, associated with a clockwise rotation of about 4° Ma^{-1} about a pole close to Manado (Walpersdorf *et al.* 1998; Rangin *et al.* 1999; Stevens *et al.* 1999; Beaudouin *et al.* 2003). Immediately east of Sulawesi's north 'arm', convergence between the Philippine Sea plate and Sundaland is partly accommodated by the Molucca Sea double subduction and the overlying Sangihe and Halmahera thrusts (e.g. Rangin *et al.* 1999; Hall 2002; Beaudouin *et al.* 2003).

Despite its setting within a collisional orogen, Sulawesi is subject to widespread and young extension. Tomini Bay encloses a deep, enigmatic basin containing up to 10 km of late Cenozoic sediments (Jablonski *et al.* 2007; Polbud *et al.* 2012). Medium to high K Pliocene to modern volcanism in the Togian Islands within the bay results from Pliocene to Recent extension (Cottam *et al.* 2011) and onshore metamorphic core complexes are in the process of being exhumed by processes related to crustal thinning (Kavaleris *et al.* 1992; van Leeuwen *et al.* 2007; Spencer 2011).

Active strike slip faults (e.g. Bellier *et al.* 2001), with left lateral slip rates of up to 39 mm a^{-1} (Socquet *et al.* 2006), characterize much of Sulawesi's onshore Quaternary deformation. Often considered to result from NW directed collision between the Sula platform and Sulawesi (e.g. Silver *et al.* 1983b; Simandjuntak 1986), modern reconstructions emphasize the process of subduction hinge rollback related to the substantial amounts of oceanic crust that have been, and continue to be, subducted around Sulawesi (e.g. Spakman & Hall 2010; Hall 2012). The occurrence of Late Miocene to apparently modern north-south directed continental extension (e.g. Spencer 2011) in a broad region adjacent to the south directed Celebes Sea subduction means that a rollback mechanism must be considered.

Palu-Koro Fault

The Palu-Koro Fault (Fig. 4) is the most prominent active fault of Sulawesi and is of particular importance because it is straddled by Palu city (population 340 000). The Palu-Koro Fault appears to pass from the SW corner of the Celebes Sea to a diffuse termination onshore at the northern end of Bone Bay, a distance of 500 km, of which 220 km is onshore.

The fault's tectonic role is disputed: sinistral shear along a joint Palu-Koro-Matano Fault system has been thought to accommodate clockwise rotation and the northwards movement of a rigid

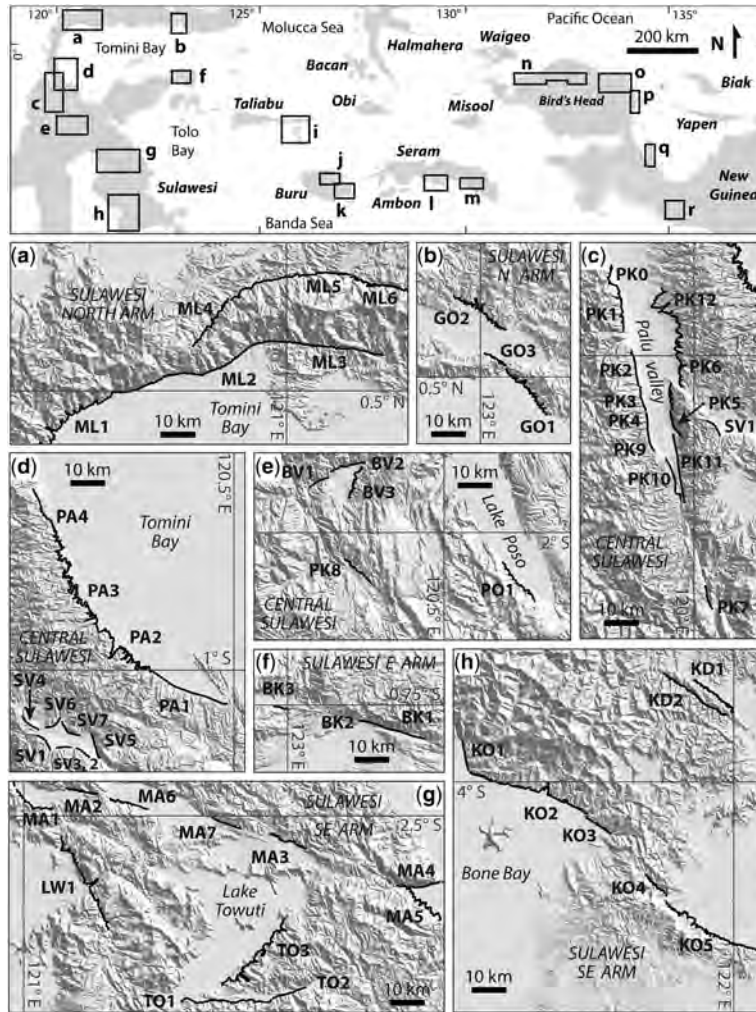


Fig. 2. Maps showing fault segments analysed for geomorphic indices. Index map at top. Bold lines are the sinuous mountain front trace (L_s) used in mountain front sinuosity calculations. Base map is a 90 m SRTM digital elevation model. All maps (a – r) drawn to the same scale. Fault segment codes correspond to the codes used in Table 2.

eastern Sulawesi block driven by collision of the Banggai Sula block in the east (e.g. Hamilton 1979; Silver *et al.* 1983b; Beaudouin *et al.* 2003). However, it is significant that the Palu Koro Fault and the North Sulawesi Trench form the western and northern limits, respectively, of a region of late Cenozoic extreme continental extension that includes deep sedimentary basins (e.g. Jablonski *et al.* 2007; Pholbud *et al.* 2012), exhumation of the mid to lower crust in settings similar to meta morphic core complexes (e.g. van Leeuwen *et al.* 2007; Watkinson 2011), exhumed low angle normal faults (Spencer 2011) and decompression related mantle melts (Cottam *et al.* 2011). These features

can be associated with the overriding plate above a retreating subduction hinge, particularly in the early stages of continent continent collision (Roy den 1993). The orientation and kinematics of the Palu Koro Fault are compatible with an interpretation that it is passively bounding a region of lithospheric extension driven by northwards rollback in the Celebes Sea, although it is unclear whether there is a hard linkage between the fault and the trench.

It is not disputed that the fault is an active zone of high strain. Geodetic measurements suggest a 39 mm a^{-1} sinistral slip rate together with 11 mm a^{-1} of extension (Socquet *et al.* 2006),

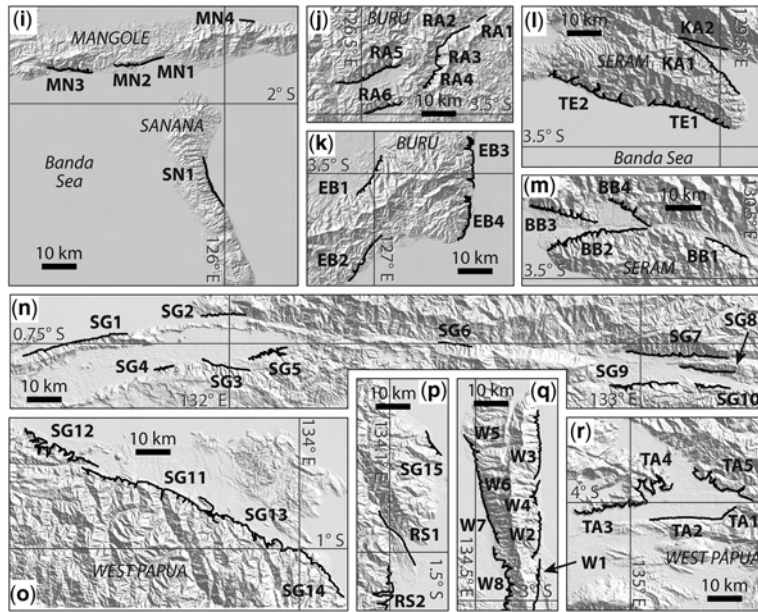


Fig. 2. Continued.

consistent with a $35 \pm 8 \text{ mm a}^{-1}$ strike slip rate determined from displaced alluvial fans 11 000 \pm 2300 years old (Bellier *et al.* 2001).

There is palaeoseismic evidence for three M_w 6.8–8.0 earthquakes during the last 2000 years, suggesting a recurrence interval of about 700 years (Beaudouin 1998; Bellier *et al.* 1998). However, even allowing for 10 m slip for each M_w 6.8–8.0 event, the resultant 30 m total displacement in 2000 years is less than the 54–86 m predicted from Holocene slip rates (Bellier *et al.* 2001). Although it has been proposed by these earlier researchers that the deficit is accommodated by aseismic creep, it is equally possible that large, undetected earthquakes occurred on unobserved fault strands and that the total recurrence interval for all the Palu Koro Fault strands is much less than 700 years. Socquet *et al.* (2006) proposed four parallel strands across a zone *c.* 50 km wide, locked at depths between 0 and 5 km.

Records of historical seismicity in Sulawesi are poor. Damaging earthquakes occurred along the Palu Koro Fault in 1905, 1907, 1909, 1927, 1934, 1968 (*c.* M_s 6.7), 1985 and 1993 (*c.* M_s 5.7) (Katili 1970; Hamilton 1979; Beaudouin 1998), but little detail is known. Large earthquakes close to the fault zone occurred in 1996 (M_w 7.7) and 1998 (M_w 6.6 and 6.0); the former caused a 2–4 m high tsunami in the Toli Toli region (Pelinovsky *et al.* 1997). However, these earthquakes originated offshore, did not clearly lie on the active Palu Koro

Fault and none had a focal mechanism indicating left lateral slip along the Palu Koro trend.

The Palu Koro Fault has the clearest geomorphological expression of any eastern Indonesian fault. It occupies a steep sided, narrow valley along much of its path through central Sulawesi, before branching into the Palu valley, which is up to 15 km wide (Fig. 5a). Two prominent scarps bound the valley and form the base of mountains that rise to >2.3 km elevation. The western scarp is highly linear, particularly the remarkable central segments *c.* 15 km south of Palu city. Mountain front sinuosity values are consistently low at 1.08–1.09, indicating maximal tectonic activity, increasing to 1.28–1.56 at the northern and southern ends of the valley, indicating rapid to moderate tectonic activity (Fig. 5a). The valley floor curvature is generally correspondingly tight, with an average V_f of 0.24 along the western scarp.

Features such as prominent triangular facets, hanging valleys and steep sided, deeply incised streams are also focused along the central western basin bounding segment (Fig. 5b). These landforms support dominantly rapid normal faulting along the basin margin faults. Wine glass canyons, in particular, indicate that the tectonic subsidence/uplift rate is faster than erosion. Lateral offset of the alluvial fans and rivers across the mountain front have been observed, notably in the northern and southern segments of the fault system (e.g. Hamilton 1979; Bellier *et al.* 2006).

Table 2. Summary of measurements of mountain front sinuosity and average valley width to height ratio for analysed fault segments

Fault	Segment	L_{mf}^*	$L_s^†$	S_{mf}^{\ddagger}	Ave. V_f^{\S}	Figure 2	Fault	Segment	L_{mf}^*	$L_s^†$	S_{mf}^{\ddagger}	Ave. V_f^{\S}	Figure 2
Malino boundary	ML1	45.16	27.17	1.66	1.01	a	Kolaka	KO1	8.79	8.38	1.05	1.25	h
Malino boundary	ML2	52.00	49.60	1.05	0.33	a	Kolaka	KO2	52.12	33.80	1.54	1.12	h
Malino boundary	ML3	28.79	27.53	1.05	0.64	a	Kolaka	KO3	10.07	8.24	1.22	1.68	h
Malino boundary	ML4	22.99	16.08	1.43	0.29	a	Kolaka	KO4	10.25	7.91	1.30	0.23	h
Malino boundary	ML5	38.22	33.86	1.13	0.22	a	Kolaka	KO5	49.44	30.21	1.64	1.19	h
Malino boundary	ML6	27.41	17.27	1.59	0.29	a		Average			1.35	1.09	
Gorontalo	GO1	33.24	16.37	2.03	0.88	b	Mangole	MN1	7.07	6.33	1.12	0.49	i
Gorontalo	GO2	39.29	16.64	2.36	1.27	b	Mangole	MN2	9.64	6.60	1.46	0.49	i
Gorontalo	GO3	12.03	6.58	1.83	1.69	b	Mangole	MN3	18.96	12.08	1.57	0.55	i
	Average			2.07	1.28	b	Sanana	MN4	4.56	3.86	1.18	N/A	i
Palu-Koro	PK0	16.94	10.99	1.54	0.31	c		SN1	2.45	1.93	1.27	0.44	i
Palu-Koro	PK1	8.94	6.60	1.35	0.22	c	Rana	Average			1.32	0.49	
Palu-Koro	PK2	10.48	9.64	1.09	0.29	c	Rana	RA1	2.86	2.83	1.01	0.35	j
Palu-Koro	PK3	7.24	6.69	1.08	0.21	c	Rana	RA2	3.68	3.12	1.18	0.23	j
Palu-Koro	PK4	4.33	3.99	1.09	0.19	c	Rana	RA3	8.19	7.73	1.06	0.18	j
Palu-Koro	PK5	9.43	7.90	1.19	0.99	c	Rana	RA4	20.19	10.31	1.96	1.53	j
Palu-Koro	PK6	11.02	6.91	1.59	0.35	c	Rana	RA5	24.35	18.31	1.33	0.28	j
Palu-Koro	PK7	7.15	6.44	1.11	0.56	c	Rana	RA6	15.49	10.40	1.49	0.68	j
Palu-Koro	PK8	10.78	9.61	1.12	0.89	e	East Buru	EB1	18.09	12.56	1.44	0.47	k
Palu-Koro	PK9	9.72	6.22	1.56	0.20	c	East Buru	EB2	18.61	15.08	1.23	0.50	k
Palu-Koro	PK10	16.34	12.80	1.28	1.10	c	East Buru	EB3	26.93	12.53	2.15	1.13	k
Palu-Koro	PK11	27.15	19.02	1.43	0.32	c	East Buru	EB4	25.16	12.62	1.99	0.75	k
Palu-Koro	PK12	64.23	27.88	2.30	0.80	c	Southern Seram	TE1	42.32	23.05	1.84	1.88	l
	Average			1.36	0.47	c	Southern Seram	TE2	49.68	23.89	2.08	1.36	l
Parigi boundary	PA1	69.67	21.44	3.25	0.90	d	Kawa	Average			1.96	1.62	
Parigi boundary	PA2	72.43	26.17	2.77	0.78	d	Kawa	KA1	27.55	20.75	1.33	0.28	l
Parigi boundary	PA3	62.33	19.92	3.13	1.45	d	Kawa	KA2	15.16	13.76	1.10	0.26	l
Parigi boundary	PA4	17.86	13.48	1.32	0.50	d		Average			1.21	0.27	
Sapu valley	SV1	6.17	5.67	1.09	0.40	d	Bobol	BB1	14.59	11.61	1.26	1.57	m
Sapu valley	SV2	3.64	3.38	1.08	N/A	d	Bobol	BB2	51.83	26.37	1.97	2.60	m
Sapu valley	SV3	4.99	3.90	1.28	N/A	d	Bobol	BB3	35.56	17.84	1.99	1.44	m
Sapu valley	SV4	6.30	5.60	1.13	N/A	d	Bobol	BB4	23.05	12.73	1.81	1.04	m
Sapu valley	SV5	6.89	4.74	1.45	N/A	d		Average			1.76	1.66	
Sapu valley	SV6	4.67	3.78	1.24	N/A	d	Sorong	SG1	33.89	28.77	1.18	1.15	n
Sapu valley	SV7	5.27	3.84	1.37	N/A	d	Sorong	SG2	13.90	11.94	1.16	1.54	n
	Average			1.23	0.40	d	Sorong	SG3	15.11	13.16	1.15	0.48	n
							Sorong	SG4	8.54	5.35	1.60	0.59	n

407
408
409
410
411
412
413
414
415
416
417
418
419
420
421
422
423
424
425
426
427
428
429
430
431
432
433
434
435
436
437
438
439
440
441
442
443
444
445
446
447
448
449
450
451
452
453
454
455
456
457
458
459
460
461
462
463
464

QUATERNARY FAULT ACTIVITY IN EASTERN INDONESIA

465
466
467
468
469
470
471
472
473
474
475
476
477
478
479
480
481
482
483
484
485
486
487
488
489
490
491
492
493
494
495
496
497
498
499
500
501
502
503
504
505
506
507
508
509
510
511
512
513
514
515
516
517
518
519
520
521
522

Bada valley	BV1	5.97	5.73	1.04	0.57	e	Sorong	SG5	29.39	10.53	2.79	4.90	n
Bada valley	BV2	10.09	9.47	1.07	0.36	e	Sorong	SG6	10.19	8.94	1.14	0.27	n
Bada valley	BV3	13.27	9.30	1.43	0.73	e	Sorong	SG7	36.50	27.47	1.33	0.45	n
	Average		1.18		0.55		Sorong	SG8	17.73	14.83	1.20	0.44	n
Poso area	PO1	18.15	13.74	1.32	0.29	e	Sorong	SG9	31.90	18.34	1.74	1.33	n
	Average		1.32		0.29		Sorong	SG10	15.44	9.57	1.61	0.40	n
Balantak	BK1	13.02	11.80	1.10	0.25	f	Sorong	SG11	65.53	40.33	1.62	0.42	o
Balantak	BK2	6.85	6.59	1.04	0.47	f	Sorong	SG12	62.92	22.04	2.85	5.10	o
Balantak	BK3	5.16	4.24	1.22	N/A	f	Sorong	SG13	54.48	30.12	1.81	8.68	o
	Average		1.12		0.36		Sorong	SG14	22.17	17.39	1.27	0.32	o
Matano	MA1	15.06	11.78	1.28	1.12	g	Sorong	SG15	11.44	7.61	1.50	0.49	p
Matano	MA2	9.21	8.66	1.06	0.25	g		Average		1.60		1.77	
Matano	MA3	12.54	10.57	1.19	0.45	g	Ransiki	RS1	18.83	17.71	1.06	N/A	p
Matano	MA4	12.56	11.63	1.08	0.23	g	Ransiki	RS2	31.31	11.87	2.64	N/A	p
Matano	MA5	23.51	12.35	1.90	0.79	g		Average		1.85		N/A	
Matano	MA6	12.34	10.52	1.17	0.72	g	Wandaman boundary	WM1	17.22	13.76	1.25	N/A	q
Matano	MA7	8.46	8.31	1.02	0.84	g	Wandaman boundary	WM2	15.55	12.08	1.29	N/A	q
	Average		1.24		0.63		Wandaman boundary	WM3	23.73	18.57	1.28	N/A	q
Kendari	KD1	24.61	14.03	1.75	0.52	h	Wandaman boundary	WM4	11.58	6.74	1.72	N/A	q
Kendari	KD2	24.62	20.42	1.21	0.58	h	Wandaman boundary	WM5	19.75	13.83	1.43	N/A	q
	Average		1.48		0.55		Wandaman boundary	WM6	9.84	9.33	1.05	N/A	q
Lawanopo	LW1	43.13	28.29	1.52	0.83	g	Wandaman boundary	WM7	9.99	7.80	1.28	N/A	q
	Average		1.52		0.83		Wandaman boundary	WM8	45.67	19.61	2.33	N/A	q
Towuti bounding	TO1	27.98	24.39	1.15	0.41	g		Average		1.45		N/A	
Towuti bounding	TO2	9.58	9.30	1.03	0.56	g	Tarera-Aiduna	TA1	6.11	5.05	1.21	N/A	r
Towuti bounding	TO3	51.16	25.10	2.04	1.22	g	Tarera-Aiduna	TA2	20.74	19.19	1.08	N/A	r
	Average		1.41		0.73		Tarera-Aiduna	TA3	32.26	19.75	1.63	N/A	r
							Tarera-Aiduna	TA4	38.83	8.48	4.58	N/A	r
							Tarera-Aiduna	TA5	35.31	18.46	1.91	N/A	r
								Average			2.08	N/A	

*Straight line length of mountain front.

†Sinuous length of mountain front.

‡Mountain front sinuosity ($S_{mf} = L_{mf}/L_s$).

§Average valley floor width to valley depth ratio ($V_f = 2V_{fw}/(E_{fd} - E_{sc}) - (E_{fd} - E_{sc})$), where V_{fw} is the valley floor width, E_{fd} and E_{sc} are the topographic elevations of the left and right valley watersheds and E_{sc} is the elevation of the valley floor).

|| Location of sinuosity segment on Figure 2.

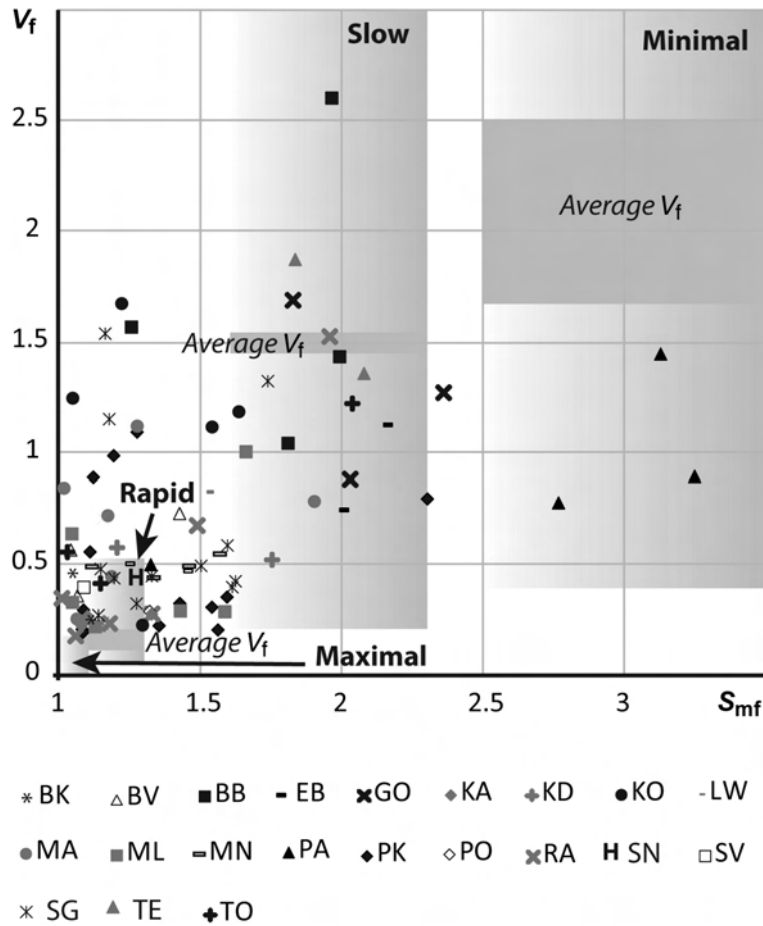


Fig. 3. Graph of mountain front sinuosity (S_{mf}) v. valley floor width to valley height index (V_f) for studied faults. Grey boxes indicate tectonic activity rates, after McCalpin (2009), with average V_f marked by the darker grey bar. BB, Bobol Fault; BK, Balantak Fault; BV, Bada valley faults; EB, East Buru faults; GO, Gorontalo Fault; KA, Kawa Fault; KD, Kendari faults; KO, Kolaka Fault; LW, Lawanopo Fault; MA, Matano Fault; ML, Malino boundary faults; MN, Mangole faults; PA, Parigi faults; PK, Palu Koro Fault; PO, Poso faults; RA, Rana Fault; SG, Sorong Fault; SN, Sanana faults; SV, Sapu valley faults; TE, Southern Seram faults; TO, Towuti faults.

A 5° releasing bend/step over is required to link the southern segments of the Palu Koro Fault, where it emerges from its narrow valley at Pakuli, with the northern segments NW of Palu city. In analogue models and other non linear strike slip faults, such releasing geometries are often associated with well defined oblique normal sidewall faults and a cross basin fault system with a more subtle surface expression that accommodates most of the strike slip strain (e.g. Mann *et al.* 1995; Mann 2007; Wu *et al.* 2009) (Fig. 6a inset).

Analysis of Palu River channels since 2003 from satellite imagery and the pattern of older filled oxbow lakes on the valley floor indicates that long reaches of the river rarely deviate from a linear

path directly along strike from the strike slip fault where it enters the Palu valley in the south (Fig. 6a, b). Many meanders have a square aspect with linear longitudinal segments parallel to the projected fault (Fig. 6c). In the south of the valley a linear braided reach is similarly parallel to the projected fault; individual braid channels are anomalously linear (Fig. 6d). Strands of the Palu Koro Fault cutting an alluvial fan and offsetting its incised drainage directly along strike to the south confirm that the river is structurally controlled. It is more reasonable to project this southern fault strand directly north across the basin than it is to consider strike slip strain transferring immediately to the western sidewall fault between Pakuli and Bolongga, particularly as

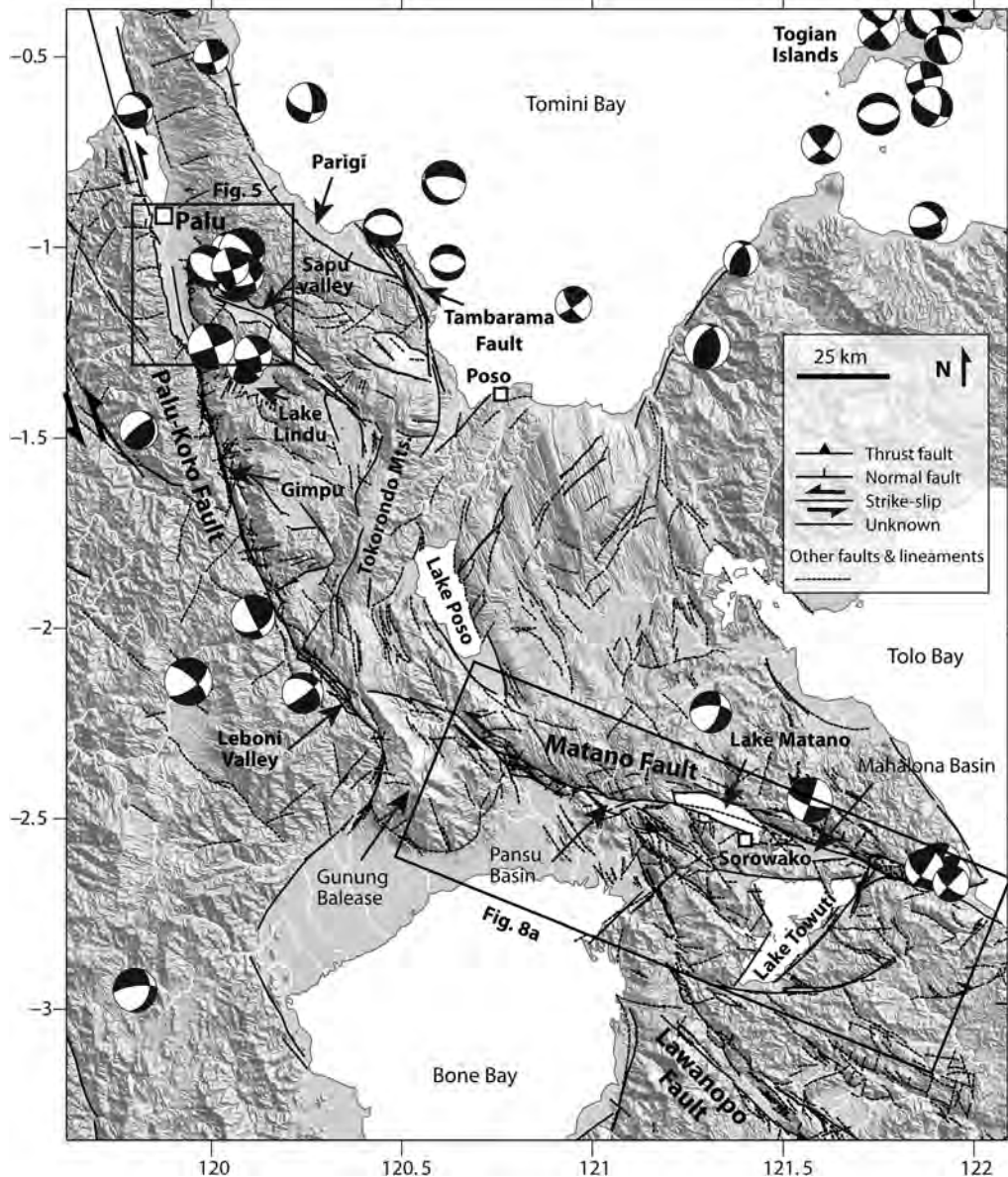


Fig. 4. Central Sulawesi overview digital elevation model (SRTM), CMT catalogue earthquakes <35 km depth and structures that show geomorphic evidence of Quaternary tectonic activity. Rivers marked in white. Illumination from NE. Location shown in Figure 1.

geomorphic indices in that region indicate a relatively low tectonic rate (Fig. 5a).

Thus we propose that much of the Palu Koro Fault strike slip strain through the Palu valley is not accommodated on the prominent sidewall faults, but on a cross basin fault system that is obscured by fluvial deposits during interseismic periods (as it is

now) (Figs 5a & 6a). The sidewall faults are largely an extensional partition, explaining the lateral slip deficit across them, noted by Bellier *et al.* (2001). Confinement of the Palu River meander belts within the strike slip cross basin fault system may be due to the development of a subtle graben, or to changes in permeability, cementation or compaction in the

639
640
641
642
643
644
645
646
647
648
649
650
651
652
653
654
655
656
657
658
659
660
661
662
663
664
665
666
667
668
669
670
671
672
673
674
675
676
677
678
679
680
681
682
683
684
685
686
687
688
689
690
691
692
693
694
695
696

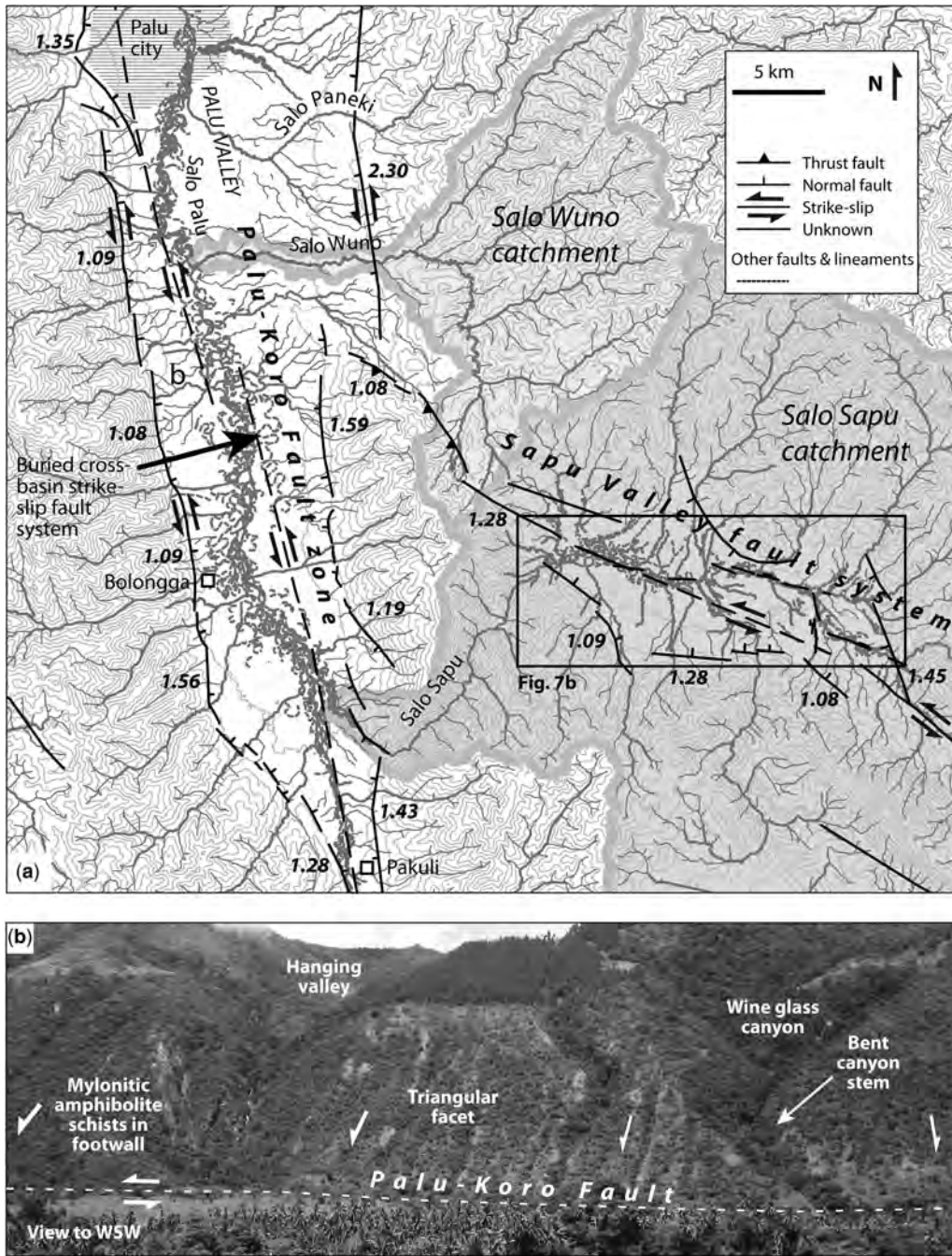


Fig. 5. (a) The Palu and Sapu valleys showing structures that with geomorphic evidence of Quaternary tectonic activity, plus topography and drainage. Mountain front sinuosity values in bold italic text. For location, see Figure 4. Major drainage basins for Salo Sapu and Salo Wuno are marked, separated by uplift at the western end of the Sapu valley fault system. (b) View of the Palu-Koro Fault scarp from the Palu valley, showing geomorphic evidence of Quaternary tectonic activity.

697
698
699
700
701
702
703
704
705
706
707
708
709
710
711
712
713
714
715
716
717
718
719
720
721
722
723
724
725
726
727
728
729
730
731
732
733
734
735
736
737
738
739
740
741
742
743
744
745
746
747
748
749
750
751
752
753
754

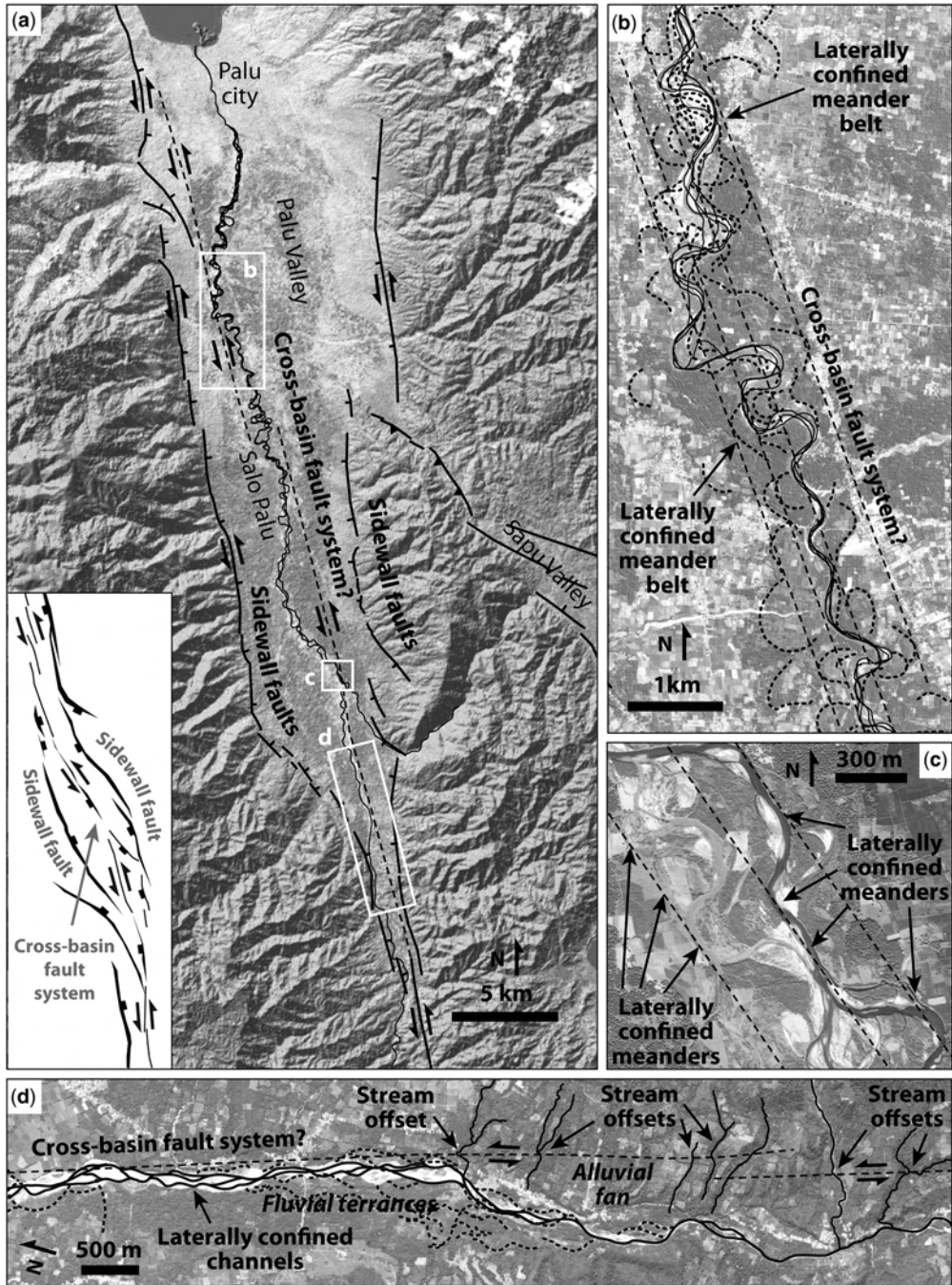
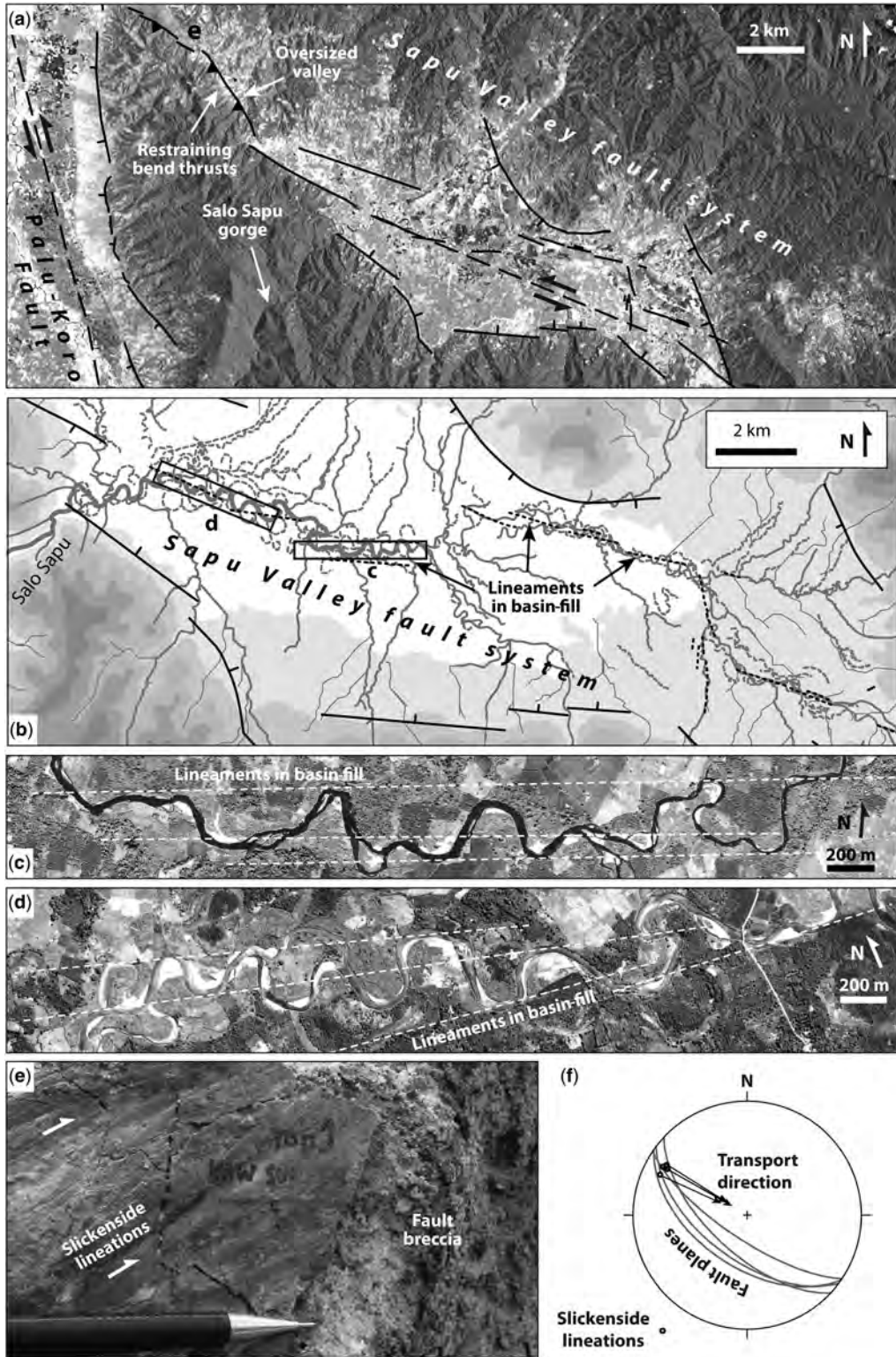


Fig. 6. Evidence of a cross basin fault system within the Palu valley Quaternary fill. (a) Overview ASTER digital elevation model draped with ESRI imagery layer. Illumination from NW. Palu River channels traced from six separate images from 2003 to 2015. Inset shows fault pattern developed in an analogue model of a releasing bend, modified after Wu *et al.* (2009), reflected and rotated to mimic the Palu valley. Sidewall faults and cross basin fault system are highlighted in the model and on the satellite imagery. (b, c) Laterally confined meander belts, interpreted as representing minor subsidence within the cross basin fault system. (d) Laterally confined river channels directly along strike from a Palu Koro Fault strand seen to offset alluvial fans in the south of the valley. (c, d, e) show ESRI imagery.

755
756
757
758
759
760
761
762
763
764
765
766
767
768
769
770
771
772
773
774
775
776
777
778
779
780
781
782
783
784
785
786
787
788
789
790
791
792
793
794
795
796
797
798
799
800
801
802
803
804
805
806
807
808
809
810
811
812



813 Quaternary valley fill resulting from penetration by
814 strike slip strands.

815 The valley's eastern sidewall fault is generally
816 much more segmented and strongly eroded than in
817 the west, with gentle slopes and irregular mountain
818 fronts (Fig. 6a). South of the intersection with the
819 Sapu valley fault system, S_{mf} values are 1.19–1.59
820 and V_f averages of 0.55 indicate rapid to moderate
821 tectonic activity. North of the Sapu valley intersec-
822 tion, S_{mf} is 2.30 and the average V_f is 0.80, indicat-
823 ing slow tectonic activity.

824 Further south along the Palu–Koro Fault, the
825 Gimpu basin exists at a small releasing step over
826 the Leboni basin occupies a releasing bend
827 near the southern termination of the fault (Fig. 4).
828 The Palu–Koro Fault bounding these flat topped
829 Quaternary basins has S_{mf} values of 1.11 and 1.12,
830 respectively, and similarly low V_f values of 0.56
831 and 0.89, indicating rapid to moderate tectonic
832 activity.

833 *Sapu valley fault system*

834 A complex NW–SE trending, 75 km long fault sys-
835 tem cuts across crystalline basement between Palu
836 valley and the Tokorondo Mountains in the east
837 (Fig. 4). The fault system is dominated by a double
838 bend: a releasing bend forming the intermontane
839 Sapu valley (c. 600 m elevation) and a restraining
840 bend associated with uplift at the head of the valley
841 (Fig. 5a). Both bends are consistent with an overall
842 left lateral shear sense for the fault system. Anec-
843 dotal reports from residents of the valley (various,
844 pers. comm. 2009) suggest that earthquakes are fre-
845 quent and well known, although there is little instru-
846 mental seismicity and no record of historical
847 earthquakes.

848 Sapu valley is an irregular rhomboidal basin
849 bounded by normal faults trending NNE–SSE and
850 east–west (Fig. 7a). Many of the faults are arcuate,
851 convex into the basin. Their range front slopes are
852 generally gentle, but S_{mf} values of 1.09–1.45 and
853 an average V_f of 0.40 suggest rapid to moderate tec-
854 tonic activity (Fig. 7b). A conspicuous feature of the
855 basin floor is the strong confinement of river chan-
856 nels to narrow linear meander belts (Fig. 7b), as dis-
857 cussed earlier for the Palu River. Both modern and
858 abandoned channels have linear meander belt mar-
859 gins and square longitudinal sections parallel to

the projected trace of the fault system through the
valley, implying fault penetration through the Qua-
ternary basin fill (Fig. 7c, d). In the same way as for
the Palu valley, this evidence supports a cross basin
fault system that accommodates most of the strike
slip strain, whereas the prominent sidewall faults
are dominantly extensional structures. The cross
basin fault system is buried by fluvial sediments,
but co-seismic subsidence, or changes in permeabil-
ity, cementation or compaction caused by periodic
surface rupture through the Quaternary basin fill
continue to influence the meander patterns.

At the head of the valley the entire fault system
curves to a more NNW–SSE trend—a restraining
geometry under sinistral shear. A broad, oversized
valley in the west is presently at 700 m elevation
(Fig. 7a), i.e. 100 m above the modern Sapu valley
floor. Exhumed brittle SW dipping reverse sinistral
faults in mica schists along the uplifted valley
support long lived uplift at this restraining bend
(Fig. 7e, f). At the foot of the westernmost obli-
que reverse fault, S_{mf} is 1.08, suggesting maximal
tectonic activity (Fig. 5a).

Drainage networks extracted from SRTM data
show that there is presently a drainage divide sepa-
rating the Salo–Wuno and Salo–Sapu catchment
basins at the position of the thrust related uplift and
oversized valley (Fig. 5a). Water presently exits
Sapu valley via a narrow, steep sided gorge (Fig.
7a). The extreme steepness and geomorphic immat-
urity of that gorge suggests that it has recently cap-
tured the Sapu valley drainage, perhaps in response
to tectonic uplift of its former well established route
to the NW via Salo–Wuno. It is likely that the Sapu
valley was internally drained for some time after
uplift in the NW and may have contained an inter-
montane lake similar to Lake Lindu to the south
(Fig. 4), explaining the flat base of the Sapu valley.

Four lines of evidence suggest the Sapu valley
fault system has been active during the Quaternary:
(1) control of the modern river meander belts by a
cross basin fault system that traverses the Quater-
nary basin fill; (2) youthful geomorphic expression
of the Salo–Sapu gorge where it has recently cap-
tured the Salo–Sapu drainage in response to tectonic
uplift in the NW; (3) rapid to moderate tectonic
activity along the transtensional segment sidewall
faults, indicated by geomorphic indices; and (4)
maximal tectonic activity along the transpressional

863
864 **Fig. 7.** Details of the Sapu valley fault system. (a) ESRI imagery of the Sapu and central Palu valleys showing
865 major structural and geomorphic features, particularly the releasing–restraining double bend and re-routing of axial
866 drainage from the NW valley to the Salo–Sapu gorge. (b) Detail of the Sapu valley showing drainage and
867 highlighting fault control of the axial river. Location shown on Figure 5a. (c, d) Laterally confined meander belts
868 and lineaments, interpreted as representing minor subsidence within the cross basin fault system. (e) Lineated
869 slickenside surface from an exhumed fault core within the Sapu restraining bend. Location shown in Figure 7a.
870 (f) Lower hemisphere stereographic projection of fault planes (great circles) and slickenside lineations (points) from
the fault shown in Figure 7e. ESRI imagery.

871 segment's reverse faults implicated in uplifting the
872 oversized palaeovalley in the east, indicated by
873 geomorphic indices.

874 *Matano Fault*

875
876
877 The Matano Fault passes from southern central
878 Sulawesi through the island's SE arm to Tolo Bay
879 (Fig. 4). It is typically shown to mark the southern
880 edge of the Sula Block, linking to the Palu Koro
881 Fault to the west and the North Sulawesi Trench to
882 the north (e.g. Hamilton 1979; Rangin *et al.* 1999).
883 A hard linkage between either the Lawanopo or
884 Matano and Palu Koro faults is a requirement of
885 many rigid block models for Sulawesi (e.g. Bellier
886 *et al.* 2006; Socquet *et al.* 2006). However, Silver
887 *et al.* (1983b) noted that the nature of the connection
888 was not known. Modern satellite imagery shows a
889 highly segmented and discontinuous westernmost
890 Matano Fault curving towards the Palu Koro
891 Fault, but the two structures remain largely isolated
892 either side of the Gunung Balease massif (Fig. 4).

893 In the east, the Matano Fault passes into the
894 northern Banda Sea. Some workers link it to the
895 Tolo Thrust (sometimes referred to as the Hamilton
896 Thrust or the East Sulawesi Trench) (Fig. 1), an
897 ESE verging thrust zone NE of Buton. Silver *et al.*
898 (1983b) suggest that the Matano and Palu Koro
899 faults act as a trench-trench transform between
900 the north Sulawesi subduction and the Tolo Thrust.
901 This thrust has been considered to accommodate
902 convergence between the Makassar block and the
903 Banda Sea block (e.g. Socquet *et al.* 2006). How-
904 ever, recent work suggests that the Tolo Thrust is
905 a gravity-driven feature at the foot of a series of
906 slumps (Rudyawan 2011), rather than a structure
907 bounding a tectonic block (e.g. Silver *et al.* 1983b;
908 Rangin *et al.* 1999).

909 Geological offsets (e.g. Ahmad 1978) and stream
910 offsets (e.g. Hamilton 1979) across the Matano
911 Fault confirm that it is a left lateral structure and
912 that it has been active during the Quaternary (Bellier
913 *et al.* 2006). Laterally offset streams are routinely
914 used to assess the shear sense and Quaternary activ-
915 ity of strike-slip faults, usually in arid environments
916 (e.g. Sieh & Jahns 1984), but also in humid, forested
917 environments (e.g. Lacassin *et al.* 1998; Wang *et al.*
918 2014). Nonetheless, such observations must be
919 interpreted cautiously, as stream offset may result
920 from stream diversion along a fault and capture by
921 another downstream reach, as well as by the genuine
922 tectonic displacement of a single stream (Wallace
923 1990). No study has used such offsets to evaluate
924 Quaternary slip rates along the Matano Fault.

925 The Matano Fault is highly segmented and lacks
926 a single through-going strand (Fig. 8a). Several lin-
927 ear basins (e.g. Pansu, Matano and Mahalona) lie
928 within or adjacent to the fault zone, often at step

overs between strands. Each basin is 4–6 km wide
and 20–30 km long. The Matano basin hosts Lake
Matano, which, at 590 m deep (Haffner *et al.*
2001), is the deepest lake in Indonesia and the
tenth deepest lake in the world. A fault passing
from the northern margin of the Pansu Basin is
very prominent as it cuts through ultramafic rocks
in the SW corner of Lake Matano, just south of
Desa Matano (Fig. 8a). The fault then steps to the
left to another very prominent fault in the NW
of the lake, from where it passes across the northern
margin of the Mahalona Basin. Rapid subsidence
in the lake and earthquake focal mechanisms record-
ing east–west extension close to the lake probably
result from this releasing geometry (McCaffrey &
Sutardjo 1982). Two major pop-ups associated
with the uplift, thrusting and exhumation of meta-
morphogenic rocks and serpentinite at restraining bends
occur east of the Mahalona Basin and west of the
Pansu Basin (Fig. 8a).

A number of consistent left lateral stream off-
sets, evidence of stream capture across two fault
strands west of Pansu Basin (Fig. 8b) and steep-
sided, narrow fault valleys (Fig. 8c) suggest youth-
ful fault activity. Geomorphic indices of oblique
basin bounding faults range from S_{mf} 1.06–1.28,
average V_f 0.69 (Pansu Basin), S_{mf} 1.02–1.17, aver-
age V_f 0.78 (Matano Basin), S_{mf} 1.19, V_f 0.45
(Mahalona Basin) to S_{mf} 1.08–1.9, average V_f
0.51 (eastern termination splay) and indicate mostly
rapid to moderate tectonic activity.

On 15 February 2011, a shallow focus M_w 6.1
earthquake near the western end of Lake Matano
(NEIC) had a focal mechanism consistent with left
lateral slip along the Matano Fault. The earthquake
caused damage to concrete walls and buildings,
including a newly built hospital in the Mahalona
valley (Fig. 8d). The earthquake's location sug-
gested that the prominent fault segment that links
the NE corner of Lake Matano with the Mahalona
Basin failed (Fig. 8e). 'Surface cracks' were
reported by local people at the eastern end of the
basin but, although we visited the area in October
2011, a surface rupture could not be located. Close
to the lake, very high resolution satellite imagery
recently made available (Bing Maps) shows three
clear lineaments cutting across boggy ground and
low-lying forest (Fig. 8f) along strike from a Mat-
ano Fault strand that offsets drainage to the left.
Although it is not possible to confirm that they rep-
resent the 2011 surface rupture, these lineaments
appear to be tectonic in origin and are clearly very
young. Linking these lineaments with the reported
surface cracks in the east, along a topographically
clearly defined fault strand, yields a postulated sur-
face rupture length of >39 km, which is longer than
expected for a M_w 6.1 earthquake from empirical
relationships (Wells & Coppersmith 1994).

929
930
931
932
933
934
935
936
937
938
939
940
941
942
943
944
945
946
947
948
949
950
951
952
953
954
955
956
957
958
959
960
961
962
963
964
965
966
967
968
969
970
971
972
973
974
975
976
977
978
979
980
981
982
983
984
985
986

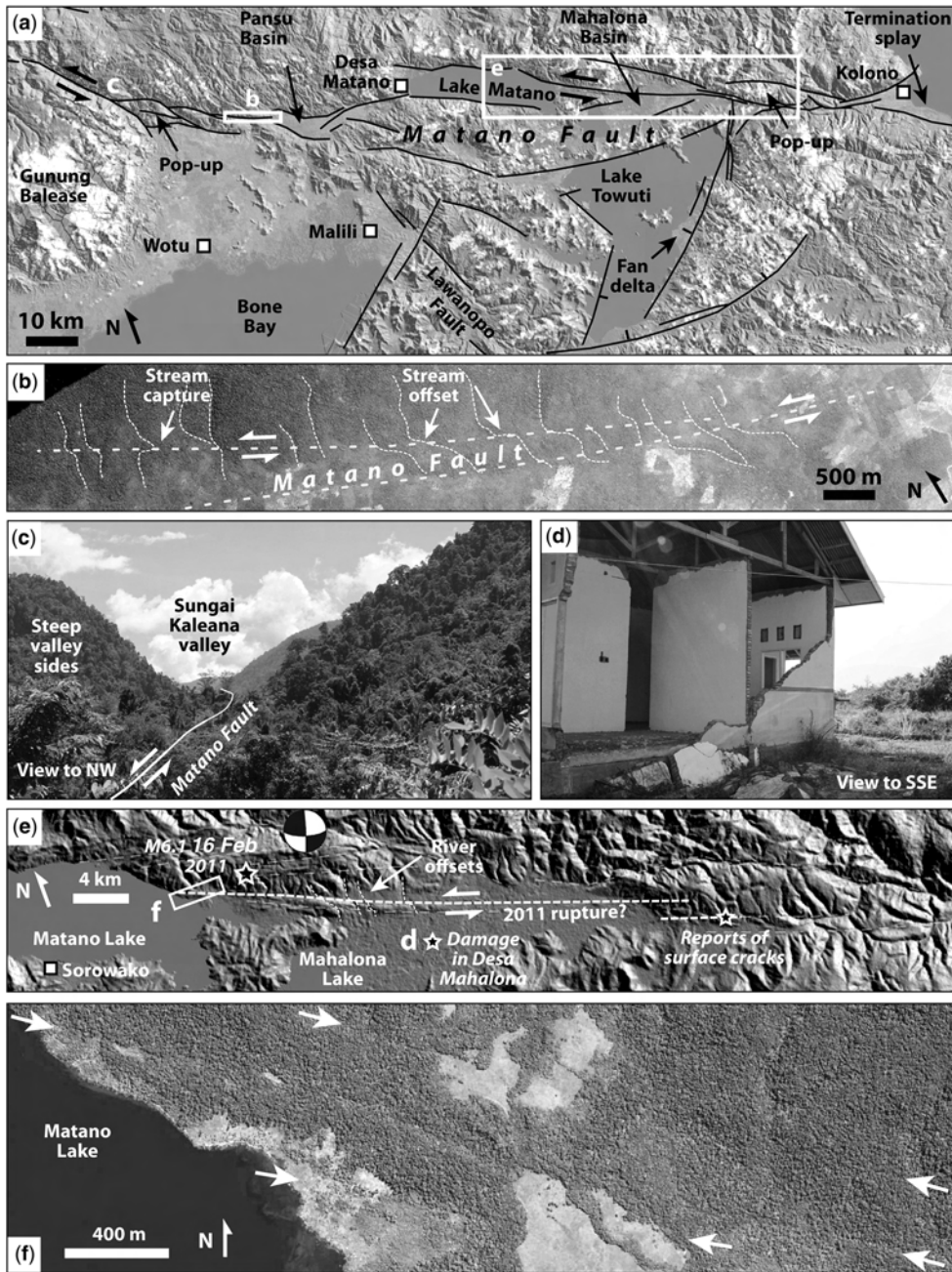


Fig. 8. Details of the Matano Fault. (a) Map of the Matano Fault, Lake Towuti and the northern part of the Lawanopo Fault. Base map is ASTER digital elevation model draped with ESRI imagery. Location shown in Figure 4. (b) Systematic stream offsets along strands of the Matano Fault west of the Pansu Basin. (c) Deep, steep sided valley marking the westernmost Matano Fault NE of Gunung Balease. (d) Hospital in the Mahalona valley damaged during the 15 February 2011 M_w 6.1 earthquake. Location shown in Figure 8e. (e) Detail of the eastern Matano and Mahalona valleys, showing features related to the 2011 earthquake and inferred surface rupture extent. ASTER base map. (f) Imagery from Bing Maps showing strong topographic lineaments in low ground in the NE corner of Lake Matano, inferred to represent recent (2011?) surface ruptures. Location shown in Figure 8e. (b) and (f) images © 2016 DigitalGlobe.

987 *Lawanopo Fault and Lake Towuti*

988 The Lawanopo Fault (Fig. 4) consists of several
989 straight NW trending fault segments that cross
990 Sulawesi's SE arm south of the Matano Fault. The
991 Lawanopo Fault is used in preference to the Matano
992 Fault by Socquet *et al.* (2006) as the southern mar-
993 gin of the 'East Sula Block'. However, discontinu-
994 ous and eroded fault traces along strands of the
995 Lawanopo Fault system suggest that it has been
996 mostly inactive during the Quaternary (Bellier
997 *et al.* 2006; Natawidjaja & Daryono 2014). None-
998 theless, recent earthquakes close to Kendari may
999 indicate that at least some strands of the Lawanopo
1000 Fault system remain active. An M_w 7.5 earthquake
1001 in the Banda Sea 170 km SE of Kendari on 19 Octo-
1002 ber 2001 had a strike slip focal mechanism and may
1003 have originated on the projected offshore trace of
1004 the Lawanopo Fault (Yeats 2010).

1005 Like the Matano Fault, the Lawanopo Fault is
1006 highly segmented and there is no through going
1007 strand at the surface (Fig. 4). Mountain front sinuos-
1008 ity values on the few segments associated with adja-
1009 cent basins range from 1.21 to 1.75 and valley depth
1010 to width ratios average 0.55–0.83, indicating mod-
1011 erate to slow tectonic activity.

1012 Lake Towuti, the largest of the Malili lakes,
1013 occupies an intermontane basin at 318 m elevation
1014 and has a maximum water depth of 203 m (Haffner
1015 *et al.* 2001). The basin lies in the wedge between
1016 the Matano and Lawanopo faults and is itself cut
1017 by linear fault strands that internally deform the
1018 wedge (Fig. 4). Two prominent curvilinear faults
1019 lie along the south and east of the lake (Fig. 8a).
1020 The closest, trending NE–SW and downthrown to
1021 the NW, forms the linear eastern lake boundary
1022 and is marked by a number of fans prograding into
1023 the lake. Its high mountain front sinuosity (2.04)
1024 and valley depth to width ratio (1.22) suggest slow
1025 tectonic activity. However, a large earthquake
1026 along this >25 km long structure could cause a sub-
1027 stantial tsunami or seiche in the lake. The second
1028 fault, to the east, is longer still (>55 km) and highly
1029 continuous. It intersects the Lawanopo Fault at a
1030 small angle and may directly transfer slip away
1031 from that structure. Mountain front sinuosity ranges
1032 from 1.03 to 1.15, suggesting maximal to rapid tec-
1033 tonic activity, although the valley floors are rather
1034 rounded (average V_f 0.49). Lake Towuti would rap-
1035 idly fill with sediment if it were not actively subsid-
1036 ing, therefore the bounding normal faults must be
1037 considered to be active during the Quaternary.

1039 *Kolaka Fault*

1040 The Kolaka Fault (Simandjuntak *et al.* 1984, 1994;
1041 **EDQ1** Surono 1994) (Fig. 9a) lies along the southern mar-
1042 gin of the Mengkoka mountains and is sub parallel
1044

to the Lawanopo Fault to its north. It is equivalent
to the Mendoke Fault of Bellier *et al.* (2006). Ham-
ilton (1979) interpreted the fault as a SW dipping
thrust and Bellier *et al.* (2006) considered the fault
as a pre Early Pleistocene strike slip continuation
of the Palu–Koro Fault, but there is little evidence
to support either hypothesis. One strand of the
Kolaka Fault is sealed by 4.4 ± 0.2 Ma dacites,
potentially placing a limit on the timing of faulting
(White *et al.* 2014).

The fault is composed of several NE–SW trend-
ing, gently arcuate segments up to 45 km long in
map view. Along the Bone Bay coast and at Kolaka
town the downthrown side is to the south and the
easternmost segment is downthrown to the north
(Fig. 9a). The polarity shift occurs across a 10 km
wide relay straddling the Anggowala mountains.
The orientation of these two apparently normal
fault systems is kinematically consistent with sinis-
tral slip along the overall Kolaka trend.

Geomorphic indices are highest closest to
Kolaka town, where S_{mf} values of 1.22–1.30 and
 V_f values of 0.23–1.68 suggest that there is rapid
to slow active dip slip across the fault, which has
a clear surface expression and is marked by triangu-
lar facets (Fig. 9c). Along strike to the NW a series
of linear valleys and low ridges near Lasusua may be
a continuation of the Kolaka Fault (Fig. 9b). An
absence of fault scarps or clearly displaced features
makes fault activity hard to evaluate, but meander
confinement within a linear graben across the Lasu-
sua alluvial plain and asymmetrical subsidence
highlighted by the river's proximity to the bounding
fault suggests recent fault activity (Fig. 9d).

Faults downthrown to the WSW at the western
end of the Kolaka Fault have very low S_{mf} and V_f
values (1.05 and 1.25, respectively), deeply incised
streams and well developed triangular facets, sug-
gesting Quaternary dip slip. These faults face into
Bone Bay and may be related to basin bounding
extensional structures accommodating subsidence
in the bay (Camplin & Hall 2014).

Balantak Fault

A prominent ENE trending linear structure, the
Balantak Fault, lies at the eastern end of Sulawesi's
east arm and separates the Batui thrust system in
the south from mountainous highlands in the north
(Fig. 10a). It has been considered to be part of
the Batui thrust system (Silver *et al.* 1983b), but
its remarkably straight outcrop, field observations
(Simandjuntak 1986) and along strike alternation
between local uplift and subsidence suggest that it
is a steep, possibly strike slip, fault.

Onshore, where the fault bends gently to the
right, small, apparently Quaternary basins are devel-
oped (Fig. 10b). There is uplift where the fault bends

1045
 1046
 1047
 1048
 1049
 1050
 1051
 1052
 1053
 1054
 1055
 1056
 1057
 1058
 1059
 1060
 1061
 1062
 1063
 1064
 1065
 1066
 1067
 1068
 1069
 1070
 1071
 1072
 1073
 1074
 1075
 1076
 1077
 1078
 1079
 1080
 1081
 1082
 1083
 1084
 1085
 1086
 1087
 1088
 1089
 1090
 1091
 1092
 1093
 1094
 1095
 1096
 1097
 1098
 1099
 1100
 1101
 1102

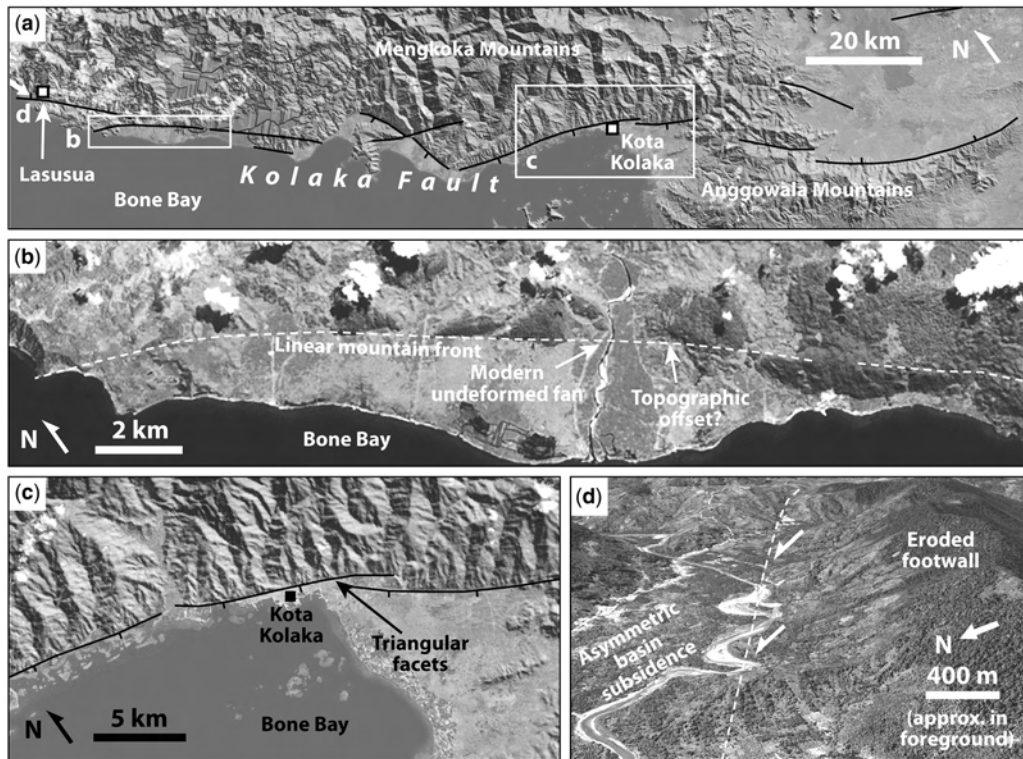


Fig. 9. Details of the Kolaka Fault. (a) Overview map of the main Kolaka Fault segments. Base map is ASTER digital elevation model draped with ESRI imagery. Location shown in Figure 1. (b) Straight segment of the Kolaka Fault associated with linear ridges and valleys. ESRI imagery. Google Earth imagery. Image © 2016 DigitalGlobe. (c) Linear fault bounded mountain front and triangular facets indicating Quaternary fault activity at Kolaka town. (d) Asymmetrical axial drainage at a splaying fault segment near the western fault termination, indicating Quaternary subsidence along the bounding fault system.

gently to the left. Both observations are kinematically compatible with a dextral shear sense. One of the zones of Quaternary subsidence is shown in Figure 10c. A basin bounding fault at a small clockwise angle from the regional Balantak Fault trend is crossed by streams that show no systematic offset, suggesting dominant dip slip. To the north, a prominent lineament crosses the basin, expressed by lines of vegetation and slightly darker (moister?) soil. This lineament's parallelism with the Balantak Fault to the east and its negligible topographic relief suggests it is the through going strike slip fault strand. Although stream avulsion across the flat topped basin is too dynamic to preserve meaningful offsets, the clear expression of the fault in the young sediments suggests the Balantak Fault has been active during the Quaternary.

The Balantak Fault's termination system offshore to the east of Poh Head is composed of left stepping segments separated by folds and thrusts (Fig. 10d). Contraction between left stepping main

segments, an apparently antithetic sinistral fault and the orientation of folds and thrusts are all kinematically compatible with dextral shear along the Balantak Fault (Watkinson *et al.* 2011). Earthquakes located onshore and west of Poh Head also suggest right lateral and reverse slip parallel to the Balantak Fault (Fig. 10a). However, a swarm of offshore earthquakes between Peleng and Taliabu to the east have focal mechanisms that support sinistral slip along the Balantak trend. This apparent contradiction is discussed in Watkinson *et al.* (2011). Here we conclude that the geological and geomorphic evidence supports long term Quaternary dextral slip. Further work is required to understand the significance of a small number of contradictory seismological signals in the area.

The Balantak Fault is almost continuous for 54 km from Balantak town in the east to Poh Bay in the west, where it probably continues just offshore for another >30 km. Extending to include the dextral fault system offshore to the SE makes the

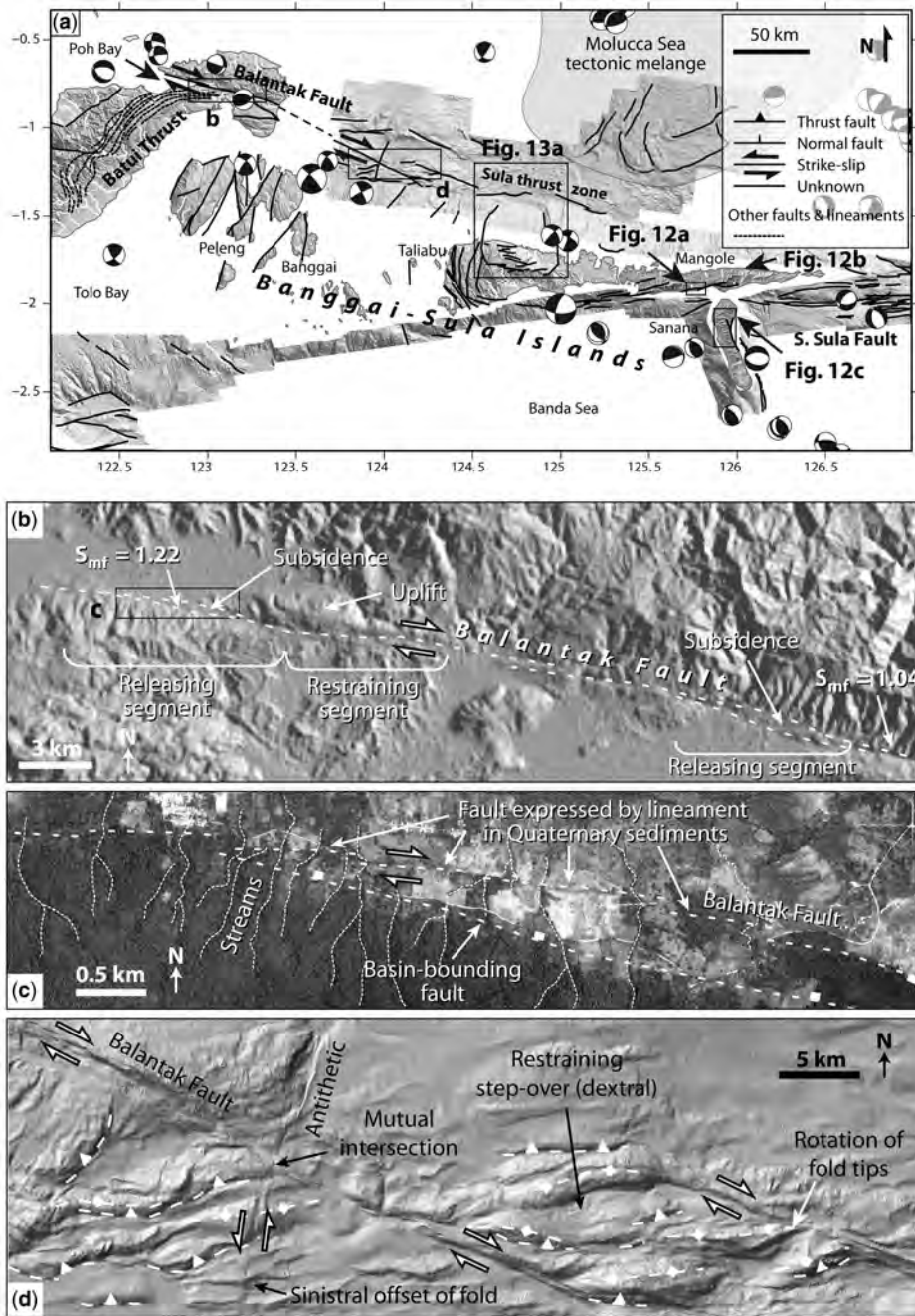


Fig. 10. (a) East arm of Sulawesi and Banggai Sula Islands digital elevation model (SRTM), multibeam bathymetry, CMT catalogue earthquakes <35 km depth and structures showing geomorphic evidence of Quaternary tectonic activity. After Watkinson *et al.* (2011). Location shown in Figure 1. (b) Subsidence and uplift associated with releasing and restraining segments of the onshore Balantak Fault. ASTER digital elevation model base map. (c) Detail of bounding fault system of a Balantak Fault releasing segment, showing a north dipping normal fault and sub parallel lineament in agricultural land, inferred to represent a through going strike slip strand. ESRI imagery base map. (d) Detail of the offshore Balantak Fault expressed in multibeam imagery (illumination from NW) showing evidence of dextral shear.

1161 fault up to 250 km long. The onshore fault scarp has
1162 exceptionally low S_{mf} values, from 1.04 to 1.22
1163 (Fig. 10b), with correspondingly low average V_f val-
1164 ues of 0.36, suggesting maximal to moderate
1165 tectonic activity.

1166 *Gorontalo Fault*

1167 The Gorontalo Fault (Katili 1973) (Fig. 11a)
1168 has been considered to be one of the major block
1169 bounding structures of Sulawesi (e.g. Socquet
1170 *et al.* 2006; Molnar & Dayem 2010). Geodetic mod-
1171 elling suggests a 11 mm a⁻¹ dextral slip rate and
1172 10 km locking depth; however, because the obser-
1173 vation points are widely spaced, it remains possible
1174 that global positioning system (GPS) data record
1175 rotation of the entire north arm of the island rather
1176 than discrete slip across a fault (Socquet *et al.*
1177 2006). There is little modern shallow seismicity in
1178 the Gorontalo area, suggesting that the fault is inac-
1179 tive or remains locked (Fig. 11a).

1180 The fault is composed of several branching
1181 segments, including major c. 30 km long segments
1182 south and north of Gorontalo city (Fig. 11b). Lim-
1183 boto Lake lies in the 7 km wide step over between
1184 these two segments, indicating local transtension.
1185 The fault is expressed by highly eroded scarps
1186 passing along the Tomini Bay coast and bounding
1187 the Gorontalo/Limboto depression. Geomorphic
1188 indices suggest that the segments experience slow
1189 to minimal tectonic activity, with S_{mf} values rang-
1190 ing from 1.83 to 2.36 and an average V_f of 1.28.
1191 Although there is considerable human development
1192 within the Gorontalo/Limboto depression, which
1193 may obscure neotectonic activity, there appears to
1194 be little evidence of deformation within the Quater-
1195 nary sediment fill, except for the presence of Lim-
1196 boto Lake subsidence at the releasing step over.

1197 *Western Tomini Bay bounding faults*

1198 A series of faults along the margin of Tomini Bay
1199 shows evidence of recent activity. The faults are
1200 arcuate and generally mark the boundary between
1201 mountainous ground along Sulawesi's narrow
1202 'neck' and Tomini Bay, which is up to 2 km deep
1203 and contains a sedimentary succession up to 10 km
1204 thick (Jablonski *et al.* 2007; Pholbud *et al.* 2012).
1205 Extension and mantle decompression across the
1206 bay are associated with Plio Pleistocene volcanism
1207 in the Togian Islands and possibly with modern vol-
1208 canism at Una Una volcano (Cottam *et al.* 2011),
1209 supporting recent extensional faulting and litho-
1210 spheric thinning both onshore and offshore (Phol-
1211 bud *et al.* 2012).

1212 The northernmost bounding fault bounds the
1213 2.5 km high Molino Metamorphic Complex (Fig.
1214 11c), a suite of quartzo feldspathic mica schists

and gneisses that may be an exhumed metamorphic
core complex (van Leeuwen & Muhandjo 2005).
The faults dip north and south on the north and
south sides of the complex, respectively, and have
crystalline basement in their footwalls. The southern
segment has a curvilinear trace >75 km long with
extremely low S_{mf} values (1.05) and well developed
triangular facets at the end of V shaped valleys with
 V_f values of 0.33–0.64 within an uplifted footwall
block. On this basis, combined with no evidence
of strike slip, it is interpreted as a normal fault.

Further SW, the Tomini Bay bounding faults are
crossed by a number of fan deltas prograding into
the bay. These are surprisingly short (<3 km),
given the potential upstream sediment source, sug-
gesting rapid and recent hanging wall subsidence
(Fig. 11d, e). Segments further south along the
'neck' have higher S_{mf} values (1.66) and the fan
delta lobe length increases to >10 km, suggesting
less significant recent subsidence (Fig. 11f).

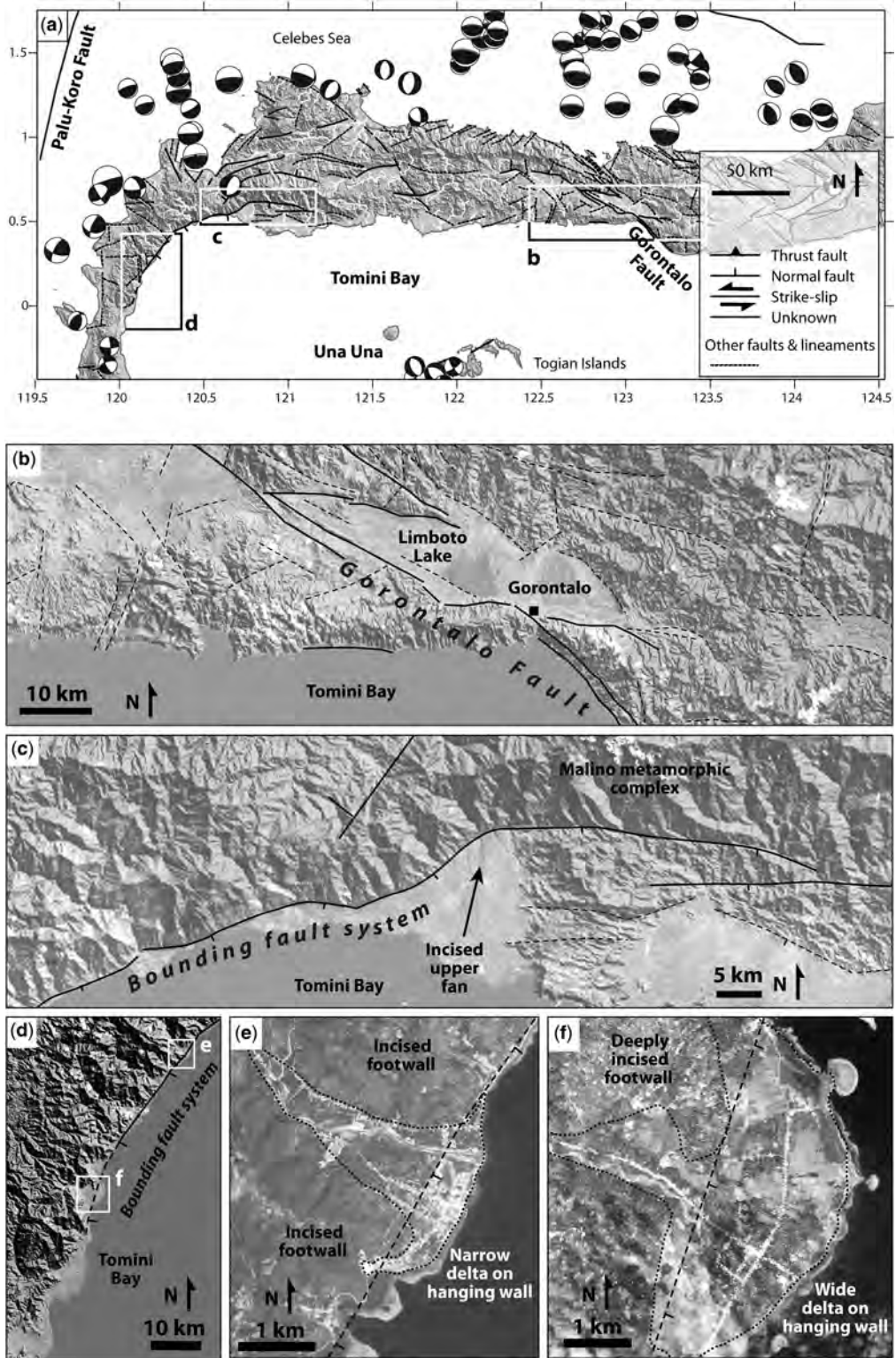
At the southern end of the neck, a NE dipping
fault system, including the Tambarama Fault (Phol-
bud *et al.* 2012), forms an apparently continuous
arcuate trace at Parigi (Fig. 4), marking the boundary
between the Palu Metamorphic Complex onshore
(van Leeuwen & Muhandjo 2005) and Tomini Bay
subsidence offshore. S_{mf} values are generally high
(2.77–3.25), although a short northern segment is
less sinuous at 1.32. A well developed apron of fan
deltas extends 6 km from the mountain front.

1215 **Maluku and North Maluku**

Maluku and North Maluku are composed of numer-
ous islands affected by disparate neotectonic pro-
cesses. In the north, Halmahera (Fig. 1) and the
Sangihe Arc are involved in the active collision of
two accretionary complexes above the subducted
Molucca Sea slab, where the Sangihe forearc is
being thrust eastwards over the Halmahera forearc
(e.g. Silver & Moore 1978; Hamilton 1979; Hall
1987; Hall *et al.* 1995). The entire system accommo-
dates 80 mm a⁻¹ of the 105 mm a⁻¹ Philippine Sea
plate Sundaland convergence (Rangin *et al.* 1999).
Splays of the left lateral Sorong Fault pass through
and to the south of Halmahera and Bacan, where
there is abundant modern seismicity (e.g. Ali &
Hall 1995; Hall *et al.* 1995) (Fig. 1).

South of Bacan, islands with Australian conti-
nental basement, such as the Banggai Sula Islands
and Obi, are bounded by strands of the Sorong Fault
and were for a long time considered to have been
translated from New Guinea along a 1900 km long
Sorong Fault passing from northern Papua New
Guinea towards Sulawesi (e.g. Visser & Hermes
1962; Audley Charles *et al.* 1972; Hamilton 1979;
Pigram *et al.* 1985; Garrard *et al.* 1988; Hutchison

1219
1220
1221
1222
1223
1224
1225
1226
1227
1228
1229
1230
1231
1232
1233
1234
1235
1236
1237
1238
1239
1240
1241
1242
1243
1244
1245
1246
1247
1248
1249
1250
1251
1252
1253
1254
1255
1256
1257
1258
1259
1260
1261
1262
1263
1264
1265
1266
1267
1268
1269
1270
1271
1272
1273
1274
1275
1276



1277 1989). New interpretations based on evidence of
 1278 extreme crustal extension and mantle exhumation,
 1279 mantle tomography and geodynamic models (e.g.
 1280 Spakman & Hall 2010; Hall 2011; Spencer 2010,
 1281 2011; Pownall *et al.* 2014) suggest that those
 1282 islands, together with others along the northern
 1283 Banda Arc such as Buru and Seram, were part of a
 1284 continental spur that was fragmented during Mio-
 1285 cene Pliocene times by lower crustal delamination
 1286 driven by Banda Sea rollback.

1287 Quaternary extension in Maluku appears to be
 1288 as important as it is in Sulawesi, despite an overall
 1289 collisional tectonic setting. Young metamorphic
 1290 core complexes exhumed in Seram (Pownall *et al.*
 1291 2013) and possibly Buru (Roques 1999) are associ-
 1292 ated with low angle and steep normal faults. A sig-
 1293 nificant component of the seismic moment release
 1294 in Maluku is by normal and strike slip earthquakes,
 1295 alongside important thrusting in the Molucca Sea
 1296 and north Seram (e.g. Rangin *et al.* 1999). Sinistral
 1297 transpression through Seram accommodates Austra-
 1298 lia Pacific convergence and links into the Tarera
 1299 Aiduna Fault of West Papua (e.g. Rangin *et al.*
 1300 1999; Stevens *et al.* 2002; Teas *et al.* 2009).

1302 *Banggai Sula Islands*

1303 The Banggai Sula Islands (Fig. 10a) occupy a frag-
 1304 ment of continental crust of Australian affinity that
 1305 has collided with the east arm of Sulawesi (e.g.
 1306 Audley Charles *et al.* 1972; Hamilton 1979; Pigram
 1307 *et al.* 1985; Garrard *et al.* 1988). The South Sula
 1308 Sorong Fault was interpreted by Hamilton (1979)
 1309 to follow the break in slope south of Taliabu and
 1310 pass between Mangole and Sanana. North of the
 1311 Banggai Sula Islands the North Sula Sorong
 1312 Fault (e.g. Hamilton 1979; Norvick 1979; Silver
 1313 *et al.* 1983b; Sukamto & Simandjuntak 1983), pre-
 1314 viously considered to pass from the Bird's Head,
 1315 past Obi and along the north margin of the Bang-
 1316 gai Sula Islands towards Sulawesi's east arm, can
 1317 not be detected in new geophysical data and must lie
 1318 below the Molucca Sea collision complex to the
 1319 north (Ferdian *et al.* 2010; Watkinson *et al.* 2011).

1320 Despite the density of deformation in the area,
 1321 there is very little shallow seismicity immediately

1322 north of the Banggai Sula margin (Engdahl *et al.*
 1323 1998; Rangin *et al.* 1999; Beaudouin *et al.* 2003),
 1324 indicating that there are few active structures, that
 1325 deformation is largely aseismic or that the main
 1326 faults have interseismic periods that exceed instru-
 1327 mental records. This is a marked contrast with the
 1328 abundant shallow seismicity associated with the
 1329 Molucca Sea collisional zone further north. How-
 1330 ever, a number of focal mechanisms north and
 1331 south of the islands indicate that there is some resid-
 1332 ual left lateral slip on east west to NW SE trend-
 1333 ing faults (Fig. 10a).

1334 Mangole Island appears to be bordered along its
 north and south sides by several linear east west
 trending normal faults, indicated by straight traces
 and well developed triangular facets (Fig. 12a, b).
 Mountain front sinuosity values range from 1.11
 to 1.57 and V_f is from 0.44 to 0.55, suggesting that
 some of the structures have been active during the
 Quaternary. Sanana Island, topographically orthog-
 onal to Mangole, is bounded by NNW SSE trend-
 ing faults that can be traced offshore in multibeam
 bathymetry. The most prominent fault, on the east
 coast, forms a well defined scarp >20 km long, dip-
 ping and downthrown to the east, making it likely to
 be a normal fault (Fig. 12c). Triangular facets, hang-
 ing valleys, deeply incised streams (Fig. 12d) and an
 absence of subaerial prograding fan delta tops wider
 than c. 400 m suggest rapid recent eastwards subsi-
 dence along the fault, supported by S_{mf} values of
 1.27–1.34.

Taliabu Island (Fig. 10a) is cut by a number of
 east west and north south trending Quaternary
 faults. The north south trending faults in the
 west have a particularly fresh geomorphic expres-
 sion. A north coast bedding parallel dip slope
 dips 6° into the Molucca Sea (Fig. 13a). Offshore
 to the north a planar detachment surface 34 km
 wide exactly corresponds to the Taliabu dip slope
 onshore and represents a submarine slope failure
 (Watkinson *et al.* 2011). Both onshore and offshore
 slopes appear to be part of a single large glide
 surface of a mega debris slide that translated
 much of north Taliabu at least 37 km north into
 the Molucca Sea, probably causing a significant
 tsunami.

Fig. 11. (a) North arm of Sulawesi digital elevation model (SRTM), CMT catalogue earthquakes <35 km depth and structures showing geomorphic evidence of Quaternary tectonic activity. Rivers marked in white. Location shown in Figure 1. (b) Detail of the onshore Gorontalo Fault and associated basins. ASTER digital elevation model draped with ESRI imagery layer. (c) Fault system bounding the Malino metamorphic complex showing remarkably straight and steep mountain front and well developed triangular facets. (d) Overview of fan deltas prograding into western Tomini Bay across the bounding fault system. (e) Narrow fan delta clearly cut by the basin bounding fault, indicating rapid subsidence. Google Earth imagery. Image © 2016 DigitalGlobe. Data SIO, NOAA, U.S. Navy, NGA, GEBCO. Image (2016) Terrametrics. Image Landsat. (f) Wide fan delta further south indicating a slower rate of hanging wall subsidence. Google Earth imagery. Image © 2016 DigitalGlobe. Data SIO, NOAA, U.S. Navy, NGA, GEBCO. Image (2016) Terrametrics. Image Landsat.

1335
1336
1337
1338
1339
1340
1341
1342
1343
1344
1345
1346
1347
1348
1349
1350
1351
1352
1353
1354
1355

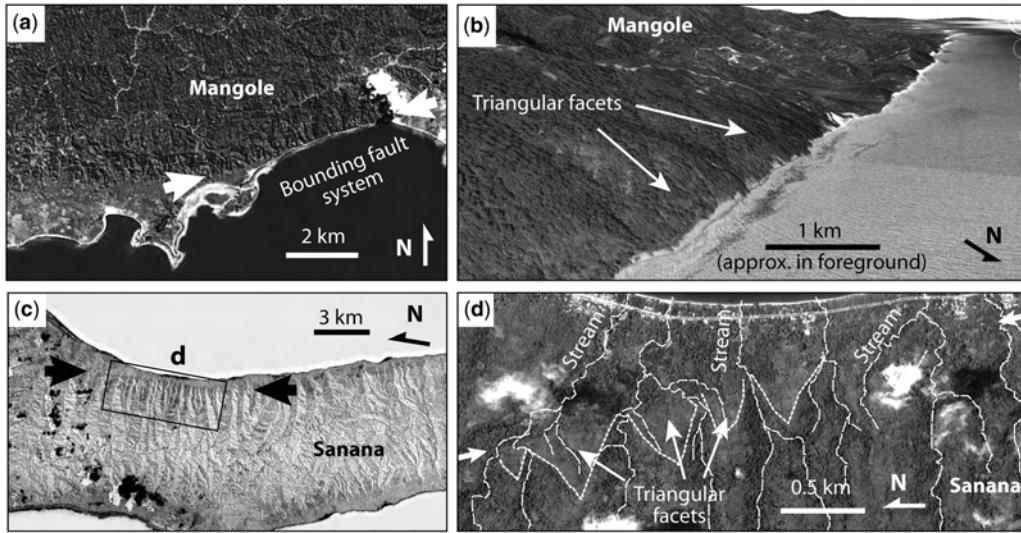


Fig. 12. Details of Quaternary faults in the Banggai Sula Islands. For locations, see Figure 10a. **(a)** Part of the linear normal fault system bounding the southern margin of Mangole Island. Google Earth image. Data SIO, NOAA, U.S. Navy, NGA, GEBCO, Image Landsat. Image © 2016 TerraMetrics. **(b)** Triangular facets along the north coast of Mangole Island. Oblique view in Google Earth. Data SIO, NOAA, U.S. Navy, NGA, GEBCO. Image © DigitalGlobe. Image © 2016 TerraMetrics. Image Landsat. **(c)** Fault control along the eastern coast of Sanana Island. Image from Google Earth (greyscale inverted for clarity). Image Landsat. Image © DigitalGlobe. Image © 2016 TerraMetrics. Data SIO, NOAA, U.S. Navy, NGA, GEBCO. **(d)** Detail of the Sanana fault, showing the extremely linear mountain front, narrow V shaped valleys and triangular facets. Image © DigitalGlobe.

1356
1357
EDQ3
1358
1359
1360
1361
1362
1363
1364
1365
1366
1367
1368
1369
1370
1371
1372
1373
1374
1375
1376
1377
1378
1379
Colour
online/
colour
hardcopy
1383
1384
1385
1386
1387
1388
1389
1390
1391
1392

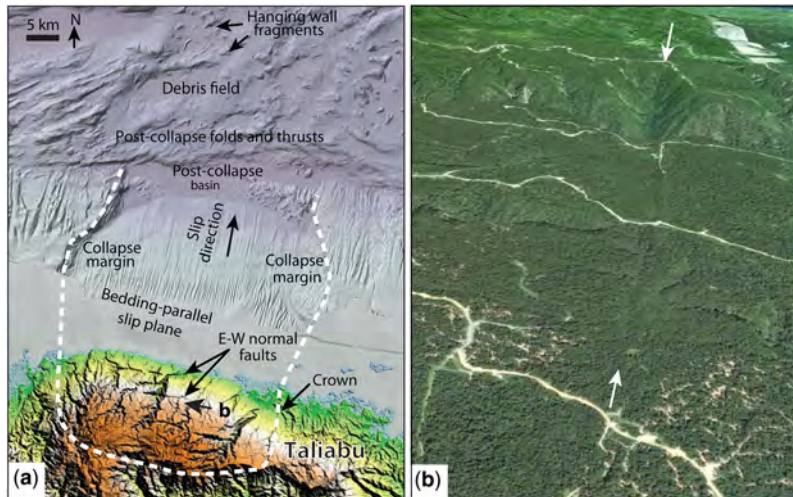


Fig. 13. **(a)** Mega debris slide and post collapse normal faults, north coast of Taliabu. Base map is SRTM topography onshore and multibeam bathymetry offshore. Location shown in Figure 10a. **(b)** Oblique perspective view from Google Earth of one of the normal faults on the north slope of Taliabu. White arrows mark fault tips. View to the west. Field of view is c. 1 km in foreground. View location and direction indicated by arrow in Figure 13a. Image Landsat. Image © DigitalGlobe. Data SIO, NOAA, U.S. Navy, NGA, GEBCO.

The north Taliabu dip slope is truncated by several prominent east west trending faults that dip steeply north. The geomorphic expression is very fresh (Fig. 13b). The footwall crests are only slightly eroded and, in most cases, the drainage runs parallel to fault scarps and has not cut across them, except for a few prominent high order streams. The faults displace the dip slope and must therefore post date the mega debris slide. Although we have no absolute constraint on the timing of the slide, reef build ups are conspicuously poorly developed along the section of coast at the foot of the dip slope, but are extensive along the coast and small islands on either side. The slide must have happened recently enough that corals have been unable to fully recolonize the new coastline, suggesting that the post slide normal faults are late Quaternary and probably still active.

Sorong Fault from Obi to Waigeo

Westward splaying segments of the Sorong Fault emanate from the western Bird's Head and pass close to the islands of Salawati, Misool, Obi, Bacan, south Halmahera and Waigeo (e.g. Katili 1975; Hamilton 1979; Ali & Hall 1995) (Fig. 1). Although there is debate about whether the Sorong Fault onshore West Papua is tectonically active (discussed later in this paper), at the latitude of Obi there is $19 \pm 8 \text{ mm a}^{-1}$ left lateral displacement between Ternate and the Bird's Head that may be accommodated by one or more strands of the Sorong Fault (Bock *et al.* 2003). Seismicity is limited in the islands immediately west of the Bird's Head, but intense seismicity occurs around Obi, Bacan and south Halmahera (Rangin *et al.* 1999), which may be where sinistral strain is transferred from Seram into the Molucca Sea.

Seram fold thrust belt

Between northern Seram and the Bird's Head is a broad zone of transpression linked to convergence between Australia and the Pacific plate (Fig. 1). A deep bathymetric trough, the Seram Trough, lies 150 km north of Seram Island and curves around the Banda Sea, linking to the Timor Trough and ultimately the Java Trench. The Seram Trough has been interpreted as a subduction trench (e.g. Hamilton 1979), a foredeep ahead of a fold thrust belt (e.g. Audley Charles 1986) and a hinge zone marking the northern limit of delaminated and subducted lower continental crust (Spakman & Hall 2010).

Convergence across the Seram Trough is presently 20 mm a^{-1} (Rangin *et al.* 1999; Stevens *et al.* 2002) and is associated with intense seismicity generated by shallow thrust faulting (McCaffrey 1989; Engdahl *et al.* 1998) mainly concentrated

along the northern edge of Seram (Fig. 14a) and entirely in the western part of the fold belt (Teas *et al.* 2009).

Seram is centred on a belt of high mountains ($>3 \text{ km}$ elevation), which include tracts of continental metamorphic rocks, ultramafic rocks and the Earth's youngest exposed ultra high temperature granulites, exhumed since 16 Ma (Pownall *et al.* 2014). The Plio Pleistocene Wahai and Fufa formations onlap the elevated pre Pliocene succession, forming low plains along the northern coast (Pairault *et al.* 2003), and are themselves overlain by modern alluvial and reef deposits. There is evidence of active contraction within these plains.

On the north coast of Seram, onshore fold growth affects the modern drainage, suggesting that the folds have been active during the Quaternary (Fig. 15a). Three large rivers draining the northern slopes of the Kobipoto Mountains are deflected from a linear route to the coast by two sets of segmented east west to NW SE trending hills. Progressive migration of the rivers away from the hilltops is recorded by a trail of abandoned and filled river channels left behind by the deflected river, expressed by oxbow shaped fields and areas of vegetation (Fig. 15b, c). Larger hills, like that in the centre of Figure 15a, cause more deflection than smaller folds, like that in the east which only deflects Wai (stream) Kobi slightly. In all cases the abandoned channels are located upslope of the modern river, suggesting that progressive uplift is forcing river avulsion. This tendency for the hills to grow symmetrically from a central axis, their elongate morphology and their asymmetry (steep northern slopes, shallow southern slopes) support the interpretation that they are the surface expression of shallow, north vergent fault propagation folds above south dipping thrusts (Fig. 15d).

Abandoned meander channels and point bars on the coastal plain in the central part of Figure 15d are not associated with any obvious modern river, but seem to originate at the foot of the central frontal thrust. Abandoned remnants of a comparably large river can also be observed in an uplifted valley immediately to the south, and directly north of a fourth major north flowing river, which presently abruptly curves around the eastern tip of the fault before joining Wai Musi. It is interpreted that the abandoned channels here represent a river that flowed directly north before the fold developed. An uplifted valley across the mid point of the fold shows that the river attempted to downcut as the fold grew, but was ultimately thwarted by a high uplift rate and swung east to be captured by Wai Musi. Deep lateral incision by the captured river into the back limb of the fold (Fig. 15b) suggests that the fold growth, and presumably underlying thrust activity, is ongoing.

1451
1452
1453
1454
1455
1456
1457
1458
1459
1460
1461
1462
1463
1464
1465
1466
1467
1468
1469
1470
1471
1472
1473
1474
1475
1476
1477
1478
1479
1480
1481
1482
1483
1484
1485
1486
1487
1488
1489
1490
1491
1492
1493
1494
1495
1496
1497
1498
1499
1500
1501
1502
1503
1504
1505
1506
1507
1508

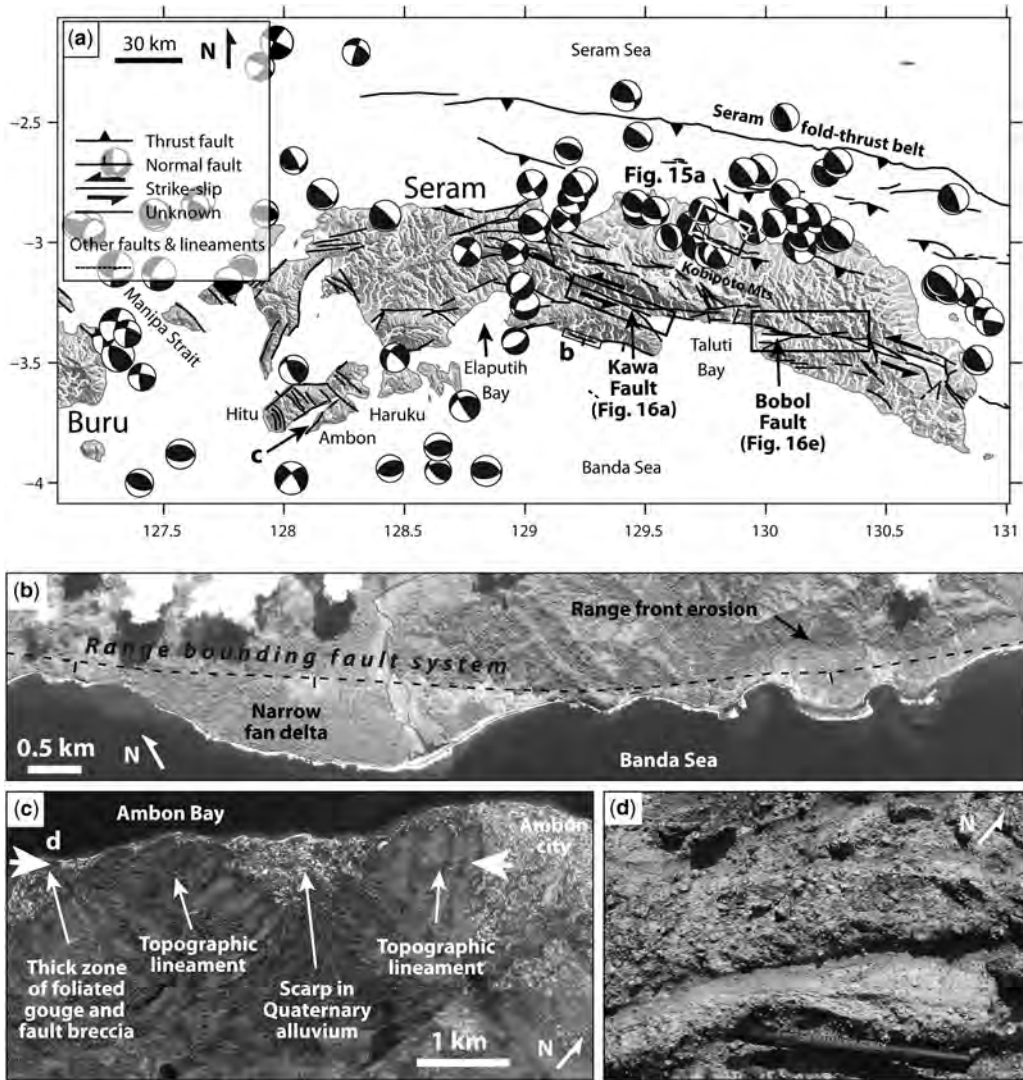


Fig. 14. (a) Seram digital elevation model (SRTM), CMT catalogue earthquakes <35 km depth and structures showing geomorphic evidence of Quaternary tectonic activity. Rivers marked in white. Offshore structures from Teas *et al.* (2009). Location shown in Figure 1. (b) Normal faults along the south coast of Seram, marked by a linear mountain front and a prominent lineament crossing a narrow fan delta. Google Earth imagery. Data SIO, NOAA, U.S. Navy, NGA, GEBCO. Image © 2016 DigitalGlobe. Image © 2016 TerraMetrics. (c) Possible Quaternary fault SW of Ambon, marked by a lineament that crosses volcanic hills and Quaternary drift. Google Earth imagery. Image © 2016 DigitalGlobe. (d) Example of foliated gouge from a thick fault zone located where the lineament illustrated in Figure 14c reaches the coast. Pen is 14 cm long.

A series of abandoned channels east of Wai Musi, the easternmost of which link to Wai Kobi, indicates that river itself may previously have been a tributary to Wai Kobi, before being deflected to the west and ultimately cut off from the trunk stream, presumably by uplift above the eastern frontal thrust.

Such evidence of recent hanging wall uplift and tectonic folding, together with the low relief of the range front, leads to the conclusion that the faults are youthful, low angle, south to SW dipping thrusts supported by focal mechanisms along the north coast (Fig. 14a). Uplifted coastal terraces in the foreland of the onshore thrusts and a

conspicuously wide coastal plain (Fig. 15d) suggest additional young uplift north of the onshore thrusts, perhaps in response to a third set of active faults just offshore. This is consistent with modern thrust activity within the broad fold thrust belt offshore (e.g. Engdahl *et al.* 1998; Teas *et al.* 2009) and a 1629 mega thrust earthquake probably originating in the Seram Trough (Liu & Harris 2013).

Kawa Fault

The Kawa Fault (Pownall *et al.* 2013) lies in the prominent ESE WNW trending deep linear valley that passes through central Seram (Fig. 14a) and is occupied by the Kawa River. The fault broadly separates upper greenschist to mid amphibolite facies Tehoru Formation rocks in the south from generally higher grade metamorphic rocks of the Saku and Taunusa complexes in the north (Germeraad 1946; Tjokrosapoetro *et al.* 1993; Pownall *et al.* 2013). The Kawa Fault coincides with the position of strongly mylonitic garnet bearing Tehoru Formation schists with a steeply dipping foliation considered by Linthout *et al.* (1991) to record dextral shear, but now recognized to have been intensely folded and possibly originating in a low angle normal fault, resulting in complexly re oriented kinematic indicators (Pownall *et al.* 2013).

A brittle fault zone up to 2 km wide (Pownall *et al.* 2013) overprints the mylonitic rocks and controls the modern topography (Fig. 16a, b). Fault strands are generally parallel to the mylonitic foliation and contain abundant serpentinite slivers and smears. Mid way along the fault is a prominent right step associated with uplift and a major drainage divide, pointing to local transpression due to left lateral slip. Stream offsets measured from Landsat and Google Earth imagery along the fault (Fig. 16a) range from 66 605 m of left lateral offset (22 measurements) to 62 334 m of right lateral offset (five measurements). Most measurements have a high uncertainty, increased by Seram's extremely humid climate and thick forest cover. Nonetheless, some measurements for example, the 268 and 253 m left lateral offsets (e.g. Fig. 16c) are considered to be robust because: (1) they lie on fault segments that are well defined (narrow linear valleys with other independent evidence of a fault origin such as triangular facets and steps/bends with the corresponding uplift/subsidence appropriate to the sense of river offset); (2) there is no evidence of stream capture; and (3) upstream and downstream valleys have a similar geomorphic character. A left lateral shutter ridge displacement and a NW SE trending fold within the Kawa River delta (Fig. 16a) support recent sinistral shear. A few earthquakes close to the western end of the fault yield CMT solutions suggesting dextral slip along NW

SE trending planes, whereas one close to the west endmost splay indicates sinistral slip (Fig. 14a).

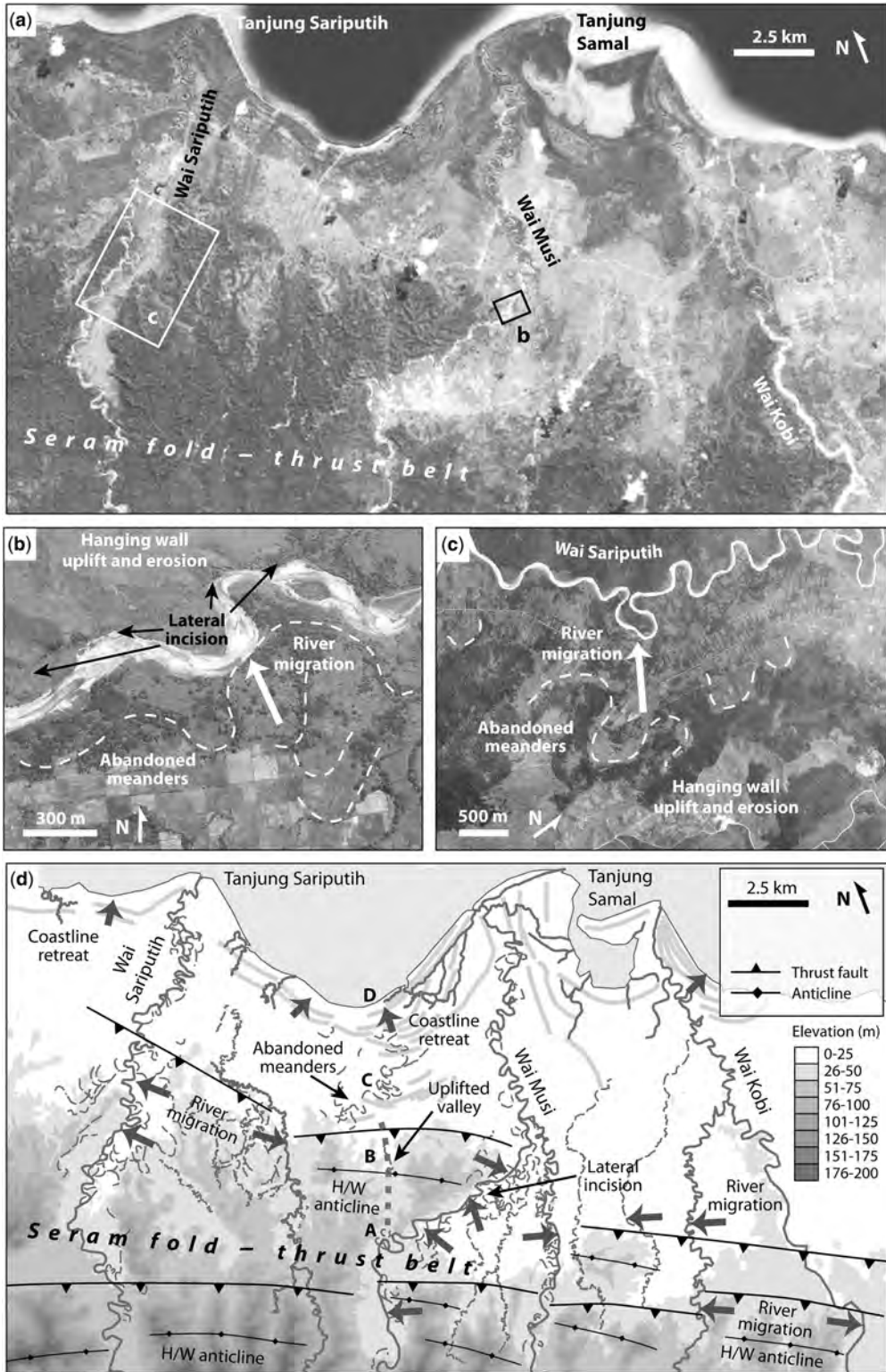
The fault zone splays as it enters Taluti Bay in the east (Fig. 16a). The splay strands are associated with well developed triangular facets that record Quaternary normal faulting (Fig. 16d). The two major splays have low S_{mf} values of 1.10 in the north and 1.33 in the south and an average V_f of 0.27, indicating rapid to moderate tectonic activity. The Kawa River flows hard against the southern splay, suggesting active subsidence along that segment, despite its higher S_{mf} indicating slower tectonic activity than in the north. However, the river's position may also be influenced by landslides, debris flows and anticline growth in the northern part of its valley. In the west, the fault splays north of Elaputih Bay, attaining a total onshore length of 90 km, or 120 km including a possible splay fault along the north coast of Taluti Bay (Fig. 14a).

Although the fault zone is thickly forested, numerous landslip scars can be recognized along the fault, indicating recent seismicity (Fig. 16a). In addition, the eastern termination is characterized by a series of discontinuous tilted blocks suggestive of slope failure along the southern margin of the Manusela Mountains (Fig. 16a). An M7.8 earthquake in 1899 triggered landslides that caused a 12 m high local tsunami at Tehoru (<http://www.ngdc.noaa.gov>; Brune *et al.* 2010), although it is unclear whether the source was the Kawa Fault or a more distant earthquake. However, all evidence points to the Kawa Fault being active during the Quaternary and capable of generating large earthquakes.

Other active faults of Seram

Along strike from the Kawa Fault on the east side of Taluti Bay, a fault zone occupies the valleys of Wai Masumang and Wai Bobol and is here termed the Bobol Fault (Fig. 14a). It is highly segmented, although with a total onshore length of 100 km and possible along strike continuity with the Kawa Fault, it is a significant structure. Four large basins are developed along its length, each bounded by ESE WNW to SE NW trending normal faults. The mountain front sinuosity along these structures ranges from 1.26 in the central section to 1.99 in the west and the average V_f is 1.66, indicating moderate to slow tectonic activity. There are a number of stream offsets both across the basin bounding faults and across parallel faults in adjacent mountains (Fig. 16e). Convincing displacements are all left lateral and range from 310 m to 2.06 km (Fig. 16f). Most strike slip fault segments within the fault zone are parallel to the Kawa Fault and the two fault systems appear to be tectonically related and part of a broader zone of active left lateral shear linking to the Tarera Aiduna Fault in West Papua.

1567
 1568
 1569
 1570
 1571
 1572
 1573
 1574
 1575
 1576
 1577
 1578
 1579
 1580
 1581
 1582
 1583
 1584
 1585
 1586
 1587
 1588
 1589
 1590
 1591
 1592
 1593
 1594
 1595
 1596
 1597
 1598
 1599
 1600
 1601
 1602
 1603
 1604
 1605
 1606
 1607
 1608
 1609
 1610
 1611
 1612
 1613
 1614
 1615
 1616
 1617
 1618
 1619
 1620
 1621
 1622
 1623
 1624



The southern margin of Seram is locally formed by linear mountain fronts flanked by narrow fan deltas not more than 1 km wide. The steep, linear aspect and high topographic relief of the mountain fronts and the topographic lineaments that cross the fans parallel to the mountain front (Fig. 14b) suggest that the mountain front is defined by Quaternary normal faults. However, the coastal range is deeply eroded, with S_{mf} values of 1.84–2.08 and an average V_f of 1.62, indicating slow tectonic activity. Earthquake focal mechanisms towards the west of the coastal fault system in the region of Elaputih Bay support shallow focus, broadly south directed, steep normal faulting (Fig. 14a).

A number of other small suspected normal fault systems occur around the SW coast of Seram, including those bounding the Ambon Islands. One fault along the northern coast of Hitu (Fig. 14a) is particularly steep and straight, with an S_{mf} of 1.16 and well developed triangular facets along its 16 km long trace. A NE–SW trending lineament that passes through Ambon city marks the southern coast of Ambon Bay (Fig. 14c) and is associated with a zone of fault breccia and foliated gouge several metres thick (Fig. 14d). An M 7.6 earthquake occurred on 8 October 1950 close to the south coast of Ambon (Bath & Duda 1979), although it is unlikely that such an event could have been caused by the relatively short, dominantly normal faults visible onshore.

Buru

Buru consists of a presumed Palaeozoic continental metamorphic basement flanked by a Mesozoic sedimentary succession (Tjokrosapoetro *et al.* 1993), both of which are probably continuous with similar units in Seram (e.g. Pigram & Panggabean 1984; Linthout *et al.* 1989). Young K–Ar ages of 4–5 Ma (Linthout *et al.* 1989) and an apatite fission track central age of 2.5 ± 0.5 Ma suggest late Neogene exhumation, possibly accommodated by low angle normal faults (Roques 1999) as similarly postulated for western Seram (Pownall *et al.* 2013).

Intense shallow seismicity associated with Seram terminates abruptly in Manipa Strait, east of Buru (Fig. 17a). A broad belt of earthquakes in

Manipa Strait have CMT solutions indicating either NNE–SSW dextral events or WNW–ESE sinistral events, including a 14 March 2006 M_w 6.7 earthquake 25 km offshore. Most earthquakes have a component of reverse slip; others are pure thrust earthquakes with a NW–SE trend.

Most of Buru's sparse population lives in the NE of the island, including the major town, Namlea. A 5–10 km wide system of NW–SE trending faults cuts through the town, across Kayeli Bay, and defines the coastline (Fig. 17b). The faults are expressed in remote sensing data by linear hills and sag ponds at releasing right step overs, notably at Jikumerasa (Fig. 17c). Fault strands that cut through basement metamorphic rocks and alluvial fans show consistent stream offsets and pass directly into Quaternary alluvium and control modern river channels (Fig. 17d). Stream offsets of up to 85 m across individual strands are mostly right lateral; where they are left lateral there is clear evidence for stream capture. Variations in offset sense and amount are to be expected—streams are dynamic and are not passively offset like pre-kinematic geological markers. The process of offset, beheading and capture, leading to stream offsets of zero or opposite to the fault's shear sense, is well documented and widely observable in active faults worldwide (e.g. Wallace 1968; Sieh & Jahns 1984; Huang 1993; Walker & Allen 2012). All these features imply Quaternary NW–SE trending dextral fault activity in NE Buru, despite the apparent discordance with the few earthquake focal mechanisms recorded.

A broad fault zone 65 km long almost bisects Buru from the NE to SW (Figs 17a & 18a). Identified as left lateral on early geological maps (e.g. Tjokrosapoetro *et al.* 1981), little else is known about the fault zone, here termed the Rana Fault. Danau (lake) Rana, in the centre of Buru, occupies an intermontane basin within a right step over between two segments of the Rana Fault, suggesting that the fault is dextral. West of Wadule, Wa (river) Geren is abruptly diverted 90° from a broad oversized valley, which would have taken it to the coast in the NE of the island, into a narrow and steep sided canyon (Fig. 18a) that links with Wa Apu and empties into Kayeli Bay further south

Fig. 15. Evidence of Quaternary thrusting along the north coast of Seram. (a) ESRI image showing a number of NE flowing rivers flowing around linear elevated and forested regions. Location shown in Figure 14a. (b, c) Migrating rivers marked by filled channels and oxbow lakes and incision into uplifting regions. Google Earth imagery. Image © 2016 DigitalGlobe. (d) Interpretation of Figure 15a. Thick arrows indicate progressive migration of river channels; short arrows show coastline regression. Abandoned channels at points A, B and C are interpreted to represent the previous route of a river that entered the sea at D north of a meander plain at C, but was cut off by thrust hanging wall (HW) uplift at B and was forced to divert east from point A to join Wai Musi, leaving previous channels abandoned. Other rivers show lateral migration away from the growing tips of thrusts in response to hanging wall fold growth. See text for further details.

1625
1626
1627
1628
1629
1630
1631
1632
1633
1634
1635
1636
1637
1638
1639
1640
1641
1642
1643
1644
1645
1646
1647
1648
1649
1650
1651
1652
1653
1654
1655
1656
1657
1658
1659
1660
1661
1662
1663
1664
1665
1666
1667
1668
1669
1670
1671
1672
1673
1674
16 EDQ3
1676
1677
1678
1679
1680
1681
1682

1683
1684
1685
1686
1687
1688
1689
1690
1691
1692
1693
1694
1695
1696
1697
1698
1699
1700
1701
1702
1703
1704
1705
1706
1707
1708
1709
1710
1711
1712
1713
1714
1715
1716
1717
1718
1719
1720
1721
1722
1723
1724
1725
1726
1727
1728
1729
1730
1731
1732
1733
1734
1735
1736
1737
1738
1739
1740

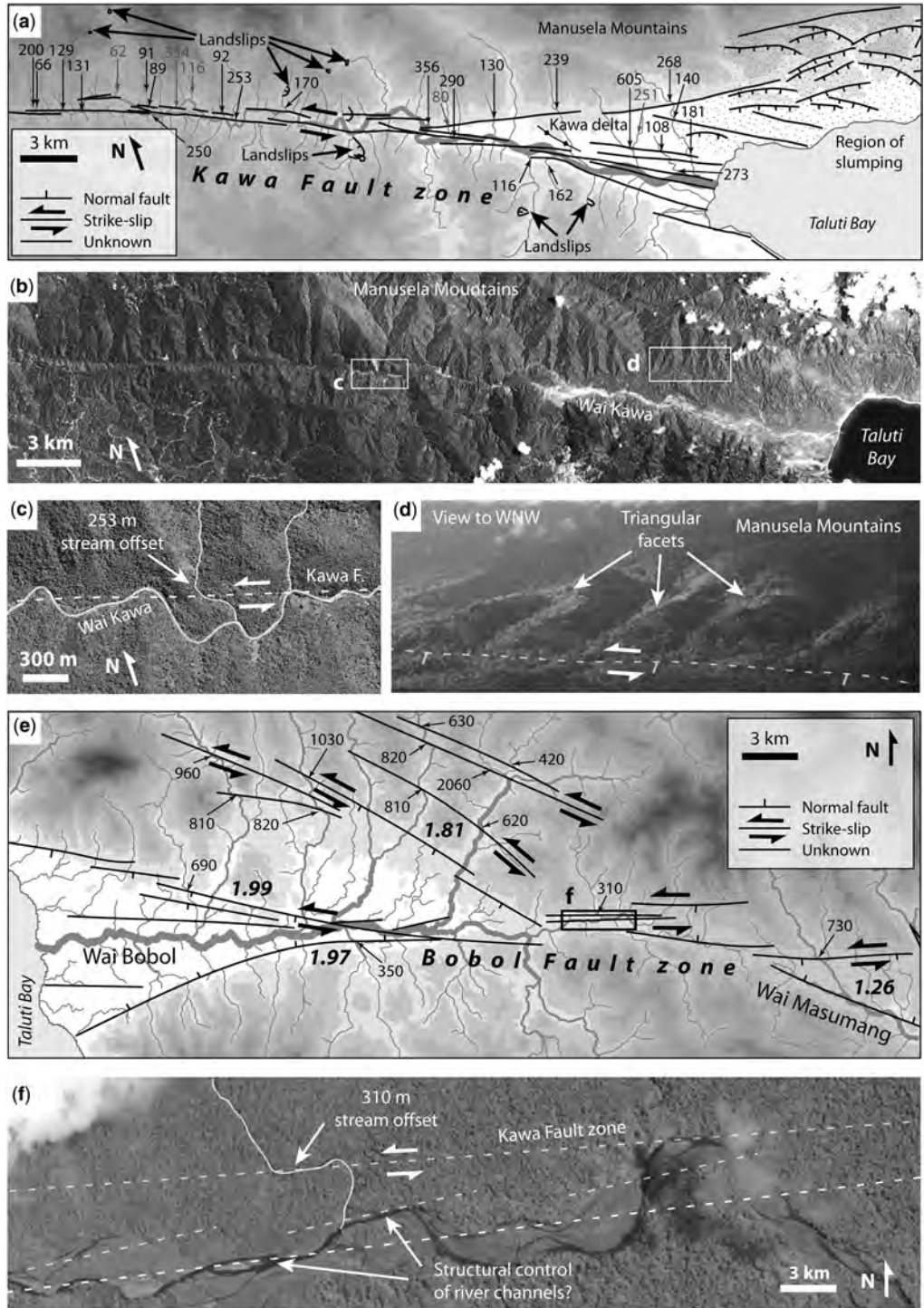


Fig. 16. Strike slip faults of southern Seram. (a) Overview map of the Kawa fault zone showing Quaternary fault strands, rivers, river offsets (in metres) and landslips. Left lateral offsets in black, right lateral offsets in grey. See Figure 14a for location. (b) ESRI image of the Kawa fault zone highlighting its clear geomorphic expression and

1741
1742
1743
1744
1745
1746
1747
1748
1749
1750
1751
1752
1753
1754
1755
1756
1757
1758
1759
1760
1761
1762
1763
1764
1765
1766
1767
1768
1769
1770
1771
1772
1773
1774
1775
1776
1777
1778
1779
1780
1781
1782
1783
1784
1785
1786
1787
1788
1789
1790
1791
1792
1793
1794
1795
1796
1797
1798

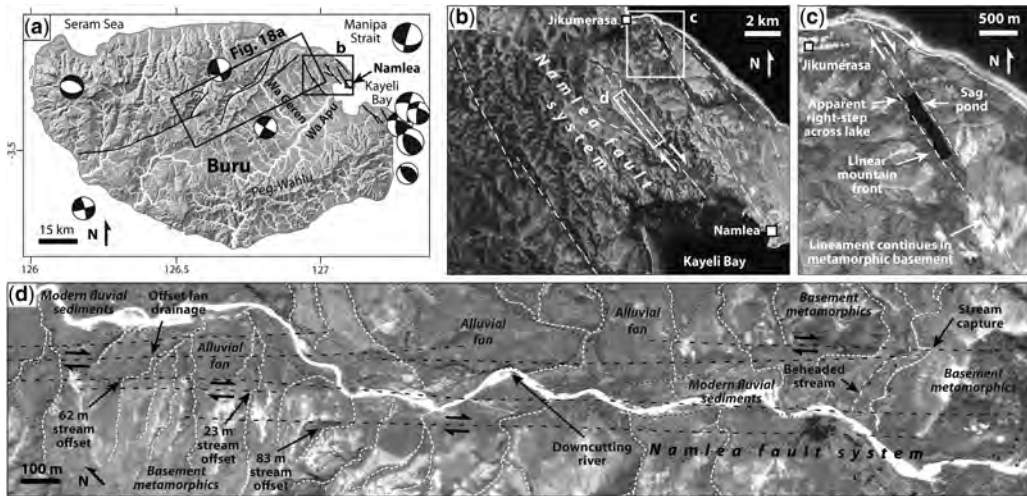


Fig. 17. Quaternary fault features in Buru. (a) Digital elevation model (SRTM), CMT catalogue earthquakes <35 km depth and structures that show geomorphic evidence of Quaternary tectonic activity. Rivers marked in white. Location shown in Figure 1. (b) Overview of topographic lineaments passing through Namlea and NE Buru. ESRI imagery. (c) Detail showing possible sag pond developed at the releasing step over between right stepping fault segments. (d) Evidence of strike slip faulting along the Namlea lineament trend. Lineaments pass from basement rock through Quaternary drift and are associated with systematic right lateral stream offsets. Image © 2016 DigitalGlobe.

(Fig. 17a). This pronounced capture of a northern drainage basin by a relatively minor tributary of Wa Apu appears to have been triggered by uplift at a left bend in the Rana Fault immediately east of the capture point (Fig. 18a), again suggesting Quaternary dextral shear.

Upstream of the Wa Geren stream capture, the Rana Fault has exceptionally fresh geomorphic expression (Fig. 18b, c), with pronounced triangular facets and very low S_{mf} values from 1.01 to 1.18 along the southern valley slope and a correspondingly low average V_f of 0.25, all suggesting a maximal to rapid tectonic rate. There are a number of beheaded and offset streams along the southern valley slope, although there is no consistent tectonic lateral offset. The axial river has migrated systematically eastwards in two places, leaving behind abandoned channels uplifted up to 10 m above the modern river channel (Fig. 18c). The uplift defines a pair of low amplitude right stepping en echelon periclinal, consistent with Quaternary right lateral shear. There is abundant evidence of revegetated

landslip scars in the surrounding hills close to the fault.

A c. 10 m high scarp along the base of alluvial fans in the valley, visible in high resolution Digital Globe satellite imagery from Google Earth, has the appearance of a normal fault surface rupture (Fig. 18d, e). The valley is relatively thinly vegetated and the scarp, discontinuous over c. 7.5 km, is well preserved. Although in places it is parallel to the modern river valley, the linear scarp also crosses higher ground, proving that it is not simply an erosional feature. By analogy with proved historical earthquake surface ruptures with a similar topographic expression for example, the 1857 Lone Pine earthquake (Beanland & Clark 1994) and the 1609 Hongyazi earthquake (Xu *et al.* 2010) the Buru scarp may have formed during the last few hundred years. The entire 10 m throw could have developed during a single M 7.5 earthquake, according to empirical relationships (Wells & Copper smith 1994), or during a number of smaller events, similar to the Star Valley Fault at Afton, Wyoming,

Fig. 16. (Continued) thick forest cover. (c) Representative stream offset across the main Kawa Fault strand, image from Google Earth. (d) View into the Kawa Fault from the Wai Kawa delta showing the linear mountain front and triangular facets developed along the northern strand of the Taluti Bay splay. Image © 2016 DigitalGlobe. (e) Overview map of the Bobol fault zone showing Quaternary fault strands, rivers and left lateral river offsets (in metres). Bold italic numbers are S_{mf} values. See Figure 14a for location. (f) Representative stream offset across the main Kawa Fault strand, also showing fault control of river channels. ESRI imagery.

1799
 1800
 1801
 1802
 1803
 1804
 1805
 1806
 1807
 1808
 1809
 1810
 1811
 1812
 1813
 1814
 1815
 1816
 1817
 1818
 1819
 1820
 1821
 1822
 1823
 1824
 1825
 1826
 1827
 1828
 1829
 1830
 1831
 1832
 1833
 1834
 1835
 1836
 1837
 1838
 1839
 1840
 1841
 1842
 1843
 1844
 1845
 1846
 1847
 1848
 1849
 1850
 1851
 1852
 1853
 1854
 1855
 1856

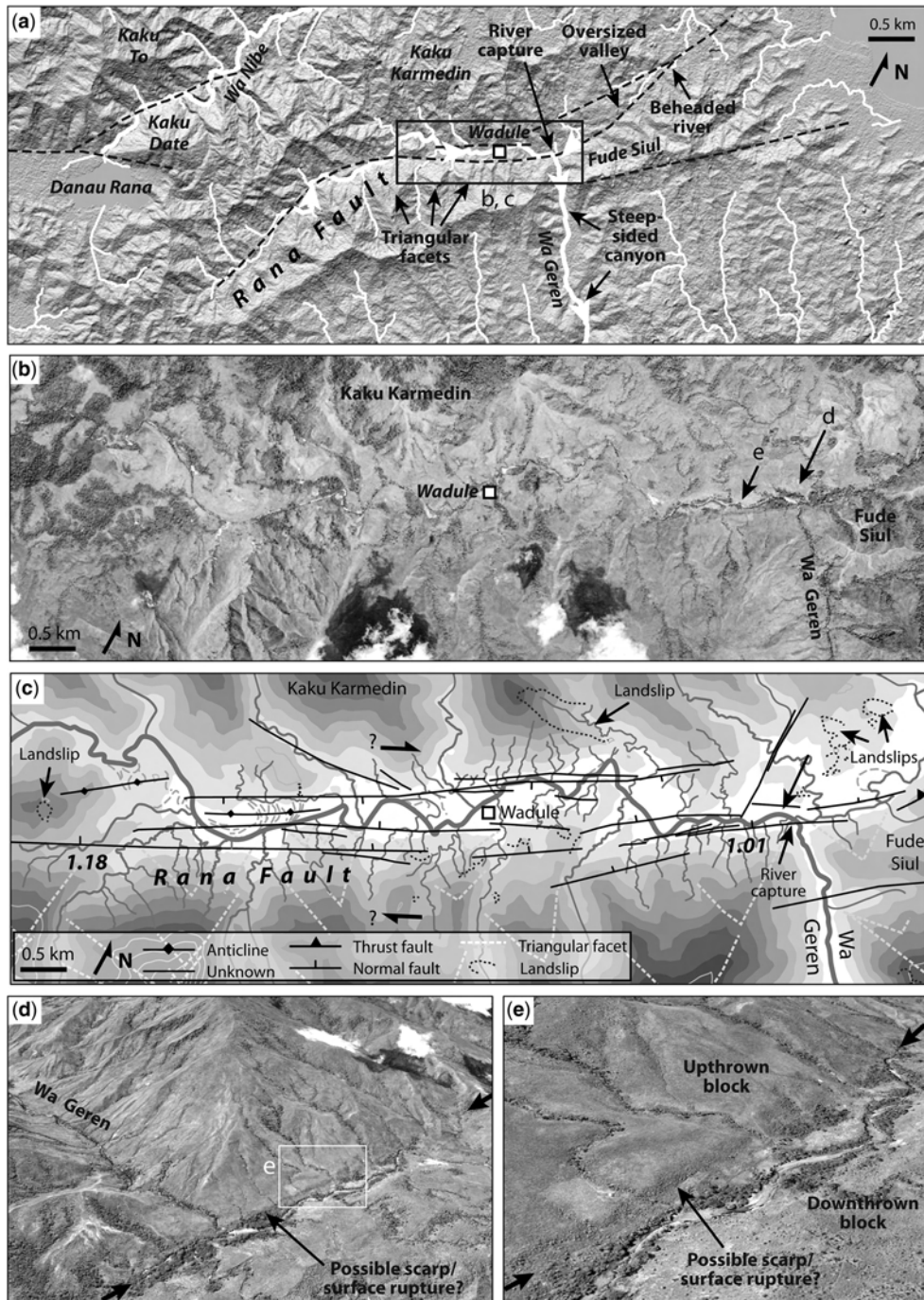


Fig. 18. Rana Fault, central Buru. (a) Overview of the Rana Fault, ASTER GDEM base map. Rivers marked in white, with white arrows showing the flow direction of major rivers discussed in the text. Location shown in Figure 17a. (b) ESRI image of the central part of the Rana Fault. (c) Interpretation of the image in (b), showing evidence of Quaternary fault activity. (d) Possible fault scarp along the foot of triangular facets marking the Rana Fault. (e) Detail of the possible fault scarp, showing steep dip, fresh geomorphic expression and straight trace. (d) and (e) are oblique views from Google Earth. Image © 2016 DigitalGlobe.

1857
1858
1859
1860
1861
1862
1863
1864
1865
1866
1867
1868
1869
1870
1871
1872
1873
1874
1875
1876
1877
1878
1879
1880
1881
1882
1883
1884
1885
1886
1887
1888
1889
1890
1891
1892
1893
1894
1895
1896
1897
1898
1899
1900
1901
1902
1903
1904
1905
1906
1907
1908
1909
1910
1911
1912
1913
1914

where an 11 m high scarp formed during three late Quaternary earthquakes (Piety *et al.* 1992). This is perhaps a more likely scenario given the relatively short length of the Rana Fault.

Elsewhere in Buru the geomorphic expression of other steep normal faults suggests rapid to moderate tectonic activity. Faults associated with the Rana Lake basin have S_{mf} values of 1.33–1.49 (Fig. 2j). Short fault segments in the SE of the island have S_{mf} values of 1.23 and 1.44, whereas those on the extreme east coast are more eroded, with S_{mf} values of 1.99 and 2.14 (Fig. 2k), indicating that they have been less active during the Quaternary.

Papua and West Papua

Oblique convergence at an angle of *c.* 60° between Australia and the Pacific is accommodated across Papua and West Papua in a complex zone of strain partitioning between shortening and left lateral shear (e.g. Abers & McCaffrey 1988; McCaffrey 1996). West of about 138° E shortening is largely accommodated on a variety of structures in the New Guinea Trench and Manokwari Trough, in the Mamberamo fold thrust belt and in the central Highlands to the south (e.g. Milsom *et al.* 1992; Puntodewo *et al.* 1994; Stevens *et al.* 2002). The largest earthquake to occur in eastern Indonesia

since 1938 was the tsunamigenic 17 February 1996 M_w 8.2 Biak earthquake, which was also the largest thrust event worldwide since 1977 (Henry & Das 2002) and may have been associated with the 1979 M 7.9 Yapen earthquake (Okal 1999).

Left lateral strain of up to 80 mm a⁻¹ resulting from oblique Australia Pacific convergence is accommodated across a 300 km wide zone of sinistral shear (Stevens *et al.* 2002) focused on the Yapen Fault system in the north and stepping across Cenderawasih Bay to the Tarera–Aiduna Fault system in the south, largely bypassing the antecedent Sorong Fault in West Papua (e.g. Puntodewo *et al.* 1994; McCaffrey 1996; Stevens *et al.* 2002; Bock *et al.* 2003). Left lateral shear is passed from the Tarera–Aiduna Fault westwards into Maluku via the highly transpressive Seram fold thrust belt (Teas *et al.* 2009).

As in Sulawesi, Maluku and North Maluku, extension is important within the overall convergent orogen. Cenderawasih Bay and the adjacent Waiyoga Basin contain thick sediment piles (e.g. Dow & Sukanto 1984; Pubellier *et al.* 1999; Charlton 2010) and metamorphic core complex exhumation at the Wandamen Peninsula (e.g. Bailly *et al.* 2009) indicates extreme lithospheric stretching. Although extension may be related to processes within the wide left lateral shear zone (Stevens *et al.* 2002), lessons from Sulawesi suggest that

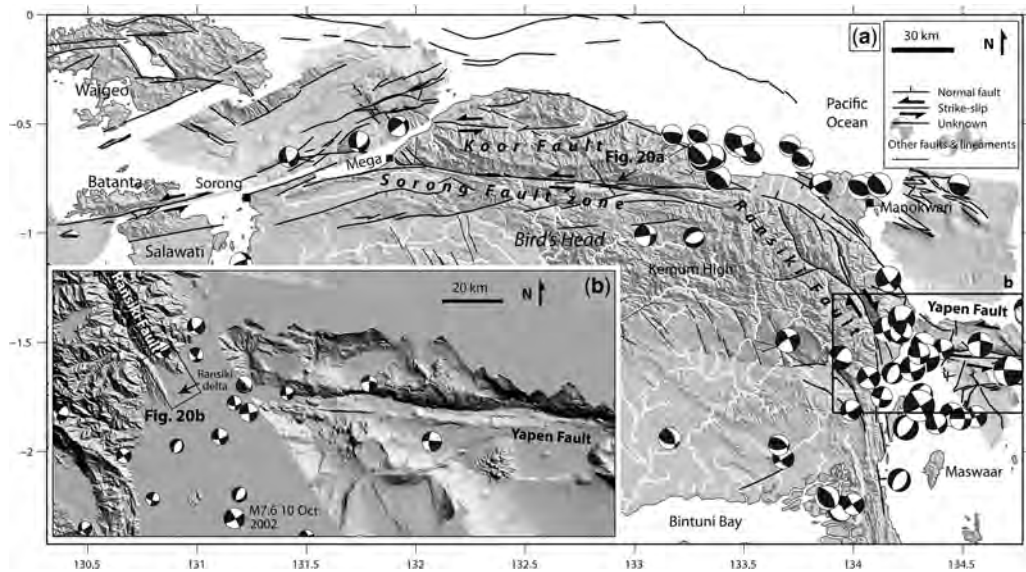


Fig. 19. (a) Bird's Head (West Papua) digital elevation model (SRTM), multibeam bathymetry, CMT catalogue earthquakes <35 km depth and structures showing evidence of Quaternary tectonic activity. Rivers marked in white. Location shown in Figure 1. Offshore structures north of the Koor Fault from Milsom *et al.* (1992). (b) Detail of the intersection between the Ransiki and Yapen faults, south of Manokwari. Eastern limit of image is to the east of the main map. SRTM onshore, multibeam bathymetry offshore.

1915 far field subduction related mechanisms may also
 1916 be significant.

1917
 1918
 1919

Sorong Fault in West Papua

1920 The Sorong Fault in West Papua is marked by a
 1921 15 km wide zone of pronounced linear ridges and
 1922 valleys trending ENE from northern Salawati
 1923 through Sorong city and into the deep valley cutting
 1924 across the northernmost mainland towards Manok
 1925 wari in the east (Fig. 19a). Hamilton (1979) ques
 1926 tioned whether this structure was significant in
 1927 post Miocene tectonics, pointing out that parts of
 1928 it were covered by post Miocene strata, and it is now
 1929 generally considered to be inactive (e.g. Puntodewo
 1930 *et al.* 1994; Decker *et al.* 2009; Charlton 2010).

1931 There is little significant seismicity along
 1932 much of the fault and geodetic measurements sug
 1933 gest that both sides of the fault are broadly moving
 1934 together and with the Pacific (e.g. Puntodewo *et al.*
 1935 1994; Stevens *et al.* 2002), with slight residual left
 1936 lateral motion between the Sorong and Fakfak GPS
 1937 stations possibly accommodated on the Sorong
 1938 Fault or the Koor Fault to the north (Bock *et al.*
 1939 2003). However, the Sorong GPS station is south
 1940 of important strands of the Sorong Fault, which lie
 1941 offshore to the north and come onshore at Mega,
 1942 and the station is certainly south of the Koor Fault,
 1943 leaving substantial uncertainty in the amount of
 1944

present day left lateral strain accommodated across
 this zone. The April 1937 M 6.9 and April 1944 M
 7.2 and 7.4 earthquakes relocated by Okal (1999)
 were located on the onshore Sorong Fault 50
 100 km west of Manokwari and had focal mecha
 nisms indicating left lateral shear. Apparent right
 lateral motion between the Sorong and Biak GPS
 stations, taken to lie on opposite sides of the Sorong
 Fault (Puntodewo *et al.* 1994), is complicated by
 other structures such as the Ransiki and Yapen
 faults, which also lie between the stations.

Numerous convincing left lateral stream offsets
 of up to 300 m are documented in the central part
 of the fault valley (Dow & Sukamto 1984) (Fig.
 20a). Similar sized displacements of Wallace
 Creek crossing the San Andreas Fault have been
 dated to 13 259 years (Sieh & Jahns 1984). It is
 unclear how long such offsets can be preserved in
 the landscape of an environment like West Papua,
 but it is unlikely they are pre Quaternary. Given
 that few such offsets are preserved in the more obvi
 ously active faults of eastern Indonesia, such as the
 Palu Koro and Matano faults, the Sorong Fault
 examples must reflect relatively recent and signifi
 cant strike slip. Mountain front sinuosity along
 those segments of the fault associated with vertical
 motions is also conspicuously low, ranging from
 1.16 to 1.17 along segments NNE of Sorong city
 to 1.14 along the central section, where Dow &

1945
 1946
 1947
 1948
 1949
 1950
 1951
 1952
 1953
 1954
 1955
 1956
 1957
 1958
 1959
 1960
 1961
 1962
 1963
 1964
 1965
 1966
 1967
 1968
 1969
 1970
 1971
 1972

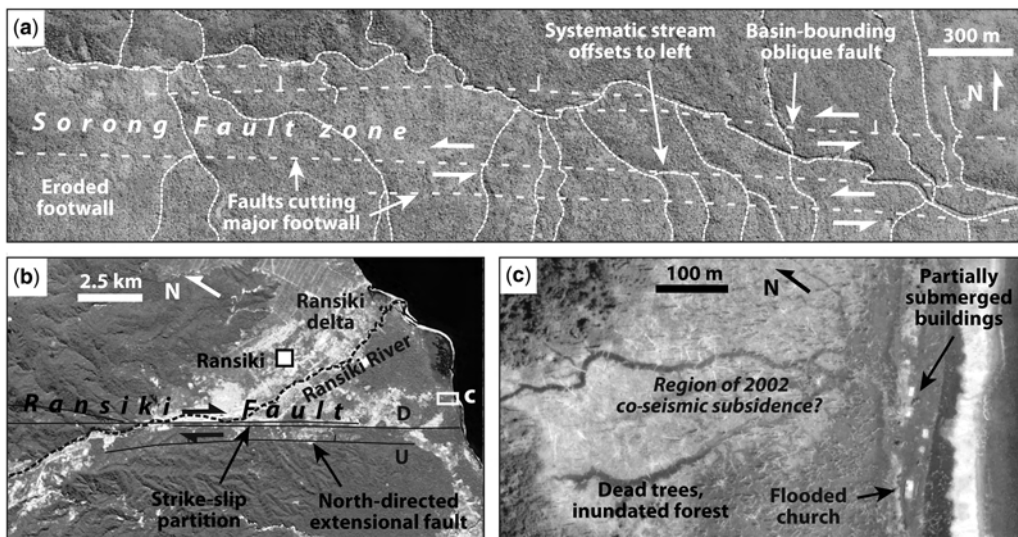


Fig. 20. Evidence of Quaternary fault activity in the Bird's Head. (a) Section of the onshore Sorong Fault showing a basin bounding normal fault in the north and two strike slip fault strands offsetting streams to the left in the south. Location shown in Figure 19a. ESRI imagery. (b) Ransiki delta at the southern end of the Ransiki Fault showing prominent western normal fault, strike-slip partition, and north-directed extensional fault. Location shown in Figure 19b. (c) Region of co seismic subsidence showing flooded forest and buildings adjacent to the western normal fault. Google Earth Imagery. Image © 2016 DigitalGlobe.

Sukamto (1984) measured displaced streams and where triangular facets and shutter ridges are well developed. In the east, S_{mf} values of 1.20 and 1.33 also suggest active tectonics. Faults adjacent to flat topped Quaternary basins associated with Sorong Fault releasing geometries are interpreted to be dominantly normal faults (Fig. 20a) and these structures have generally higher S_{mf} values, including 1.60, 1.61, 1.74 and 2.79. The average V_f value for all these fault segments is 1.15, consistent with moderate to slow tectonic activity.

Koor Fault and Ransiki Fault

The Koor Fault is an east west trending structure 20–30 km north of the Sorong Fault (Fig. 19a), which lies within a boundary zone between the oceanic Pacific plate and continental crust in the south (Dow & Sukamto 1984). The NNW trending Ransiki Fault (Fig. 19a) has been viewed as a dextral shear zone linking the easternmost Sorong Fault and the Yapen Fault (e.g. Robinson & Ratman 1978; Milsom *et al.* 1992; Charlton 2010).

Like the Sorong Fault in West Papua, both the Koor and Ransiki faults have been considered to be inactive (e.g. Hamilton 1979; Puntodewo *et al.* 1994). However, a shallow M 7.6 earthquake on 10 October 2002 at the southern end of the Ransiki Fault (Fig. 19b) had a focal mechanism and after shock distribution consistent with dextral slip along the Ransiki Fault (NEIC), although the possibility of sinistral slip along a NE–SW trending splay of the Yapen Fault cannot be excluded. Topographic and bathymetric data from the intersection (Fig. 19b) could be interpreted to show the two structures curving gently into each other, leading to the possibility of contraction in the Ransiki area.

Mountain front sinuosity measured along two splays of the southern Ransiki Fault yields values of 2.64 for a clearly inactive, c. north–south trending southwestern strand, and 1.06 for the linear fault bounding the southern margin of Ransiki delta (Figs 2p & 19b). The very low S_{mf} and the asymmetrical position of the Ransiki River close to the fault scarp (Fig. 20b) support recent extensional activity along the fault. A 2 m high coseismic surface rupture formed close to the fault scarp during the 2002 earthquake and was associated with subsidence of the delta that flooded a low lying church (D. Gold, pers. comm. 2013), visible in satellite imagery to be coincident with a large region of flooded forest (Fig. 20c).

Yapen Fault

The Yapen Fault (Fig. 21a) is a highly linear east–west trending structure that crosses the 320 km wide northern Cenderawasih Bay and is similar in

character to the Sorong Fault in West Papua (e.g. Hamilton 1979; Dow & Sukamto 1984). In the east, the Yapen Fault vanishes into the Mamberamo delta (Fig. 21a), where it forms a subtle linear valley delineated by active mud volcanoes (Dow & Sukamto 1984) and may dissipate into the Mamberamo fold–thrust belt (Puntodewo *et al.* 1994). In the west, the Yapen Fault has an unclear termination, variously interpreted as being dextrally offset from the Sorong Fault along the Ransiki Fault (Puntodewo *et al.* 1994; Charlton 2010), linking/terminating against the Ransiki Fault (Milsom *et al.* 1992) and unconnected to inactive Ransiki/onshore Sorong faults, but transferring strain south to the Wandamen fault system (Bailly *et al.* 2009).

Geodetic measurements indicate a fast left lateral slip rate of 46 ± 12 mm a⁻¹ across the Yapen Fault (Bock *et al.* 2003), expressed by intense seismicity and focal mechanisms indicating left lateral slip along east–west trending subvertical planes (e.g. Okal 1999; Stevens *et al.* 2002). The 12 September 1979 M 7.9 tsunamigenic earthquake on the south coast of Yapen island (Fig. 21a) was associated with sinistral slip along a ESE–WNW trending plane focused at a depth of 5 km and probably caused 2 m of displacement (Okal 1999).

The Randaway Fault Zone (Dow & Hartono 1982) is a set of NW–SE trending faults onshore Yapen that link to strands of the Yapen Fault in the north (Fig. 21b). Interpreted as post Pliocene normal faults, they have previously been used to support a period of right lateral shear along the Yapen Fault zone (Charlton 2010). However, we saw no geomorphic evidence of significant normal faulting along the Randaway trend – instead we saw a small linear basin and lake near the northern tip of the Randaway Fault at a left step over and a deeply incised stream offset to the left by almost 1 km – both evidence of Quaternary sinistral shear (Fig. 21b).

Although the north coast of Yapen is remarkably straight and clearly fault controlled, the main fault mostly lies just offshore to the north, meaning that geomorphic indices could not be usefully measured along the Yapen Fault. Multibeam bathymetry east of the island shows the Yapen Fault expressed by a straight, narrow lineament marked by pressure ridges and parallel to a prominent set of curvilinear normal faults (Fig. 21c). Splays of the fault curving to the WSW delimit at least two rhomboidal pull apart basins. At the western limit of the multibeam data a splay appears to enter a third pull apart basin, which is associated with a prominent north–south trending sidewall fault. It is significant that this structure is parallel to, and 60 km north, of the Wandamen Peninsula – perhaps support for the southwards transfer of sinistral shear from the Yapen

1973
1974
1975
1976
1977
1978
1979
1980
1981
1982
1983
1984
1985
1986
1987
1988
1989
1990
1991
1992
1993
1994
1995
1996
1997
1998
1999
2000
2001
2002
2003
2004
2005
2006
2007
2008
2009
2010
2011
2012
2013
2014
2015
2016
2017
2018
2019
2020
2021
2022
2023
2024
2025
2026
2027
2028
2029
2030

2031
 2032
 2033
 2034
 2035
 2036
 2037
 2038
 2039
 2040
 2041
 2042
 2043
 2044
 2045
 2046
 2047
 2048
 2049
 2050
 2051
 2052
 2053
 2054
 2055
 2056
 2057
 2058
 2059
 2060
 2061
 2062
 2063
 2064
 2065
 2066
 2067
 2068
 2069
 2070
 2071
 2072
 2073
 2074
 2075
 2076
 2077
 2078
 2079
 2080
 2081
 2082
 2083
 2084
 2085
 2086
 2087
 2088

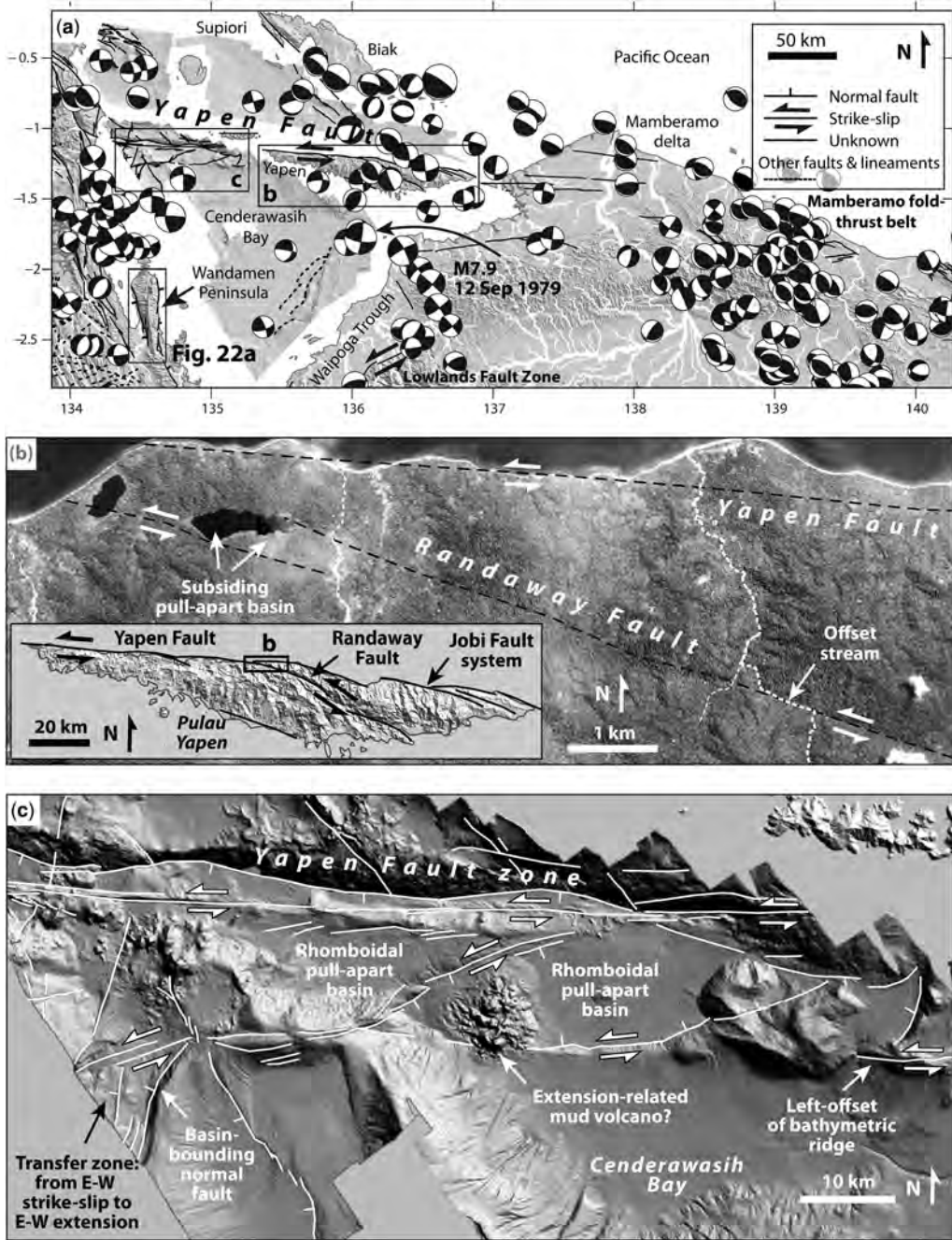


Fig. 21. Northern Papua and Cenderawasih Bay digital elevation model (SRTM), multibeam bathymetry, CMT catalogue earthquakes <35 km depth and structures showing geomorphic evidence of Quaternary tectonic activity. Rivers marked in white. Location shown in Figure 1. (b) Expression of the Yapen and Randaway faults along the northern coast of Pulau Yapen, showing evidence for Quaternary sinistral slip along the Randaway Fault. Inset shows the topography and major structures of Yapen. ESRI imagery. (c) Multibeam bathymetry detail showing the Yapen Fault to the west of Pulau Yapen; the southern strands appear to transfer to north-south extension via a series of pull-apart basins.

2089
2090
2091
2092
2093
2094
2095
2096
2097
2098
2099
2100
2101
2102
2103
2104
2105
2106
2107
2108
2109
2110
2111
2112
2113
2114
2115
2116
2117
2118
2119
2120
2121
2122
2123
2124
2125
2126
2127
2128
2129
2130
2131
2132
2133
2134
2135
2136
2137
2138
2139
2140
2141
2142
2143
2144
2145
2146

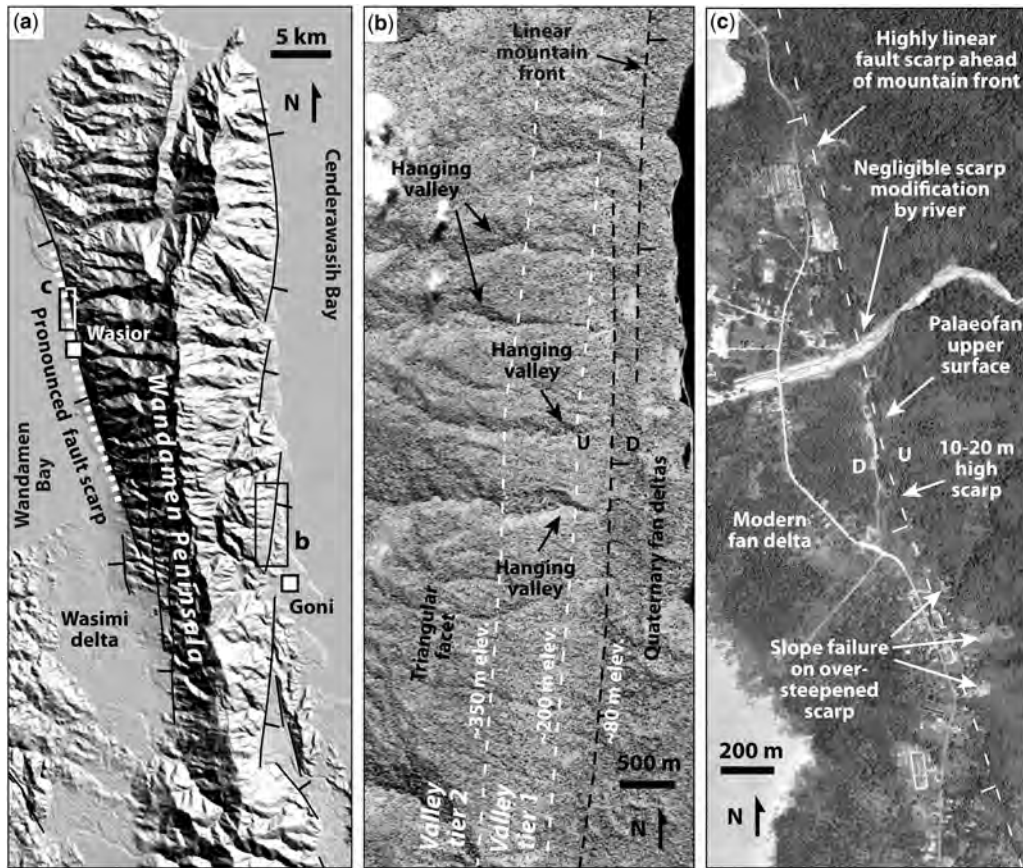


Fig. 22. Evidence of Wandamen Peninsula Quaternary fault activity. (a) Overview digital elevation model (SRM) showing bounding normal faults. Location shown in Figure 21a. (b) Pronounced triangular facets and hanging valleys along the eastern bounding fault system. ESRI imagery. (c) Inferred Quaternary fault trace across the top of alluvial fans crossing the western fault system. Google Earth imagery. Image © 2016 DigitalGlobe.

Fault via a region of east west extension, as proposed by Bailly *et al.* (2009).

south (Puntodewo *et al.* 1994; McCaffrey 1996; Bock *et al.* 2003) (Fig. 1).

Mamberamo fold thrust belt

Wandamen Peninsula faults

The Mamberamo fold thrust belt (Fig. 21a) probably accommodates some Australia Pacific shortening in eastern Papua and lies north of the Highlands thrust belt of central New Guinea (e.g. Dow & Sukanto 1984). Unlike the complex oblique convergence and strain partitioning further west, the belt contains relatively simple NW trending active structures oriented normal to convergence (McCaffrey 1996). Despite intense and widespread seismicity, less than 15 mm a⁻¹ of shortening occurs across the Mamberamo belt, leaving much of the remaining 45 mm a⁻¹ Australia Pacific convergence and 100 mm a⁻¹ of left lateral motion to offshore structures to the north and the Highlands thrust belt to the

The Wandamen Peninsula projects into Cenderawasih Bay from the eastern edge of the Lengguru fold belt, and is bounded on the east and west sides by north south trending faults (Fig. 22). We refer here specifically to these faults, not to the Wandamen Fault Zone of Dow & Sukanto (1984) that connects the Sorong Fault with the Tarera Aiduna fault system via the Ransiki Fault.

The peninsula is considered to represent the exhumed internal zone of the Lengguru fold belt and is composed of an amphibolite eclogite grade metamorphic dome rising to >2 km elevation (Robinson *et al.* 1990; Bailly *et al.* 2009; Charlton 2010), which may be a metamorphic core complex

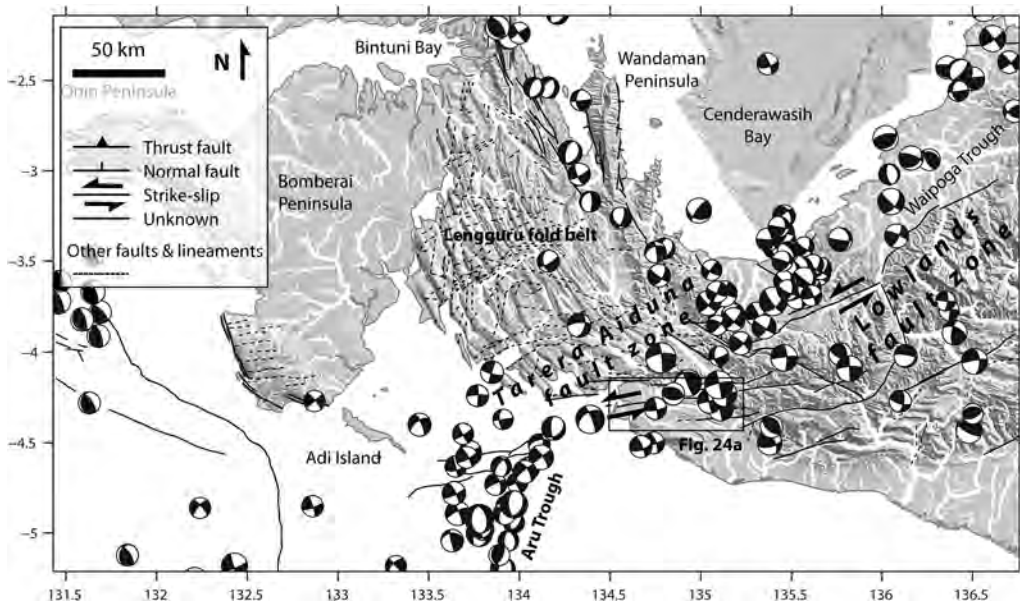
2147 (e.g. Hill *et al.* 2002). Seismicity and GPS vectors
 2148 either side of Cenderawasih Bay (Stevens *et al.*
 2149 2002) suggest active extension accommodated on
 2150 north south trending structures close to the Wan
 2151 damen Peninsula, which may connect to the western
 2152 releasing termination array of the Yapen Fault in the
 2153 north (Fig. 21c).

2154 Normal faults bounding the peninsula are
 2155 expressed by curvilinear en echelon segments up
 2156 to 20 km long trending north south to NNW
 2157 SSE. These make up the east and west detachment
 2158 systems of Bailly *et al.* (2009). Triangular facets,
 2159 hanging valleys and V shaped valleys are common
 2160 and indicate rapid tectonic activity (Fig. 22b).
 2161 Two tiers of hanging valleys on the eroded scarp
 2162 of the eastern fault system are defined by changes
 2163 in valley width or orientation at common elevations
 2164 along the scarp. They probably record variations
 2165 in the tectonic rate or climate during exhumation
 2166 of the fault surface. Mountain front sinuosity values
 2167 of four segments on the east side are uniform
 2168 at 1.25, 1.28 and 1.29, with one more eroded seg
 2169 ment of 1.72. Fan deltas are well developed at
 2170 relays between the fault segments, notably at Goni
 2171 and another smaller delta 21 km further north
 2172 (Fig. 22a). As well as localizing sediment transport,
 2173 the relays are likely to be sites of active displac
 2174 e ment minima, allowing subaerial delta progradat
 2175 ion on the hanging wall.

On the west of the peninsula, S_{mf} values range
 from 1.05 to 1.43, indicating maximal to rapid
 tectonic activity. A 21 km long section of the west
 ern fault system passing through Wasior shows
 evidence of recent normal faulting (Fig. 22c).
 Upper modern fan deltas are abruptly terminated
 by a linear scarp, above which are narrow truncated
 palaeofans. Rivers vertically incised into footwall
 palaeofans show little evidence of lateral erosion
 and small landslides are localized along the over
 steepened scarp. The scarp is marked by a linear
 change in topography, lines of vegetation and
 often an abrupt change from meandering rivers up
 stream to anastomosing rivers downstream of the
 scarp. A southern continuation of the Wandamen
 fault system bounds the eastern margin of the
 Wasimi delta and has an S_{mf} value of 2.33, indicat
 ing slow to minimal tectonic activity.

Other circum-Cenderawasih Bay structures

The locus of active Australia Pacific left lateral
 strain partitioning shifts from the Yapen Fault sys
 tem to the Tarera Aiduna Fault system across Cen
 derawasih Bay, defining a 300 km wide shear zone
 that involves a complex array of Quaternary faults
 within the two bounding strike slip zones (e.g. Ste
 vens *et al.* 2002; Bock *et al.* 2003). Along the east
 ern margin of Cenderawasih Bay, the NE trending



2202 **Fig. 23.** Southern West Papua and Cenderawasih Bay digital elevation model (SRTM),
 2203 multibeam bathymetry, CMT catalogue earthquakes <35 km depth and structures showing geomorphic evidence of Quaternary tectonic
 2204 activity. Rivers marked in white. Location shown in Figure 1. Offshore structures from Teas *et al.* (2009).

2205 Lowlands Fault Zone (bounding the Waipoga
2206 Trough of Visser & Hermes 1962) and the Paniai
2207 Fault Zone are associated with thrust and left lateral
2208 strike slip earthquakes (Fig. 23), offset drainage and
2209 high fault scarps, indicating modern tectonic activ-
2210 ity (Pubellier *et al.* 1999; Stevens *et al.* 2002). The
2211 faults have a soft linkage with the Tarera Aiduna
2212 Fault system in the south and splays curve into par-
2213 allelism with the Yapen Fault and Mamberamo
2214 fold thrust belt in the north.

2215 The Lengguru fold belt (Visser & Hermes 1962)
2216 lies SW of Cenderawasih Bay and the Wandamen
2217 Peninsula, east of Bintuni Bay and the Bomberai
2218 Peninsula, and is bounded by the Tarera Aiduna
2219 fault system in the south (Fig. 23). Compressional
2220 deformation terminated during the Pleistocene
2221 (Decker *et al.* 2009) and the belt is presently largely
2222 inactive, except for a few earthquakes related to
2223 gravitational collapse (Bailly *et al.* 2009), often
2224 with a left lateral component related to residual Tar-
2225 era Aiduna strain.

2226

2227

2228

Tarera Aiduna Fault

2229

2230

2231

2232

2233

2234

2235

2236

2237

2238

2239

2240

2241

2242

2243

2244

2245

2246

2247

2248

2249

2250

2251

2252

2253

2254

2255

2256

2257

2258

2259

2260

2261

2262

The Tarera Aiduna Fault (Visser & Hermes 1962) is an east west trending left lateral shear zone that forms the southern boundary of the Lengguru fold belt and passes offshore to the west, north of the Aru Trough (Fig. 23). The Tarera Aiduna Fault *sensu stricto* is part of a wide system of faults that pass, via a diffuse zone of sinistral transpression, into the Seram fold thrust belt in the west (Teas *et al.* 2009). The fault system is at least 130 km long onshore (Fig. 24) and is expressed by straight lineaments clearly visible on satellite imagery (Hamilton 1979) and a set of en echelon folds (Katili 1986). Including possible soft linkage to Seram via sinistral transpression within the Seram fold thrust belt, imaged in multibeam bathymetric data (Teas *et al.* 2009), the whole fault system may be >700 km long. Geodetic measurements show high relative motion between the Bird's Head north of the Tarera Aiduna Fault and GPS stations south of the fault, such as Aru and Timika (Bock *et al.* 2003). Earthquake focal mechanisms showing sinistral slip along east west trending vertical planes (e.g. Seno & Kaplan 1988) suggest that the motion onshore is seismic and occurs along a broad zone (Fig. 23). Seismicity is largely absent west of the Bomberai peninsula, suggesting either a wide zone of aseismic deformation linking the Tarera Aiduna Fault with the Seram sinistral transpression (Teas *et al.* 2009), a region of seismic deformation with recurrence times longer than the instrumental record, or no structural connection between the two regions.

The onshore Tarera Aiduna Fault has a geomorphic expression typical of a major strike slip fault

zone (Fig. 24a). In the west it passes across a low lying mangrove plain with minimal topographic relief. It is possible to trace several fault strands from linear features revealed by abandoned river channels and coastline segments (Fig. 24b). Its central section is expressed by a series of linear ridges of moderate relief bounding a wide rhomboidal basin (Fig. 24c), across which the captured Aru River passes into the Uruma River in the south. The river is abruptly deflected as it crosses two prominent fault strands, with 65–75 m left lateral displacement, which may reflect recent Tarera Aiduna Fault slip (Fig. 24d, e), although this offset is rather speculative.

An asymmetrical graben developed at the eastern termination of the Tarera Aiduna Fault is bounded by NE–SW trending normal faults (Fig. 24f). Rivers pressed hard against the NW dipping bounding faults and a SE dipping set of antithetic faults indicate active subsidence. The easternmost Tarera Aiduna Fault itself has a significant dip slip component, forming the northern margin of an 800 m high ridge. The Tarera Aiduna Fault and the eastern bounding normal fault have S_{mf} values of 1.08 and 1.21, respectively, indicating that they are both active. Bounding faults along the northern margin of the rhomboidal basin, including segments corresponding to the Aria River Fault of Hamilton (1979), have S_{mf} values of 1.63, 1.91 and >4.00, pointing to slow to inactive tectonics.

Discussion

Challenges

The identification of Quaternary/modern fault activity in eastern Indonesia has historically proved difficult (e.g. Hamilton 1979; Dow & Sukanto 1984; Puntodewo *et al.* 1994; Socquet *et al.* 2006; Bailly *et al.* 2009; Teas *et al.* 2009). In part, this is because eastern Indonesia cannot be well described in terms of rigid plate tectonics, involving instead diffuse boundaries and boundary linkages, lithospheric strength heterogeneity and lower crustal flow (Hall 2011). All the fault zones in the region that are relatively well constrained by geodetic data display strain gradients that can be explained in terms of multiple fault strands, distributed deformation or elastic strain surrounding a locked fault (e.g. Walpersdorf *et al.* 1998; Rangin *et al.* 1999; Stevens *et al.* 2002; Bock *et al.* 2003; Socquet *et al.* 2006). Poor historical earthquake records and few palaeoseismic data mean that it is difficult to distinguish between these options and so attention is naturally focused on geomorphologically prominent faults and lineaments or structures with instrumentally recorded seismicity. Faults or segments of fault systems with recurrence intervals greater than

2263
2264
2265
2266
2267
2268
2269
2270
2271
2272
2273
2274
2275
2276
2277
2278
2279
2280
2281
2282
2283
2284
2285
2286
2287
2288
2289
2290
2291
2292
2293
2294
2295
2296
2297
2298
2299
2300
2301
2302
2303
2304
2305
2306
2307
2308
2309
2310
2311
2312
2313
2314
2315
2316
2317
2318
2319
2320

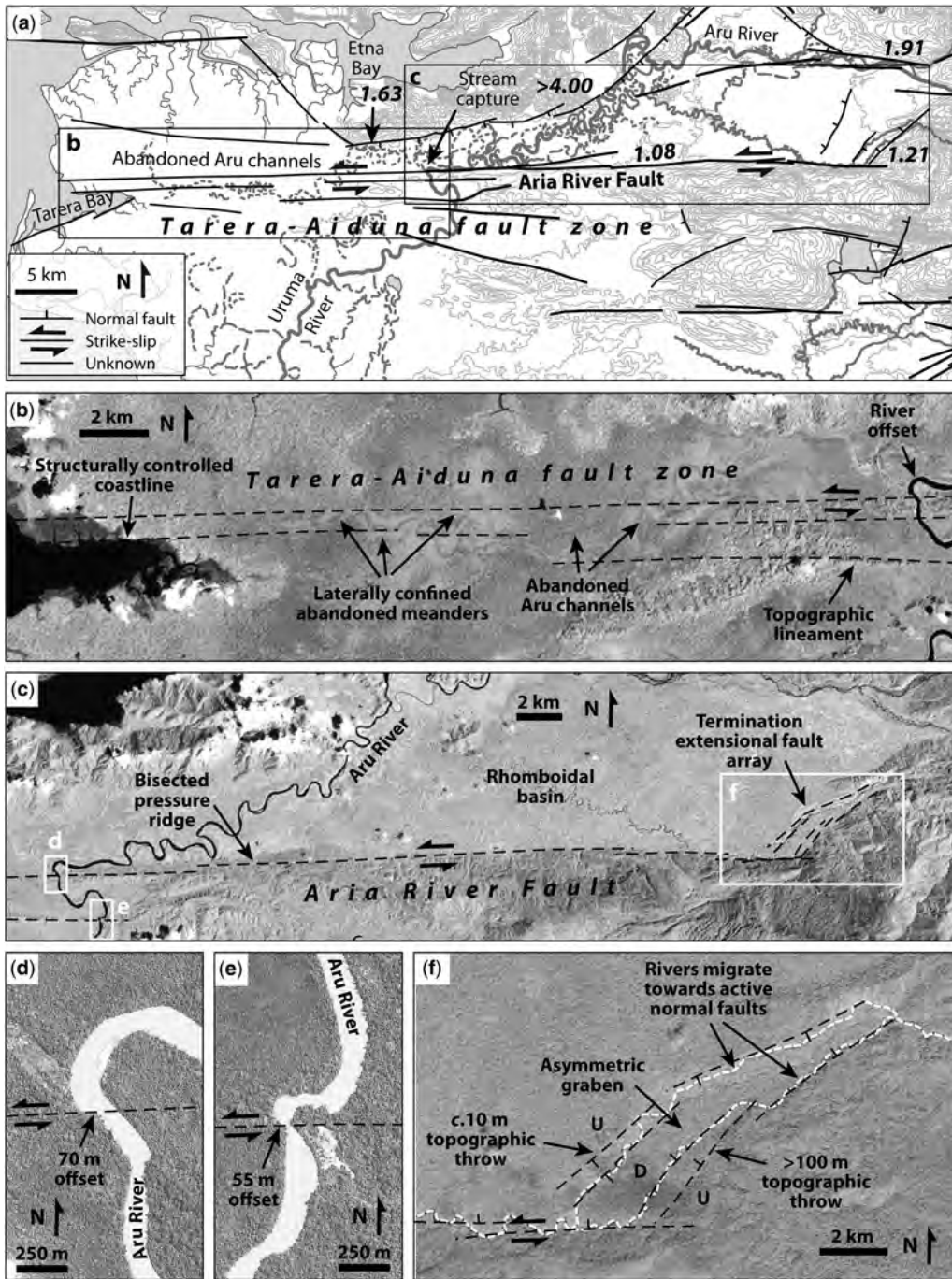


Fig. 24. (a) Map of the onshore Tarera–Aiduna Fault showing structures with geomorphic evidence of Quaternary tectonic activity. Bold italic numbers are S_{mf} values. Location shown in Figure 23. (b) Detail from greyscale Landsat TM 432 image showing linear confinement of abandoned River Aru channels, indicating strike slip strands across the plain. (c) Major strand of the Tarera–Aiduna Fault bounding a steep sided ridge and rhomboidal basin. (d, e) Possible river offset across the Tarera–Aiduna Fault. (f) Termination extensional fault array developed at the eastern end of the main Tarera–Aiduna Fault strand. (d, e, f) from ESRI imagery.

2321 the short period of instrumental or even historical
2322 seismic records inevitably remain undocumented.

2323 Additional challenges to the identification of
2324 Quaternary faults include thick forest over most of
2325 the islands (e.g. Pubellier *et al.* 1999), the abun-
2326 dance of important structures located entirely off
2327 shore and not readily available for study (e.g.
2328 Silver *et al.* 1983b; Henry & Das 2002; Teas *et al.*
2329 2009; Liu & Harris 2013), the rapid erosion of tec-
2330 tonic landforms in the humid environment, the
2331 rapid burial of co seismic features by a high sedi-
2332 ment flux (e.g. Suggate & Hall 2003) and the high
2333 density of active and inactive structures within a
2334 large region (e.g. Puntodewo *et al.* 1994; Stevens
2335 *et al.* 2002).

2336 Of the 27 fault systems described here, none
2337 can be confidently described as inactive during the
2338 Quaternary. Eleven show evidence of 'maximal'
2339 tectonic activity according to the classification sum-
2340 marized in McCalpin (2009) and a further five show
2341 evidence of 'rapid' tectonic activity (Table 3). It is
2342 important to note that the Quaternary faults dis-
2343 cussed here are not exhaustive there are numerous
2344 other active faults in the region, in addition to major
2345 offshore seismic sources, such as the Molucca Sea
2346 collision complex, the Banda Sea and Molucca
2347 Sea subducted slabs, and ongoing subduction of
2348 the Celebes Sea (e.g. Cardwell & Isacks 1978; Sil-
2349 ver & Moore 1978; Cardwell *et al.* 1980; Silver
2350 *et al.* 1983a; Engdahl *et al.* 1998), which also
2351 need to be taken into account in any hazard analysis.

2352 *Quaternary fault geometry and earthquakes*

2353 The largest earthquakes in eastern Indonesia have
2354 been thrust and mega thrust events, including those
2355 of the Seram Trough (1629, $M > 8.5$), the Banda
2356 Sea (1938, $M > 8.0$) and Biak (1996, M_w 8.2)
2357 (e.g. Wichmann 1918; Henry & Das 2002; Okal &
2358 Reymond 2003; Liu & Harris 2013). However,
2359 many major historical earthquakes in the studied
2360 region have occurred on strike slip faults, in-
2361 cluding the Sorong Fault (1944, M 7.5), the Yapen
2362 Fault (1979, M 7.9) the Ransiki Fault (2002, M
2363 7.6) and perhaps the Kawa Fault (1899, M 7.8)
2364 (e.g. Okal 1999; Brune *et al.* 2010; NEIC). Sixteen
2365 of the studied faults are dominantly strike slip and
2366 an additional five may have a substantial strike slip
2367 component (Table 3). As they are often long, straight,
2368 geometrically simple and subvertical, strike slip
2369 faults are capable of generating large, shallow and
2370 damaging earthquakes for example, the 1906 M
2371 7.7 San Francisco earthquake (e.g. Wald *et al.*
2372 1993), the 2001 M_w 7.8 Kunlun Shan earthquake
2373 (e.g. Lin *et al.* 2003) and the 2002 M_w 7.9 Denali
2374 earthquake (e.g. Haeussler *et al.* 2004).

2375 A crucial barrier to the propagation of lateral
2376 ruptures and hence earthquake magnitude, even on

2377 straight strike slip faults, is the presence of discon-
2378 tinuities or step overs (e.g. Segal & Pollard 1980;
2379 Sibson 1985; Barka & Kadinsky Cade 1988). The
2380 majority of historical strike slip earthquake ruptures
2381 were arrested by step overs wider than 3–5 km
2382 (Lettis *et al.* 2002; Wesnousky 2006). For example,
2383 the 1999 M_w 7.1 Düzce earthquake ruptured a 40 km
2384 segment of the North Anatolian Fault (Aydın &
2385 Kalafat 2002) and terminated in the >4 km wide
2386 Eften releasing bend in the west and the 4–5 km
2387 wide Bakacak releasing step over in the east
2388 (Duman *et al.* 2005). Straight, continuous faults are
2389 therefore capable of generating larger earthquakes
2390 than curved or segmented faults, of generating rup-
2391 tures that penetrate below the seismogenic layer
2392 (King & Wesnousky 2007) and of sustained super-
2393 shear rupture propagation, causing enhanced ground
2394 motion (Robinson *et al.* 2010). Eastern Indonesia's
2395 major strike slip faults show a variety of levels of
2396 segmentation, which may be viewed as an indi-
2397 cation of their structural maturity, with high cumu-
2398 lative displacements empirically known to remove
2399 fault zone complexities (e.g. Wesnousky 1988;
2400 Stirling *et al.* 1996; King & Wesnousky 2007).
2401 Other properties such as block rotation and pre-
2402 existing weaknesses may complicate this simple
2403 relationship.

2404 The Matano Fault is an example of a structurally
2405 immature fault zone. Its onshore length of 195 km is
2406 punctuated by three major basins, each one 4–6 km
2407 wide, and two major restraining bends. The resul-
2408 tant maximum potential rupture length is 90 km
2409 (Table 3). Empirical rupture length magnitude
2410 relationships (Wells & Coppersmith 1994) suggest
2411 a potential M 7.4 earthquake for such a rupture
2412 length. Uncertainties in this estimate include the
2413 unknown ability of a rupture to bypass the relatively
2414 gentle restraining bend east of the Mahalona Basin,
2415 the possibility of a through going strike slip fault at
2416 seismogenic depths below Lake Matano, the effect
2417 on fault strength of widespread serpentinite smears
2418 along the fault zone and the unknown length to
2419 which the fault continues offshore to the east.

2420 The Sorong Fault in West Papua, part of the fault
2421 system at the southern end of the Philippine Sea
2422 plate, is a much more established fault zone with a
2423 long history of slip (e.g. Ali & Hall 1995), reflected
2424 in an apparent absence of step overs >1 km and a
2425 continuous, straight onshore length of 420 km
2426 equating to a potential $M > 8.0$ earthquake if the
2427 entire linked system failed. The M_w 7.9 Yapen
2428 earthquake of 1979 ruptured an unknown length of
2429 the potentially 420 km long quasi continuous
2430 Yapen Fault (Okal 1999), showing that such a sce-
2431 nario is possible. Despite evidence that most left
2432 lateral strain is focused south of the Sorong Fault
2433 in West Papua, a conservative slip rate estimate of
2434 2 mm a^{-1} could accumulate 2 m of elastic

2379
2380
2381
2382
2383
2384
2385
2386
2387
2388
2389
2390
2391
2392
2393
2394
2395
2396
2397
2398
2399
2400
2401
2402
2403
2404
2405
2406
2407
2408
2409
2410
2411
2412
2413
2414
2415
2416
2417
2418
2419
2420
2421
2422
2423
2424
2425
2426
2427
2428
2429
2430
2431
2432
2433
2434
2435
2436

Table 3. Summary of observations made from Quaternary faults in eastern Indonesia, with hypothetical earthquake magnitudes, styles and tsunami risk

Fault	Typical segment length (km)	Maximum observed total length (km)	Step-over/relay width (km)	Potential rupture length (km) [§]	Attributable seismicity	Notable historical events	S_{nr} range	V_r range	Tectonic activity class [†]	Potential earthquake magnitude [‡]	Potential earthquake style	Associated tsunami?
Malino boundary	25–75	130	1.2	130	Y		1.05–1.66	0.22–1.01	Maximal to slow	7.6	Normal	Y
Gorontalo	30	95	7	35	N		1.83–2.36	0.88–1.69	Slow to minimal	6.9	Strike-slip	Y
Palu–Koro	10–35	220	<1	135	Y	M _w 7.7, 1996	1.08–2.30	0.24–0.89	Maximal to slow	7.6	Strike-slip	Y
Parigi boundary	10–45	95	3	80	Y		1.32–3.25	0.50–1.45	Minimal	7.3	Normal	Y
Sapu valley	5–20	75	? <2	75	N		1.08–1.45	0.40	Maximal to moderate	7.3	Strike-slip	N
Balantak	54	250	10 (offshore)	54	Y		1.04–1.22	0.25–0.47	Maximal to moderate	7.1	Strike-slip	Y
Matano	10–60	195	6	90	Y	M _w 6.1, 2011	1.02–1.9	0.23–0.78	Maximal to slow	7.4	Strike-slip	Y (lake)
Lawanopo and Kendari	10–45	200	7	70	?	M _w 7.5, 2001?	1.21–1.75	0.55–0.83	Moderate to slow	7.2	Strike-slip	N
Towuti bounding	25–55	55	<1	55	N		1.03–2.04	0.41–1.22	Maximal to slow	7.1	Normal	Y (lake)
Kolaka	5–45	175	10	50	Y		1.05–1.64	0.23–1.68	Maximal to slow	7.0	Strike-slip	Y
Mangole	20	135	2	135	Y		1.12–1.57	0.49–0.55	Rapid to slow	7.6	Normal/strike-slip	Y
Sanana Rana	5–20 10	60 65	? 3–4	60 >40	Y N	S _{ic} rupture?	1.27 1.01–1.96	0.44 0.23–1.53	Rapid Maximal to slow	7.2 >6.9	Normal/strike-slip ?Strike-slip	Y N
East Buru	10	48	<1	48	Y	M 7.6, 1950	1.84–2.08	1.36–1.88	Slow	7.0	Strike-slip	Y
Southern Senam	5–15	60	2	60	Y					7.2	Normal	Y

2495 displacement across the northern Bird's Head (sim-
2496 ilar to the 1979 Yapen earthquake release; Okal
2497 1999) in 1000 years. Even if all of this occurred
2498 west of the 1937 and 1944 earthquakes, and assum-
2499 ing complete stress release during those events, the
2500 remaining *c.* 200 km western portion of the fault
2501 could still generate a $M > 7.7$ earthquake.

2502 The apparently very young and highly seg-
2503 mented Tarera Aiduna fault zone and structures
2504 in the near offshore Seram fold thrust belt (Teas
2505 *et al.* 2009) and onshore Seram (Kawa and Bobol
2506 faults) could be part of a single soft linked fault
2507 system and seem to partition much of the present
2508 day left lateral motion between Australia and the
2509 Bird's Head. This fault system may thus be taking
2510 over the Pre Pleistocene role of the Sorong Fault.
2511 Although there is not yet a through going fault on
2512 the scale of the Sorong Fault, the individual compo-
2513 nents of the Tarera Aiduna Fault and left lateral
2514 faults in Seram are each capable of generating
2515 $M > 7$ earthquakes. Geomorphic observations sug-
2516 gest that they have all been active during the Quater-
2517 nary, even if some segments (e.g. the Bobol Fault)
2518 lack instrumental seismicity records. A major uncer-
2519 tainty in assessing the Tarera Aiduna fault system
2520 is the type and degree of linkage along its segments.
2521 The longest segment onshore with geomorphic evi-
2522 dence for rapid activity is 60 km long and may
2523 be traced, via an abrupt releasing bend 3 km wide,
2524 another 30 km to the east. Assuming rupture is not
2525 terminated by the bend, an $M 7.4$ earthquake is pos-
2526 sible on this 90 km long segment. It is reasonable to
2527 assume that the fault passes some distance offshore
2528 before the next terminating step over, so the maxi-
2529 mum magnitude is likely to be larger.

2530 In a similar manner, the maximum potential
2531 magnitudes for observed quasi continuous seg-
2532 ments of the Kawa and Bobol faults of southern
2533 Seram are 7.5 and 7.4, respectively, but a continuous
2534 rupture linking across Taluti Bay could achieve a
2535 length of 240 km and an earthquake magnitude of
2536 7.8. The 1899 $M 7.8$ event, which caused slope fail-
2537 ure north of Tehoru and a tsunami around Taluti
2538 Bay, could have originated from such a rupture.

2539 The Palu valley has previously been considered
2540 to represent a pull apart basin between two strands
2541 of the Palu Koro Fault (Bellier *et al.* 2001, 2006;
2542 Beaudouin *et al.* 2003; Socquet *et al.* 2006). The
2543 width between the two strands would be about
2544 6 km, ample to terminate earthquake rupture, limit-
2545 ing the maximum length and magnitude of Palu
2546 Koro Fault earthquakes to the segments north and
2547 south of Palu valley. However, the possibility of a
2548 continuous, buried cross basin fault system within
2549 the Palu valley as proposed here has significant
2550 implications for seismic hazard assessment in the
2551 densely populated valley. A continuous cross basin
2552 fault within the Palu valley, as seen in analogue

models (e.g. Wu *et al.* 2009) and natural strike slip
basins (e.g. the Clonard Basin, Haiti; Mann *et al.*
1995), means that the Palu Koro Fault may be
straighter and more continuous than previously sug-
gested and palaeoseismic trenches across the border
faults may not record major historical strike slip
earthquakes. The postulated buried and locked
section alone is 50 km long and is thus capable of
generating an $M 7.0$ earthquake. The total onshore
length of the Palu Koro Fault between Leboni
valley and Palu city, lacking step overs wider than
1 km and bends greater than 5° , is 135 km. As
such, the Palu Koro Fault must qualify as a 'fault
superhighway', potentially capable of sustained
super shear rupture speeds (Robinson *et al.* 2010)
and earthquakes up to $M 7.6$.

Other smaller structures that are geologically
less significant because they are either not associ-
ated with instrumental seismicity (e.g. the Sapu
valley fault system), have very low geomorphic
tectonic activity indices (e.g. the Gorontalo Fault)
or are composed of short and discontinuous fault
segments (e.g. the Namlea fault system) are of par-
ticular importance from a hazard analysis perspec-
tive because of their proximity to large population
centres with little to no earthquake resistance. Sim-
ilarly, structures such as the Kolaka Fault, which has
its most geomorphologically youthful segment
bounding steep uplifted topography immediately
adjacent to Kolaka town, may also be associated
with secondary seismic hazards such as landslides.
Large earthquakes along many of the faults, partic-
ularly the Palu Koro, Matano and Balantak faults
and the Molino, Towuti and Wandamen Peninsula
boundary faults, may also trigger local tsunami, as
has been already demonstrated in Palu and Taluti
bays (e.g. Prasetya *et al.* 2001; Brune *et al.* 2010).

Conclusions

Neotectonic deformation in eastern Indonesia is
rarely focused on discrete shear zones bounding
rigid blocks, although this is often how it is inter-
preted. The pattern of seismicity and the broad
distribution of Quaternary faults suggests that the
region is more closely approximated by continuum
mechanics than by rigid microplates (e.g. Thatcher
1995). All of the studied faults show geomorphic
evidence of Quaternary tectonic activity, even in
areas where high strain rates are not inferred from
geodetic measurements (e.g. Buru, south Seram
and northern West Papua).

The zone of left lateral deformation that includes
the Yapen Fault, the Tarera Aiduna Fault and
strike slip associated with the Seram fold thrust
belt is perhaps the most active onshore/nearshore
fault system of eastern Indonesia as recorded by

2553 instrumental seismicity and geodetics. However, in
2554 terms of seismic risk, the Palu Koro Fault is con-
2555 sidered to be the most significant structure due to
2556 its proximity to Palu city, the possibility of a cross
2557 basin fault system close to the city, the fault's unpre-
2558 dictability as a result of its poorly known seismic
2559 history, and the fault's potential to cause large, shal-
2560 low focus, super shear earthquakes. Additional fac-
2561 tors increasing the risk of the Palu Koro Fault
2562 include the possibility of liquefaction in the deep
2563 Quaternary sedimentary basin on which Palu city
2564 is built and the low lying city's vulnerability to tsu-
2565 nami travelling down the narrow Palu Bay.

2566 The Sorong Fault in West Papua should be
2567 viewed as the wildcard of eastern Indonesian active
2568 tectonics. Although GPS measurements appear to
2569 show little sinistral strike slip motion, or even a
2570 degree of dextral slip, station locations in Sorong
2571 and Biak cannot resolve the complexity of the
2572 Sorong Yapen Ransiki Fault and may omit shear
2573 to the north. Convincing left lateral stream offsets
2574 and low mountain front sinuosity values show that
2575 the fault has been active during the Quaternary. A
2576 dearth of seismicity, rather than indicating that the
2577 fault is benign, may instead indicate that it is locked
2578 and accumulating elastic strain. Magnitude 6.9, 7.2
2579 and 7.4 earthquakes in 1937 and 1944, located on
2580 the fault west of Manokwari, prove that the fault is
2581 capable of generating large earthquakes. The Sor-
2582 ong Fault's contribution to the seismic hazard of
2583 West Papua should not be underestimated, parti-
2584 cularly given its proximity to large towns such as
2585 Sorong and Manokwari.

2586 There is great potential for the palaeoseismic
2587 study of some of the faults discussed in this paper
2588 to confirm Quaternary activity and to provide
2589 more detailed answers to questions about seismic
2590 hazards, particularly characteristic earthquake sizes
2591 and recurrence intervals. It is recommended that
2592 trenching work is carried out across possible surface
2593 ruptures identified along the Matano, Balantak,
2594 Rana, Ransiki and Wandamen Peninsula faults.
2595 Geophysical studies to image shallow fault strands
2596 in the Quaternary sedimentary fill of several strike
2597 slip basins, including the Palu, Sapu and Mahalona
2598 valleys, would help to confirm the existence of
2599 cross basin strike slip fault systems that may pose
2600 a previously unrecognized seismic hazard.

2601 We are grateful to TGS (<http://www.tgs.com>), who pro-
2602 vided the multibeam data, to John Decker, Phil Teas and
2603 the crew of the Shakti dive boat for support and valuable
2604 discussions during Banda Sea fieldwork. Alfend Rudy-
2605 wan, Dave Gold, Ferry Yulian, Ega Abang Surya Nugraha,
2606 Jonathan Pownall and Benjamin Sapiie are thanked for
2607 their assistance and contributions to the ideas discussed
2608 here. Two anonymous reviewers are thanked for detailed
2609 and constructive reviews, which considerably improved
2610 the final paper. Recent fieldwork was funded by the SE

Asia Research Group, Royal Holloway University of
London.

References

- ABERS, G. & McCAFFREY, R. 1988. Active deformation in the New Guinea Fold and Thrust Belt: seismological evidence for strike slip faulting and basement involved thrusting. *Journal of Geophysical Research*, **93**, 13332–13354.
- AHMAD, W. 1978. Geology along the Matano Fault Zone, East Sulawesi, Indonesia. In: WIRYOSUJONO, S. & SUDRADJAT, A. (eds) *Proceedings: Regional Conference on the Geology and Mineral Resources of South East Asia*, Jakarta, Indonesia, 4–7 August 1975. Indonesian Association of Geologists, 143–150.
- ALI, J.R. & HALL, R. 1995. Evolution of the boundary between the Philippine Sea Plate and Australia: palaeomagnetic evidence from eastern Indonesia. *Tectonophysics*, **251**, 251–275.
- AUDLEY CHARLES, M.G. 1986. Timor Tanimbar Trough: the foreland basin to the evolving Banda orogen. In: ALLEN, P.A. & HOMEWOOD, P. (eds) *Foreland Basins*. International Association of Sedimentologists, Special Publications, **8**, 91–102.
- AUDLEY CHARLES, M.G., CARTER, D.J. & MILSON, J. 1972. Tectonic development of Eastern Indonesia in relation to Gondwanaland dispersal. *Nature*, **239**, 35–39.
- AYDIN, A. & KALAFAT, D. 2002. Surface ruptures of the 17 August and 12 November 1999 Izmit and Duzce earthquakes in northwestern Anatolia, Turkey: their tectonic and kinematic significance and the associated damage. *Bulletin of the Seismological Society of America*, **92**, 95–106.
- BAILLY, V., PUBELLIER, M., RINGENBACH, J. C., DE SIGOYER, J. & SAPIN, F. 2009. Deformation zone 'jumps' in a young convergent setting: the Lenguru fold and thrust belt, New Guinea Island. *Lithos*, **113**, 306–317.
- BARKA, A. & KADINSKY CADE, K. 1988. Strike slip fault geometry in Turkey and its influence on earthquake activity. *Tectonics*, **7**, 663–684.
- BATH, M. & DUDA, S.J. 1979. *Some Aspects of Global Seismicity*. Seismological Institute, Uppsala, 1–79.
- BEANLAND, S. & CLARK, M. 1994. *The Owens Valley Fault Zone, Eastern California, and Surface Faulting Associated with the 1872 Earthquake*. US Geological Survey Bulletin, **1982**. US Government Printing Office, Washington DC.
- BEAUDOUIN, T. 1998. *Tectonique active et sismotectonique du système de failles décrochantes de Sulawesi Central*. Thèse de Doctorat, Université Paris Sud.
- BEAUDOUIN, T., BELLIER, O. & SEBRIER, M. 2003. Present day stress and deformation fields within the Sulawesi Island area (Indonesia): geodynamic implications. *Bulletin de la Société géologique de France*, **174**, 305–317.
- BELLIER, O., BEAUDOUIN, T. ET AL. 1998. Active faulting in central Sulawesi (eastern Indonesia). In: WILSON, P. & MICHEL, G.W. (eds) *The Geodynamics of S, SE Asia (GEODYSSSEA Project)*. GeoForschungsZentrum, Potsdam, 276–312.

- 2611 BELLIER, O., SEBRIER, M. *ET AL.* 2001. High slip rate for a
2612 low seismicity along the Palu Koro active fault in cen-
2613 tral Sulawesi (Indonesia). *Terra Nova*, **13**, 463–470.
- 2614 BELLIER, O., SEBRIER, M., SEWARD, D., BEAUDOUIN, T.,
2615 VILLENEUVE, M. & PUTRANTO, E. 2006. Fission
2616 track and fault kinematics analyses for new insight
2617 into the Late Cenozoic tectonic regime changes in
2618 West Central Sulawesi (Indonesia). *Tectonophysics*,
2619 **413**, 201–220.
- 2620 BOCK, Y., PRAWIRODIRDJO, L. *ET AL.* 2003. Crustal motion
2621 in Indonesia from global positioning system measure-
2622 ments. *Journal of Geophysical Research*, **108**, 2367.
- 2623 BRUNE, S., BABEYKO, A.Y., LADAGE, S. & SOBOLEV, S.V.
2624 2010. Landslide tsunami hazards in the Indonesian
2625 Sunda Arc. *Natural Hazards Earth Systems Science*,
2626 **10**, 589–604.
- 2627 BULL, W.B. 1978. *Geomorphic Tectonic Activity Classes*
2628 *of the South Front of the San Gabriel Mountains, Cal-
2629 ifornia*. Final Report, US Geological Survey, Contract
2630 No. 14 08 0001 G 394.
- 2631 BULL, W.B. 2007. *Tectonic Geomorphology of Mountains:
2632 a New Approach to Paleoseismology*. Blackwell Pub-
2633 lishing, Malden, MA.
- 2634 BULL, W.B. & McFADDEN, L.D. 1977. Tectonic geomor-
2635 phology north and south of the Garlock fault, Califor-
2636 nia. In: DOEHERING, D.O. (ed.) *Geomorphology in Arid
2637 Regions. Proceedings at the Eighth Annual Geomor-
2638 phology Symposium*. State University of New York,
2639 Binghamton, NY, 115–138.
- 2640 BURCHFIEL, B.C., ROYDEN, L.H. *ET AL.* 2008. A geologi-
2641 cal and geophysical context for the Wenchuan earth-
2642 quake of 12 May 2008, Sichuan, People's Republic of
2643 China. *Geological Society of America Today*, **18**,
2644 4–11.
- 2645 CAMPLIN, D.J. & HALL, R. 2014. Neogene history of None
2646 Gulf, Sulawesi, Indonesia. *Marine and Petroleum
2647 Geology*, **57**, 88–108.
- 2648 CARDWELL, R.K. & ISACKS, B.L. 1978. Geometry of the
2649 subducted lithosphere beneath the Banda Sea in eastern
2650 Indonesia from seismicity and fault plane solutions.
2651 *Journal of Geophysical Research*, **83**, 2825–2838.
- 2652 CARDWELL, R.K., ISACKS, B.L. & KARIG, D.E. 1980. The
2653 spatial distribution of earthquakes, focal mechanism
2654 solutions, and subducted lithosphere in the Philippine
2655 and northeastern Indonesian islands. In: HAYES, D.E.
2656 (ed.) *The Tectonic, Geologic Evolution of Southeast
2657 Asian Seas, Islands*. American Geophysical Union,
2658 Geophysical Monograph, **23**, 1–35.
- 2659 CHARLTON, T.R. 2010. The Pliocene Recent anticlock-
2660 wise rotation of the Bird's Head, the opening of the
2661 Aru Trough Cenderawasih Bay sphenochasm, and the
2662 closure of the Banda double arc. In: *Proceedings,
2663 Indonesian Petroleum Association, 34th Annual Con-
2664 vention and Exhibition*. IPA10 G 008.
- 2665 CHEN, W. P. & HSU, L. 2013. Historic seismicity near the
2666 source zone of the great 2008 Wenchuan earthquake:
2667 implications for seismic hazards. *Tectonophysics*,
2668 **584**, 114–118.
- 2669 COTTAM, M.A., HALL, R., FORSTER, M.A. & BOUDAGHER
2670 FADEL, M.K. 2011. Basement character and basin for-
2671 mation in Gorontalo Bay, Sulawesi, Indonesia: new
2672 observations from the Togian Islands. In: HALL, R.,
2673 COTTAM, M.A. & WILSON, M.E.J. (eds) *The SE
2674 Asian Gateway: History, Tectonics of the Australia
2675 Asia Collision*. Geological Society, London, Special
2676 Publications, **355**, 177–202, <https://doi.org/10.1144/SP355.9>
- 2677 DECKER, J., BERGMAN, S.C., TEAS, P.A., BAILLIE, P. &
2678 ORANGE, D.L. 2009. Constraints on the tectonic evolu-
2679 tion of the Bird's Head, West Papua. In: *Proceedings,
2680 Indonesian Petroleum Association, 33rd Annual Con-
2681 vention and Exhibition*, IPA09 G 139.
- 2682 DEHBOZORGI, M., POURKERMANI, M., ARIAN, M., MAT
2683 KAN, A.A., MOTAMEDI, H. & HOSSEINIASL, A. 2010.
2684 Quantitative analysis of relative tectonic activity in
2685 the Sarvestan area, central Zagros, Iran. *Geomorphol-
2686 ogy*, **121**, 329–341.
- 2687 DEMETS, C., GORDON, R., ARGUS, D. & STEIN, S. 1994.
2688 Effects of recent revisions to the geomagnetic reversal
2689 time scale on estimates of current plate motions. *Geo-
2690 physical Research Letters*, **21**, 2191–2194.
- 2691 DOW, D.B. & HARTONO, U. 1982. The nature of the crust
2692 underlying Cenderawasih (Geelvink) Bay, Irian Jaya.
2693 *Proceedings of the Indonesian Petroleum Association*,
2694 **11**, 203–210.
- 2695 DOW, D.B. & SUKAMTO, R. 1984. Western Irian Jaya: the
2696 end product of oblique plate convergence in the Late
2697 Tertiary. *Tectonophysics*, **106**, 109–139.
- 2698 DUMAN, T.Y., EMRE, O., DOGAN, A. & OZALP, S. 2005.
2699 Step over and bend structures along the 1999 Duzce
2700 Earthquake surface rupture, North Anatolian Fault,
2701 Turkey. *Bulletin of the Seismological Society of
2702 America*, **95**, 1250–1262, [https://doi.org/10.1785/
2703 0120040082](https://doi.org/10.1785/0120040082)
- 2704 ENGD AHL, E.R., VAN DER HILST, R. & BULAND, R.
2705 1998. Global teleseismic earthquake relocation with
2706 improved travel times and procedures for depth deter-
2707 mination. *Bulletin of the Seismological Society of
2708 America*, **88**, 722–743.
- 2709 ESHGHI, S. & ZARE, M. 2003. Bam (SE Iran) Earthquake
2710 of 26 December 2003, Mw 6.5. A Preliminary Recon-
2711 naissance Report, [www.iiees.ac.ir/en/wp-content/
2712 uploads/2010/12/Bam-report-zare.pdf](http://www.iiees.ac.ir/en/wp-content/uploads/2010/12/Bam-report-zare.pdf) [last accessed
2713 29 October 2016].
- 2714 FERDIAN, F., HALL, R. & WATKINSON, I. 2010. A structural
2715 re-evaluation of the north Banggai Sula area, eastern
2716 Indonesia. In: *Proceedings, Indonesian Petroleum
2717 Association, 34th Annual Convention*, IPA07 G 009,
2718 1–20.
- 2719 FU, B., NINOMIYA, Y., LEI, X., TODA, S. & AWATA, Y.
2720 2004. Mapping active fault associated with the 2003
2721 M_w 6.6 Bam (SE Iran) earthquake with ASTER 3D
2722 images. *Remote Sensing of Environment*, **92**, 153–157.
- 2723 GARRARD, R.A., SUPANDJONO, J.B. & SURONO, 1988. The
2724 geology of the Banggai Sula microcontinent, eastern
2725 Indonesia. In: *Proceedings, Indonesian Petroleum
2726 Association, 17th Annual Convention*, 23–52.
- 2727 GERMERAAD, J.H. 1946. Geology of central Seran. In:
2728 RUTTEN, L. & HOTZ, W. (eds) *Geological, Petro-
2729 graphical, and Palaeontological Results of Explora-
2730 tions Carried Out September 1917 June 1919,
2731 Island of Ceram*. de Bussy, Amsterdam.
- 2732 HAEUSSLER, P.J., SCHWARTZ, D.P., DAWSON, T.E.,
2733 STENNER, H.D., LIENKAEMPER, J.J., SHERRON, B. &
2734 PERSONIUS, S.F. 2004. Surface rupture and slip distri-
2735 bution of the Denali and Totschunda faults in the 3
2736 November 2002 M 7.9 earthquake, Alaska. *Bulletin
2737 of the Seismological Society of America*, **94**, S23–S52.

QUATERNARY FAULT ACTIVITY IN EASTERN INDONESIA

- 2669 HAFFNER, G.D., HEHANUSSA, P.E. & HARTOTO, D. 2001.
 2670 The biology and physical processes of large lakes of
 2671 Indonesia: Lakes Matano and Towuti. In: MUNAWAR,
 2672 M. & HECKY, R.E. (eds) *The Great Lakes of the*
 2673 *World (GLOW): Food Web, Health, Integrity, Ecovi-*
 2674 *sion*. Ecovision World Monograph Series. Backhuys
 2675 Publishers, Leiden, 183–192.
- 2676 HALL, R. 1987. Plate boundary evolution in the Halmahera
 2677 region, Indonesia. *Tectonophysics*, **144**, 337–352.
- 2678 HALL, R. 1996. Reconstructing Cenozoic SE Asia. In:
 2679 HALL, R. & BLUNDELL, D.J. (eds) *Tectonic Evolution*
 2680 *of SE Asia*. Geological Society, London, Special Pub-
 2681 lications, **106**, 153–184, [https://doi.org/10.1144/](https://doi.org/10.1144/GSL.SP.1996.106.01.11)
 2682 [GSL.SP.1996.106.01.11](https://doi.org/10.1144/GSL.SP.1996.106.01.11)
- 2683 HALL, R. 2002. Cenozoic geological and plate tectonic
 2684 evolution of SE Asia and the SW Pacific: computer
 2685 based reconstructions, model and animations. *Journal*
 2686 *of Asian Earth Sciences*, **20**, 353–434.
- 2687 HALL, R. 2011. Australia–SE Asia collision: plate tecton-
 2688 ics and crustal flow. In: HALL, R., COTTAM, M.A. &
 2689 WILSON, M.E.J. (eds) *The SE Asian Gateway: History,*
 2690 *Tectonics of the Australia–Asia Collision*. Geological
 2691 Society, London, Special Publications, **355**, 75–109,
 2692 <https://doi.org/10.1144/SP355.5>
- 2693 HALL, R. 2012. Late Jurassic–Cenozoic reconstructions of
 2694 the Indonesian region and the Indian Ocean. *Tectono-*
 2695 *physics*, **570**, 1–41.
- 2696 HALL, R., FULLER, M., ALI, J.R. & ANDERSON, C.D. 1995.
 2697 The Philippine Sea plate: magnetism and reconstruc-
 2698 tions. In: TAYLOR, B. & NATLAND, J.H. (eds) *Active*
 2699 *Margins, Marginal Basins: a Synthesis of Western*
 2700 *Pacific Drilling Results*. American Geophysical
 2701 Union Monograph, **88**, 371–404.
- 2702 HAMILTON, W. 1979. *Tectonics of the Indonesian Region*.
 2703 US Geological Survey, Professional Papers, **1078**.
- 2704 HARRIS, R.A. 1992. Peri collisional extension and the for-
 2705 mation of Oman type ophiolites in the Banda Arc and
 2706 Brooks Range. In: PARSON, L.M., MURTON, B.J. &
 2707 BROWNING, P. (eds) *Ophiolites, their Modern Oceanic*
 2708 *Analogues*. Geological Society, London, Special Pub-
 2709 lications, **60**, 301–325, [https://doi.org/10.1144/](https://doi.org/10.1144/GSL.SP.1992.060.01.19)
 2710 [GSL.SP.1992.060.01.19](https://doi.org/10.1144/GSL.SP.1992.060.01.19)
- 2711 HENNIG, J., ADVOKAAT, E., RUDYAWAN, A. & HALL, R.
 2712 2014. Large sediment accumulations and major sub-
 2713 sidence offshore; rapid uplift on land: consequences
 2714 of extension of Gorontalo Bay and Northern Sulawesi.
 2715 In: *Proceedings, Indonesian Petroleum Association,*
 2716 *38th Annual Convention and Exhibition*, IPA14
 2717 G 304.
- 2718 HENRY, C. & DAS, S. 2002. The M_w 8.2, 17 February 1996
 2719 Biak, Indonesia, earthquake: rupture history, after
 2720 shocks, and fault plane properties. *Journal of Geo-*
 2721 *physical Research*, **107**, [https://doi.org/10.1029/](https://doi.org/10.1029/2001jb000796)
 2722 [2001jb000796](https://doi.org/10.1029/2001jb000796)
- 2723 HILL, K.C., HOFFMAN, N., LUNT, P. & PAUL, R. 2002.
 2724 Structure and hydrocarbons in the Sareba block,
 2725 ‘Bird’s Neck’, West Papua. In: *Proceedings, Indone-*
 2726 *sian Petroleum Association, 28th Annual Convention,*
 2727 *IPA01 G 115*, 227–248.
- 2728 HOLZER, L.T. & SAVAGE, J.C. 2013. Global earthquake
 2729 fatalities and population. *Earthquake Spectra*, **29**,
 2730 155–175.
- 2731 HUANG, W. 1993. Morphologic patterns of stream chan-
 2732 nels on the active Yishi Fault, southern Shandong
 2733 Province, Eastern China: implications for repeated
 2734 great earthquakes in the Holocene. *Tectonophysics*,
 2735 **219**, 283–304.
- 2736 HUTCHISON, C.S. 1989. *Geological Evolution of South*
 2737 *East Asia*. Clarendon Press, Oxford.
- 2738 JABLONSKI, D., PRIYONO, P., WESTLAKE, S. & LARSEN,
 2739 O.A. 2007. Geology and exploration potential of the
 2740 Gorontalo basin, central Indonesia—eastern extension
 2741 of the North Makassar Basin? In: *Proceedings, Indone-*
 2742 *sian Petroleum Association, 31st Annual Convention*
 2743 *and Exhibition*. IPA07 G 083.
- 2744 KATILI, J.A. 1970. Additional evidence of transcurrent
 2745 faulting in Sumatra and Sulawesi. *Bandung National*
 2746 *Institute of Geology and Mining Bulletin*, **3**, 15–28.
- 2747 KATILI, J.A. 1973. On fitting certain geological and geo-
 2748 physical features of the Indonesian island arc to the
 2749 new global tectonics. In: COLEMAN, P.J. (ed.) *The*
 2750 *Western Pacific: Island Arcs, Marginal Seas, Geo-*
 2751 *chemistry*. Western Australia University Press, Perth,
 2752 287–305.
- 2753 KATILI, J.A. 1975. Volcanism and plate tectonics in the
 2754 Indonesian island arcs. *Tectonophysics*, **26**, 165–188.
- 2755 KATILI, J.A. 1986. Geology and hydrocarbon potential of
 2756 the Arafura Sea. In: HALBOUTY, M.T. (ed.) *Future*
 2757 *Petroleum Provinces of the World*. AAPG Memoirs,
 2758 **40**, 487–501.
- 2759 KAVALIERIS, I., VAN LEEUWEN, T.M. & WILSON, M. 1992.
 2760 Geological setting and styles of mineralization, north
 2761 arm of Sulawesi, Indonesia. *Journal of Southeast*
 2762 *Asian Earth Sciences*, **7**, 113–130.
- 2763 KELLER, E.A. 1986. Investigation of active tectonics: use
 2764 of surficial Earth processes. In: WALLACE, R.E. (ed.)
 2765 *Active Tectonics, Studies in Geophysics*. National
 2766 Academy Press, Washington, DC, 136–147.
- 2767 KING, G.C.P. & WESNOUSKY, S.G. 2007. Scaling of fault
 2768 parameters for continental strike slip earthquakes. *Bul-*
 2769 *letin of the Seismological Society of America*, **97**,
 2770 1833–1840.
- 2771 LACASSIN, R., REPLUMAZ, A. & LELOUP, P.H. 1998.
 2772 Hairpin river loops and slip sense inversion on
 2773 Southeast Asian strike slip faults. *Geology*, **26**,
 2774 703–706.
- 2775 LETTIS, W., BACHHUBER, J. ET AL. 2002. Influence of
 2776 releasing step overs on surface fault rupture and fault
 2777 segmentation: examples from the 17 August 1999
 2778 Izmit earthquake on the North Anatolian Fault, Turkey.
 2779 *Bulletin of the Seismological Society of America*, **92**,
 2780 19–42.
- 2781 LIN, A., KIKUCHI, M. & FU, B. 2003. Rupture segmenta-
 2782 tion and process of the 2001 M_w 7.8 central Kunlun
 2783 earthquake, China. *Bulletin of Seismological Society*
 2784 *of America*, **93**, 2477–2492.
- 2785 LINTHOUT, K., HELMERS, H., SOPAHELWAKAN, J. &
 2786 SURYA NILA, E. 1989. Metamorphic complexes in
 2787 Buru and Seram, northern Banda Arc. *Netherlands*
 2788 *Journal of Sea Research*, **24**, 345–356.
- 2789 LINTHOUT, K., HELMERS, H. & ANDRIESEN, P.A.M.
 2790 1991. Dextral strike slip in Central Seram and 3–
 2791 4.5 Ma Rb/Sr ages in pre-Triassic metamorphics
 2792 related to Early Pliocene counterclockwise rotation
 2793 of the Buru Seram microplate (E. Indonesia). *Journal*
 2794 *of Southeast Asian Earth Sciences*, **6**, 335–342.
- 2795 LIU, Z.Y. C. & HARRIS, R.A. 2013. Discovery of possible
 2796 mega thrust earthquake along the Seram Trough from

- 2727 records of 1629 tsunamis in eastern Indonesian region.
 2728 *Natural Hazards*, **72**, 1311–1328.
- 2729 MANN, P. 2007. Global catalogue, classification and
 2730 tectonic origins of restraining and releasing bends
 2731 on active and ancient strike slip fault systems. In:
 2732 CUNNINGHAM, W.D. & MANN, P. (eds) *Tectonics of*
 2733 *Strike Slip Restraining and Releasing Bends*. Geologi-
 2734 cal Society, London, Special Publications, **290**,
 2735 13–142, <https://doi.org/10.1144/SP290.2>
- 2735 MANN, P., TAYLOR, F.W., LAWRENCE EDWARDS, R. &
 2736 TEH LUNG, KU. 1995. Actively evolving microplate
 2737 formation by oblique collision and sideways motion
 2738 along strike slip faults: an example from the northeast
 2739 ern Caribbean plate margin. *Tectonophysics*, **246**,
 2740 1–69.
- 2741 McCAFFREY, R. 1989. Seismological constraints and spec-
 2742 ulations on Banda arc tectonics. *Netherlands Journal*
 2743 *of Sea Research*, **24**, 141–152.
- 2743 McCAFFREY, R. 1996. Slip partitioning at convergent plate
 2744 boundaries of SE Asia. In: HALL, R. & BLUNDELL, D.J.
 2745 (eds) *Tectonic Evolution of Southeast Asia*. Geological
 2746 Society, London, Special Publications, **106**, 3–18,
 2747 <https://doi.org/10.1144/GSL.SP.1996.106.01.02>
- 2747 McCAFFREY, R. & SUTARDJO, R. 1982. Reconnaissance
 2748 microearthquake survey of Sulawesi, Indonesia. *Geo-*
 2749 *physical Research Letters*, **9**, 793–796.
- 2750 MCCALPIN, J.P. (ed.) 2009. *Palaeoseismology*. 2nd ed.
 2751 International Geophysics Series, **95**. Academic Press,
 2752 Burlington, USA.
- 2753 MICHETTI, A.M., AUDEMARD, F.A. & MARCO, S. 2005.
 2754 Future trends in palaeoseismology: integrated study
 2755 of the seismic landscape as a vital tool in seismic haz-
 2756 ard analyses. *Tectonophysics*, **408**, 3–21.
- 2757 MILSOM, J., MASSON, D., NICHOLS, G., SIKUMBANG, N.,
 2758 DWIYANTO, B., PARSON, L. & KALLAGHER, H. 1992.
 2759 The Manokwari Trough and the western end of the
 2760 New Guinea Trench. *Tectonics*, **11**, 145–153.
- 2760 MOLNAR, P. & DAYEM, K.E. 2010. Major intercontinental
 2761 strike slip faults and contrasts in lithospheric strength.
 2762 *Geosphere*, **6**, 444–467.
- 2763 NATAWIDJAJA, D.H. & DARYONO, M.R. 2014. The Lawa-
 2764 nopo Fault, Central Sulawesi, East Indonesia. In: *Pro-*
 2765 *ceedings, 4th International Symposium on Earthquake*
 2766 *and Disaster Mitigation 2014 (ISED 2014)*, 11–12
 2767 November 2014, Bandung, Indonesia, [https://doi-](https://doi.org/10.1063/1.4915009)
 2768 [org/10.1063/1.4915009](https://doi.org/10.1063/1.4915009)
- 2768 NATIONAL EARTHQUAKE INFORMATION CENTRE (NEIC).
 2769 <http://earthquake.usgs.gov/contactus/golden/neic.php>
 2770 [last accessed 29 October 2016].
- 2771 NATIONAL GEOPHYSICAL DATA CENTER/WORLD DATA SER-
 2772 VICE. Global Significant Earthquake Database. National
 2773 Geophysical Data Center, NOAA, [https://doi.org/10.](https://doi.org/10.7289/V5TD9V7K)
 2774 [7289/V5TD9V7K](https://doi.org/10.7289/V5TD9V7K) [last accessed 29 October 2016].
- 2774 NORVICK, M.S. 1979. The tectonic history of the Banda
 2775 arcs, eastern Indonesia: a review. *Journal of the Geo-*
 2776 *logical Society, London*, **136**, 519–527, [https://doi-](https://doi.org/10.1144/gsjgs.136.5.0519)
 2777 [org/10.1144/gsjgs.136.5.0519](https://doi.org/10.1144/gsjgs.136.5.0519)
- 2777 OKAL, E.A. 1999. Historical seismicity and seismotectonic
 2778 context of the great 1979 Yapen and Biak, Irian Jaya
 2779 earthquakes. *Pure and Applied Geophysics*, **154**,
 2780 633–675.
- 2780 OKAL, E.A. & REYMOND, D. 2003. The mechanism of
 2781 great Banda sea earthquake of 1 February 1938: apply-
 2782 ing the method of preliminary determination of focal
 2783 mechanism to a historical event. *Earth and Planetary*
 2784 *Science Letters*, **216**, 1–15.
- PAIRAULT, A.A., HALL, R. & ELDERS, C.F. 2003. Tectonic
 Evolution of the Seram Trough, Indonesia. In:
Proceedings, Indonesian Petroleum Association, 29th
Annual Convention, 355–370.
- PAVLIDES, S.B. 1989. Looking for a definition of neotec-
-
- tonics.
- Terra Nova*
- ,
- 1**
- , 233–235,
- [https://doi.org/10.](https://doi.org/10.1111/j.1365.3121.1989.tb00362.x)
-
- [1111/j.1365.3121.1989.tb00362.x](https://doi.org/10.1111/j.1365.3121.1989.tb00362.x)
- PELINOVSKY, E., YULIADI, D., PRASETYA, G. & HIDAYAT,
-
- R. 1997. The 1996 Sulawesi tsunami.
- Natural Hazards*
- ,
-
- 16**
- , 29–38.
PHOLBUD, P., HALL, R., ADVOKAAT, E., BURGESS, P. &
-
- RUDYAWAN, A. 2012. A new interpretation of
-
- Gorontalo Bay, Sulawesi. In:
- Proceedings, Indonesian*
-
- Petroleum Association, 36th Annual Convention*
- ,
-
- IPA12 G 029, 197–224.
PIETY, L., SULLIVAN, J.T. & ANDERS, M.H. 1992. Segmen-
-
- tation and paleoseismicity of the Grand Valley Fault,
-
- southeastern Idaho and western Wyoming. In: LINK,
-
- P.K., KUNTZ, M.A. & PLATT, L.B. (eds)
- Regional*
-
- Geology of Eastern Idaho and Western Wyoming*
- .
-
- Geological Society of America, Memoirs,
- 179**
- ,
-
- 155–182.
PIGRAM, C.J. & PANGGABEAN, H. 1984. Rifting of the east-
-
- ern margin of the Australian continent and the origin of
-
- some microcontinents in Indonesia.
- Tectonophysics*
- ,
-
- 107**
- , 331–353.
PIGRAM, C.J., SURONO & SUPANDJONO, J.B. 1985. Origin
-
- of the Sula Platform, eastern Indonesia.
- Geology*
- ,
- 13**
- ,
-
- 246–248.
POWNALL, J.M., HALL, R. & WATKINSON, I.M. 2013.
-
- Extreme extension across Seram and Ambon, eastern
-
- Indonesia: evidence for Banda slab rollback.
- Solid*
-
- Earth*
- ,
- 4**
- , 277–314.
POWNALL, J.M., HALL, R., ARMSTRONG, R.A. & FORSTER,
-
- M.A. 2014. Earth's youngest known ultrahigh temper-
-
- ature granulites discovered on Seram, eastern Indone-
-
- sia.
- Geology*
- ,
- 42**
- , 279–282.
PRASETYA, G.S., DE LANGE, W.P. & HEALY, T.R. 2001.
-
- The Makassar Strait Tsunamiogenic Region, Indonesia.
-
- Natural Hazards*
- ,
- 24**
- , 295–307.
PUBELLIER, M., DESFONTAINES, B., CHOROWICZ, J.,
-
- RUDANT, J. P. & PERMANA, H. 1999. Active denuda-
-
- tion morphostructures from SAR ERS 1 images (SW
-
- Irian Jaya).
- International Journal of Remote Sensing*
- ,
-
- 20**
- , 789–800.
PUNTODEWO, S.S.O., McCAFFREY, R. ET AL. 1994. GPS
-
- measurements of crustal deformation within the
-
- Pacific Australia plate boundary zone in Irian Jaya,
-
- Indonesia.
- Tectonophysics*
- ,
- 237**
- , 141–153.
QUIGLEY, M., VAN DISSEN, R. ET AL. 2012. Surface rupture
-
- during the 2010
- M_w
- 7.1 Darfield (Canterbury) earth-
-
- quake: implications for fault rupture dynamics and
-
- seismic hazard analysis.
- Geology*
- ,
- 40**
- , 55–58.
RAMÍREZ HERRERA, M.T. 1998. Geomorphic assessment
-
- of active tectonics in the Acambay Graben, Mexican
-
- Volcanic Belt.
- Earth Surface Processes and Land*
-
- forms*
- ,
- 23**
- , 317–332.
RANGIN, C., LE PICHON, X. ET AL. 1999. Plate conver-
-
- gence measured by GPS across the Sundaland/Philip-
-
- pine Sea plate deformed boundary: the Philippines and
-
- eastern Indonesia.
- Geophysical Journal International*
- ,
-
- 139**
- , 296–316.

QUATERNARY FAULT ACTIVITY IN EASTERN INDONESIA

- 2785 ROBINSON, D.P., DAS, S. & SEARLE, M.P. 2010. Earth
2786 quake fault superhighways. *Tectonophysics*, **493**,
2787 236–243.
- 2788 ROBINSON, G.P. & RATMAN, N. 1978. The stratigraphic
2789 and tectonic development of the Manokwarai area,
2790 Irian Jaya. *BMR Journal of Australian Geology & Geo-
2791 physics*, **3**, 19–24.
- 2792 ROBINSON, G.P., RYBURN, R.J., HARAHAP, B.H., TOBING,
2793 S.L. & ACHDAN, A. 1990. *Geology of the Steenkool
2794 Sheet Area, Irian Jaya. 1:250,000 Scale*. Geological
2795 Research and Development Centre, Bandung.
- 2796 ROCKWELL, T.K., KELLER, E.A. & JOHNSON, D.L. 1984.
2797 Tectonic geomorphology of alluvial fans and mountain
2798 fronts near Ventura, California. In: MORISAWA, M.
2799 (ed.) *Tectonic Geomorphology. Proceedings of the
2800 15th Annual Geomorphology Symposium*. Allen and
2801 Unwin, Boston, MA, 183–207.
- 2802 ROQUES, D. 1999. *The Metamorphic Core of Buru*. South
2803 east Asia Research Group, London, Report No. 204.
- 2804 ROYDEN, L.H. 1993. Evolution of retreating subduction
2805 boundaries formed during continental collision. *Tec-
2806 tonics*, **12**, 629–638.
- 2807 RUDYAWAN, A. 2011. *Tectonostratigraphy and structural
2808 style of the South Banggai Sula Block and NW Banda
2809 Basin, Indonesia*. MSc thesis, University of London.
- 2810 SEGAL, P. & POLLARD, D.D. 1980. Mechanics of discontin-
2811 uous faults. *Journal of Geophysical Research*, **85**,
2812 4337–4350.
- 2813 SENO, T. & KAPLAN, D.E. 1988. Seismotectonics of west-
2814 ern New Guinea. *Journal of Physics of the Earth*, **36**,
2815 107–124.
- 2816 SIBSON, R.H. 1985. Stopping of earthquake ruptures at
2817 dilational fault jogs. *Nature*, **316**, 248–251.
- 2818 SIEH, K.E. & JAHNS, R.H. 1984. Holocene activity of the
2819 San Andreas fault at Wallace Creek, California. *Jour-
2820 nal of Geophysical Research*, **95**, 883–896.
- 2821 SILVA, P.G., GOY, J.L., ZAZO, C. & BARDAJÍ, T. 2003.
2822 Fault generated mountain fronts in southeast Spain:
2823 geomorphologic assessment of tectonic and seismic
2824 activity. *Geomorphology*, **50**, 203–225.
- 2825 SILVER, E.A. & MOORE, J.C. 1978. The Molucca Sea
2826 collision zone, Indonesia. *Journal of Geophysical
2827 Research*, **83**, 1681–1691.
- 2828 SILVER, E.A., McCAFFREY, R. & SMITH, R.B. 1983a. Col-
2829 lision, rotation and the initiation of subduction in the
2830 evolution of Sulawesi, Indonesia. *Journal of Geophys-
2831 ical Research*, **88**, 9407–9418.
- 2832 SILVER, E.A., McCAFFREY, R., JOYODIWIROYO, Y. & STE-
2833 VENS, S. 1983b. Ophiolite emplacement by collision
2834 between the Sula Platform and the Sulawesi Island
2835 Arc, Indonesia. *Journal of Geophysical Research*, **88**,
2836 9419–9435.
- 2837 SIMANDJUNTAK, T.O. 1986. *Sedimentology and tectonics
2838 of the collision complex in the East Arm of Sulawesi,
2839 Indonesia*. PhD thesis, University of London.
- 2840 SIMANDJUNTAK, T.O., SURONO & SUKIDO. 1984. *Geolog-
2841 ical Report of the Kolaka Quadrangle, 394 Sulawesi,
2842 Scale 1:250,000*. Open File Report. Indonesian Geo-
2843 logical Research and Development 395 Centre,
2844 Bandung.
- 2845 SIMANDJUNTAK, T.O., SURONO & SUKIDO. 1994. *Geo-
2846 logical Map of the Kolaka Quadrangle, Sulawesi,
2847 1:250,000 scale*. Geological Research and Develop-
2848 ment Centre, Bandung.
- 2849 SOCQUET, A., VIGNY, C., CHAMOT ROOKE, N., SIMONS,
2850 W., RANGIN, C. & AMBROSIOUS, B. 2006. India and
2851 Sunda plates motion and deformation along their bound-
2852 ary in Myanmar determined by GPS. *Journal of Geo-
2853 physical Research*, **111**, [https://doi.org/10.1029/
2005JB003877](https://doi.org/10.1029/2005JB003877)
- 2854 SOHONI, P.S., MALIK, J.N., MERH, S.S. & KARANTH, R.V.
2855 1999. Active tectonics astride Katrol Hill Zone,
2856 Kachchh, Western India. *Journal of the Geological
2857 Society of India*, **53**, 579–586.
- 2858 SPAKMAN, W. & HALL, R. 2010. Surface deformation and
2859 slab–mantle interaction during Banda Arc subduction
2860 rollback. *Nature Geoscience*, **3**, 562–566.
- 2861 SPENCER, J.E. 2010. Structural analysis of three exten-
2862 sional detachment faults with data from the 2000
2863 Space Shuttle Radar Topography Mission. *Geological
2864 Society of America Today*, **20**, 4–10.
- 2865 SPENCER, J.E. 2011. Gently dipping normal faults identi-
2866 fied with Space Shuttle radar topography data in central
2867 Sulawesi, Indonesia, and some implications for fault
2868 mechanics. *Earth and Planetary Science Letters*, **308**,
2869 267–276.
- 2870 STEIN, S., GELLER, R.J. & LIU, M. 2012. Why earthquake
2871 hazard maps often fail and what to do about it. *Tecto-
2872 nophysics*, **562–563**, 1–25.
- 2873 STEVENS, C.W., McCAFFREY, R. ET AL. 1999. GPS
2874 evidence for rapid rotations about a vertical axis in a
2875 collisional setting: the Palu fault of Sulawesi, Indone-
2876 sia. *Geophysical Research Letters*, **26**, 2677–2680.
- 2877 STEVENS, C.W., McCAFFREY, R., BOCK, Y., GENRICH,
2878 J.F., PUBELLIER, M. & SUBARYA, C. 2002. Evidence
2879 for block rotations and basal shear in the world's fastest
2880 slipping continental shear zone in NW New Guinea. In:
2881 STEIN, S. & FREYMUËLLER, J. (eds) *Plate Boundary
2882 Zones*. American Geophysical Union, Geodynamics
2883 Series, **30**, 87–99.
- 2884 STIRLING, M.W., WESNOUSKY, S.G. & SHIMAZAKI, K.
2885 1996. Fault trace complexity, cumulative slip, and
2886 the shape of the magnitude frequency distribution for
2887 strike slip faults: a global survey. *Geophysical Journal
2888 International*, **124**, 833–868.
- 2889 SUGGATE, S. & HALL, R. 2003. Predicting sediment yields
2890 from SE Asia: a GIS approach. In: *Proceedings, Indo-
2891 nesian Petroleum Association, 29th Annual Conven-
2892 tion*, IPA03 G 015, 289–304.
- 2893 SUKAMTO, R. & SIMANDJUNTAK, T.O. 1983. Tectonic
2894 relationship between geologic provinces of western
2895 Sulawesi, eastern Sulawesi and Banggai Sula in the
2896 light of sedimentological aspects. *Bulletin Geological
2897 Research and Development Centre, Bandung*, **7**, 1–12.
- 2898 SURONO & BACHRI, S. 1994. Stratigraphy of the southeast
2899 Sulawesi continental terrane, Eastern Indonesia. *Jour-
2900 nal of Geology and Mineral Resources*, **4**, 4–11.
- 2901 TEAS, P.A., DECKER, J., ORANGE, D. & BAILLIE, P.
2902 2009. New insight into structure and tectonics of the
2903 Seram Trough from SEASEPTM high resolution
2904 bathymetry. In: *Proceedings, Indonesian Petroleum
2905 Association, 33rd Annual Convention and Exhibition*,
2906 IPA09 G 091.
- 2907 THATCHER, W. 1995. Microplate v. continuum descrip-
2908 tions of active tectonic deformation. *Journal of Geo-
2909 physical Research*, **100**, 3885–3894.
- 2910 TJOKROSAPETRO, S., BUDHITRISNA, T. & RUSMANA, D.
2911 1981. *Geological Map of the Buru Island Quadrangle*,

- 2843 *Maluku, 1:250,000 Scale*. Geological Research and
2844 Development Centre, Bandung.
- 2845 TJOKROSAPOETRO, S., ACHDAN, A., SUWITODIRDJO, K.,
2846 RUSMANA, E. & ABIDIN, H.Z. 1993. *Geological Map*
2847 *of the Masohi Quadrangle, 2200 Maluku, 1:250000*.
2848 Geological Research and Development Centre,
2849 Bandung.
- 2850 USGS EARTHQUAKE HAZARDS PROGRAM. Significant
2851 Earthquakes, [http://earthquake.usgs.gov/earthquakes/
2852 browse/significant.php](http://earthquake.usgs.gov/earthquakes/browse/significant.php) [last accessed 29 October 2016].
- 2853 VAN LEEUWEN, T.M. & MUHARDJO, 2005. Stratigraphy
2854 and tectonic setting of the Cretaceous and Paleogene
2855 volcanic-sedimentary successions in northwest Sula-
2856 wes, Indonesia implications for the Cenozoic evolu-
2857 tion of Western and Northern Sulawesi. *Journal of*
2858 *Asian Earth Sciences*, **25**, 481–511.
- 2859 VAN LEEUWEN, T., ALLEN, C.M., KADARUSMAN, A.,
2860 ELBURG, M., PALIN, J.M., MUHARDJO & SUWIANTO
2861 2007. Petrologic, isotopic, and radiometric age con-
2862 straints on the origin and tectonic history of the Malino
2863 Metamorphic Complex, NW Sulawesi, Indonesia. *Journal of Asian Earth Sciences*, **29**, 751–777.
- 2864 VECCHIOTTI, F. 2008. Calculating geomorphic indices
2865 in SE Asia using a SRTM derived DEM: a worked
2866 example from West Sulawesi, Indonesia. In: MICHEL,
2867 U., CIVCO, D.L., EHLERS, M. & KAUFMAN, H.J. (eds)
2868 *Remote Sensing for Environmental Monitoring*. GIS
2869 Applications and Geology VIII, SPIE Proceedings,
2870 **7110**, <https://doi.org/10.1117/12.800240>
- 2871 VISSER, W.A. & HERMES, J.J. 1962. *Geological Results of*
2872 *the Exploration for Oil in Netherlands New Guinea*.
2873 Verhandelingen Koninklijk Nederlands Geologisch
2874 en Mijnbouwkundig Genootschap, Geologische Serie
2875 20. Staatsdrukkerij-en Uitgeverijbedrijf, The Hague.
- 2876 WALD, D.J., KANAMORI, H., HELMBERGER, D.V. &
2877 HEATON, T.H. 1993. Source study of the 1906
2878 San Francisco earthquake. *Bulletin of the Seismologi-
2879 cal Society of America*, **83**, 981–1019.
- 2880 WALKER, F. & ALLEN, M.B. 2012. Offset rivers, drainage
2881 spacing and the record of strike-slip faulting: the Kuh
2882 Banan Fault, Iran. *Tectonophysics*, **530–531**, 251–263.
- 2883 WALLACE, R.E. 1968. Notes on stream channels offset by
2884 the San Andreas fault, southern Coast Ranges, Cali-
2885 fornia. In: DICKINSON, W. & GRANTZ, A. (eds) *Confer-
2886 ence on Geologic Problems of San Andreas Fault*
2887 *System*. Proceedings. Stanford University Publications
2888 in the Geological Sciences, **11**, 6–21.
- 2889 WALLACE, R.E. 1986. *Active Tectonics: Impacts on Soci-
2890 ety*. Studies in Geophysics. National Academy Press,
2891 Washington, DC.
- 2892 WALLACE, R.E. (ed.) 1990. *The San Andreas Fault System,
2893 California*. US Geological Survey, Professional
2894 Papers, **1515**.
- 2895 WALPERSDORF, A., VIGNY, C., SUBARYA, C. & MANUR-
2896 UNG, P. 1998. Monitoring of the Palu-Koro Fault
2897 (Sulawesi) by GPS. *Geophysical Research Letters*,
2898 **25**, 2313–2316.
- 2899 WANG, Y., SIEH, K., SOE THURA TUN, LAI, K.-Y. & THAN
2900 MYINT, 2014. Active tectonics and earthquake poten-
2901 tial of the Myanmar region. *Journal of Geophysical*
2902 *Research: Solid Earth*, **119**, 3767–3822, [https://doi.
2903 org/10.1002/2013JB010762](https://doi.org/10.1002/2013JB010762)
- 2904 WATKINSON, I.M. 2011. Ductile flow in the metamorphic
2905 rocks of central Sulawesi. In: HALL, R., COTTAM,
2906 M.A. & WILSON, M.E.J. (eds) *The SE Asian Gateway:
2907 History and Tectonics of the Australia–Asia Collision*.
2908 Geological Society, London, Special Publications,
2909 **355**, 157–176, <https://doi.org/10.1144/SP355.8>
- 2910 WATKINSON, I.M., HALL, R. & FERDIAN, F. 2011. Tectonic
2911 re-interpretation of the Banggai-Sula–Molucca Sea
2912 margin, Indonesia. In: HALL, R., COTTAM, M.A. &
2913 WILSON, M.E.J. (eds) *The SE Asian Gateway: History*
2914 *and Tectonics of the Australia–Asia Collision*. Geo-
2915 logical Society, London, Special Publications, **355**,
2916 203–224, <https://doi.org/10.1144/SP355.10>
- 2917 WELLS, D.L. & COPPERSMITH, K.J. 1994. New empirical
2918 relationships among magnitude, rupture length, rupture
2919 width, rupture area, and surface displacement. *Bulletin*
2920 *of the Seismological Society of America*, **84**, 974–1002.
- 2921 WELLS, S.G., BULLARD, T.F. ET AL. 1988. Regional varia-
2922 tions in tectonic geomorphology along a segmented
2923 convergent plate boundary, Pacific Coast of Costa
2924 Rica. *Geomorphology*, **1**, 239–265.
- 2925 WESNOUSKY, S.G. 1988. Seismological and structural evo-
2926 lution of strike-slip faults. *Nature*, **335**, 340–342.
- 2927 WESNOUSKY, S.G. 2006. Predicting the endpoints of earth-
2928 quake ruptures. *Nature*, **444**, 358–360.
- 2929 WHITE, L.T., HALL, R. & ARMSTRONG, R.A. 2014. The age
2930 of undeformed dacite intrusions within the Kolaka
2931 fault zone, SE Sulawesi, Indonesia. *Journal of Asian*
2932 *Earth Sciences*, **94**, 105–112.
- 2933 WICHMANN, A. 1918. Die Erdbeben des Indischen Archi-
2934 pels Bis Zum Jahre 1857. *Verhandelingen der Konin-
2935 klijke Akademie van Wetenschappen te Amsterdam*,
2936 **20**, 193 [in Dutch].
- 2937 WU, J.E., MCCLAY, K., WHITEHOUSE, P. & DOOLEY, T.
2938 2009. 4D analogue modelling of transtensional pull-
2939 apart basins. *Marine and Petroleum Geology*, **26**,
2940 1608–1623.
- 2941 WYSS, M. 2005. Human losses expected in Himalayan
2942 earthquakes. *Natural Hazards*, **34**, 305–314.
- 2943 XU, X., YEATS, R.S. & YU, G. 2010. Five short historical
2944 earthquake surface ruptures near the silk road, Gansu
2945 Province, China. *Bulletin of the Seismological Society*
2946 *of America*, **100**, 541–561.
- 2947 YEATS, R. 2010. *Active Faults of the World*. Cambridge
2948 University Press, Cambridge.
- 2949 YILDIRIM, C. 2014. Relative tectonic activity assessment
2950 of the Tuz Gölü Fault Zone; Central Anatolia, Turkey.
2951 *Tectonophysics*, **630**, 183–192.